



DOCTORAL THESIS

**EVALUATION OF THE FATIGUE RESISTANCE OF
POWER LINE CONDUCTORS FUNCTION OF THE H/w
PARAMETER**

REMY KALOMBO BADIBANGA

Brasília, December 2017

UNIVERSITY OF BRASÍLIA

**COLLEGE OF TECHNOLOGY
DEPARTMENT OF MECHANICAL ENGINEERING**

**UNIVERSITY OF BRASÍLIA
FACULTY OF TECHNOLOGY
DEPARTAMENT OF MECHANICAL ENGINEERING**

**EVALUATION OF THE FATIGUE RESISTANCE OF
POWER LINE CONDUCTORS FUNCTION OF THE H/w
PARAMETER**

REMY KALOMBO BADIBANGA

SUPERVISOR: Prof. Dr. JOSÉ ALEXANDER ARAÚJO

CO-SUPERVISOR: Prof. Dr. JORGE LUIZ ALMEIDA FERREIRA

DOCTORAL THESIS IN MECHANICAL ENGINEERING

PUBLICATION: ENM-DT – 45/2017

BRASÍLIA/DF: DECEMBER – 2017

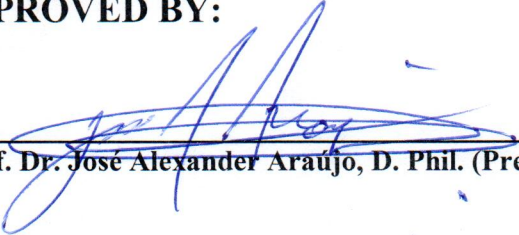
UNIVERSITY OF BRASÍLIA
FACULTY OF TECHNOLOGY
DEPARTAMENT OF MECHANICAL ENGINEERING

EVALUATION of the FATIGUE RESISTANCE of POWER
LINE CONDUCTORS FUNCTION of the H/w PARAMETER

REMY KALOMBO BADIBANGA

A thesis submitted to University of Brasilia in partial fulfilment of the
requirements of the degree of Doctor in mechanical engineering.

APPROVED BY:


Prof. Dr. José Alexander Araujo, D. Phil. (Presidente da banca) (ENM-UnB) (Orientador)


Prof. Dr. Raimundo Carlos Silverio Freire Júnior, Dr. (UFRN) (External examiner)


Prof. Dr. Luis Augusto Veloso, Dr. (UnB) (External examiner)


Prof. Dr. Cosme Roberto Moreira da Silva, Ph.D (UnB) (Internal examiner)

Brasília/DF, December 2017

FICHA CATALOGRÁFICA

REMY KALOMBO BADIBANGA

EVALUATION OF THE FATIGUE RESISTANCE OF POWER LINE CONDUCTORS
FUNCTION OF THE H/w PARAMETER - [Distrito Federal] 2017.

xxi, 157 p., 210 x 297 mm (ENM/FT/UnB, Doutor, Ciências Mecânicas, 2017).

Dissertação de Doutorado – Universidade de Brasília. Faculdade de Tecnologia.

Departamento de Engenharia Mecânica.

1. Parâmetro H/w

2. Tensão média

3. Fadiga por *fretting*

4. Curva de *Wöhler*

5. Cabo Condutor

I. ENM/FT/UnB

II. ENM-DT 45/2017

REFERÊNCIA BIBLIOGRÁFICA

KALOMBO, R.B.,(2017), Evaluation of the fatigue resistance of power line conductors function of the H/w parameter, Dissertação de Doutorado em Ciências Mecânicas, Publicação ENM-DT 45/2017, Departamento de Engenharia Mecânica, Universidade de Brasília, Brasília, DF, 157 p.

CESSÃO DE DIREITOS

AUTOR: Remy Kalombo Badibanga.

TÍTULO: Evaluation of the fatigue resistance of power line conductors function of the H/w parameter - [Distrito Federal] 2017.

GRAU: Doutor

ANO: 2017

É concedida à Universidade de Brasília permissão para reproduzir cópias desta dissertação de doutorado e para emprestar ou vender tais cópias somente para propósitos acadêmicos e científicos. O autor reserva outros direitos de publicação e nenhuma parte dessa dissertação de doutorado pode ser reproduzida sem autorização por escrito do autor.

Remy Kalombo Badibanga
remyunb@gmail.com

Acknowledgements

Glory and Praise to Jehovah, the Almighty God who allowed me to achieve this set of thesis.

I express my sincerest gratitude to Prof. D. Phil José Alexander Araujo and Prof. Dr. Jorge Luiz Almeida Ferreira for their dedicated supervision and priceless assistance throughout this study. I gratefully acknowledge all academics staffs and technicians of GFFM (*Grupo de Fadiga, Fatura e Materiais*) of University of Brasília and to all my colleagues, academics and technicians.

I would like to thank *TAESA, ATE II, ATE III, EATE, TME, AETE e Brasnorte* who are funding this research through the GFFM. Without the funding, this thesis would not have been possible.

Further, I would like to take this opportunity to thank my Mum and Dad who taught me to never give up. Also, I want to thank all my brothers, sisters, nieces, nephews and cousins.

Special thanks to Rachel Kalunga Lusinga and to all my sons who deserves a medal for their patience and support. I will forever be thankful to all my friends for the moral support provided.

Lastly, I would like to thank all those who have contributed, either directly or indirectly to the preparation, research and compilation of this thesis.

Preface

This thesis is an account of the research programme carried out by the author in the department of mechanical engineering at University of Brasília (UnB). The work is conducted under the supervision of Prof. Dr. Phil José Alexander Araújo and the co-supervision of Prof Dr. Jorge Luiz Almeida Ferreira

Some of the works, listed below, described in this thesis has been published or are under submission:

Remy B. Kalombo, Túlio A. Guimarães, Jorge L. A. Ferreira, Cosme R. M. da Silva, Gliender P. de Mendonça, José A. Araújo, 2015, Relação H/w : estudo crítico e planejamento de ensaios para avaliar a validade do parâmetro como critério de projeto contra fadiga eólica, VIII congresso de inovação tecnológica em energia eléctrica (CITENEL), Bahia, Brasil.

R.B. Kalombo, J.M.G. Martínez, J.L.A. Ferreira, C.R.M. da Silva, J.A. Araújo, 2015, Comparative fatigue tests and analysis between an All Aluminium Alloy Conductor (AAAC) and an Aluminium Conductor Steel Reinforced (ACSR), Procedia Engineering, 133, 223-232.

R.B. Kalombo, J.A. Araújo, J.L.A. Ferreira, C.R.M. da Silva, R. Alencar, A.R. Capra, 2015, Assessment of the fatigue failure of an All Aluminium Alloy Cable (AAAC) for a 230 kV transmission line in the Center-West of Brazil, Engineering Failure Analysis, 61, 77–87.

R.B. Kalombo, M.S. Pestana, J.L.A. Ferreira, C.R.M. da Silva, J.A. Araújo, 2017, Influence of the catenary parameter (H/w) on the fatigue life of overhead conductors, Tribology International, Vol. 108, pp. 141-149.

Remy K. Badibanga, Pedro Henrique C. Rocha, Renato E. R. Vieira, Thiago B. Miranda, Miélla S. Pestana, Jorge, L. A. Ferreira, Cosme R. M. Silva, Alessandro C. S. Berrêdo, Fabio S. Coutinho, Alberto R. Sousa, José A. Araújo, 2017, Comportamento em Fadiga de Cabos Condutores CA e CAL Utilizando o Critério de Projeto H/w , IX congresso de inovação tecnológica em energia eléctrica (CITENEL), Paraíba, Brasil.

Renato E. R. Vieira, **Remy K. Badibanga**, Pedro Henrique C. Rocha, Thiago B. Miranda, Miélla S. Pestana, Jorge L. A. Ferreira, José A. Araújo, Cosme R M. Silva, Alessandro C.

S. Berrêdo, Fabio S. Coutinho, Alberto R. Sousa, 2017, Efeito do Parâmetro H/w na Deformação/Tensão Dinâmica Atuante em um Cabo Tipo CA, IX congresso de inovação tecnológica em energia eléctrica (CITENEL), Paraíba, Brasil.

R.B. Kalombo, Pedro Henrique C. R., T.B. Miranda, J.L.A. Ferreira, C.R.M. da Silva, J.A. Araújo, 2017, Fatigue Performance of Overhead Conductors Tested Under the Same Value of H/w parameter, Procedia Engineering, Senlis, France. (**Accepted for publication**)

R.B. Kalombo, P.H.C. Rocha, T.B. Miranda, J.L.A. Ferreira, C.R.M. da Silva, J.A. Araújo, 2018, The effect of mean stress on the fatigue behaviour of overhead conductor function of the H/w parameter, 12th International fatigue congress, Poitiers, France. (**Abstract accepted**)

Resumo

Deste 1960, um grupo instituído pela CIGRÉ (*Conseil Intrntional des Grands Réseaux Électriques*) propôs o uso do *Every Day Stress* (EDS) para projeto de linhas de transmissão aéreas. Porém, investigações em campo chamaram atenção para ocorrência de danos devidos à fadiga em condutores, mesmo com o uso de EDS recomendados. Mais recentemente, a CIGRÉ propôs o uso do parâmetro H/w para projeto, com a intenção de generalizar o comportamento em fadiga dos condutores aéreos.

O objetivo deste trabalho, então, é conduzir um estudo experimental para avaliar os efeitos do parâmetro catenário (H/w) na vida em fadiga de condutores aéreos. Comparações entre as curvas S-N geradas mostraram que o condutor CAA Tern sustenta um número significativamente maior de ciclos antes da falha por fadiga ocorrer do que o CAL 900 MCM, para os valores de H/w . Enquanto isso, o CA Orchid apresentou uma vida em fadiga localizada entre os dois condutores citados e similar à do ACAR 750 MCM. Os dados experimentais dos testes estáticos se adequaram bem aos valores teóricos estimados. Análises de falha de amostras de quebradas (fios) revelaram, não apenas que as trincas tiveram início nas áreas de escorregamento dos fios de alumínio, mas também, sua morfologia apresentou clara evidência de falhas por fadiga, assim como marcas de praia e trincas secundárias. Adicionalmente, uma análise de falha foi realizada, não só em termos da camada em que ocorreu a quebra do fio e do tipo de superfície de falha, mas também de acordo com a posição relativa à boca do grampo em que as falhas ocorreram dentro do grampo de suspensão.

Dados apresentados nesse estudo podem ser utilizados em vários programas de elementos finitos não lineares para melhor entender o comportamento mecânico dos condutores. Ademais, a informação gerada pode ser útil para planejamento de manutenção em linhas de transmissão. Baseada na avaliação do parâmetro H/w apresentada nesse trabalho, foi verificado que o parâmetro representa um claro avanço no projeto de linhas de transmissão contra fadiga devido a vibrações eólicas quando comparado com o anteriormente recomendado *Every Day Stress* (EDS). Isso é suportado pelo fato de que, quando utilizado o parâmetro H/w , os dados estáticos são consistentes com aqueles previstos pelo uso de equações apropriadas.

Palavras-chave: Parâmetro H/w , Tensão média, Fadiga por *fretting*, Curva de Wöhler, Cabo condutor.

Abstract

Since 1960, a panel instituted by CIGRÉ (*Conseil International des Grands Réseaux Électriques*) proposed the use of the Every Day Stress (EDS) for overhead conductor design. But field investigations drew attention to the occurrence of fatigue damage of conductors even though the recommended EDS were adhered. More recently, then, CIGRÉ proposed the use of H/w (The ratio between the horizontal tensile load, H , and the conductor weight per unit length, w) parameter for design purpose with the goal of generalising the fatigue behaviour of overhead conductors.

The objective of this work, then, was to conduct an experimental study to evaluate the effects of the catenary parameter (H/w) on the fatigue life of overhead conductors. Comparison between the generated S-N curves proved that the ACSR Tern conductor could sustain a significantly higher number of cycles before fatigue failure than the AAAC 900 MCM for different values of H/w . Meanwhile, the AAC Orchid presented a fatigue life which is located between the two conductors cited above and presents a similar fatigue life as the ACAR 750 MCM. The experimental data from static tests agreed quite well with the estimated theoretical values. Failure analysis of the broken samples (wires) revealed not only that cracks initiated in the fretted areas of the aluminium wires, but also that their morphology presented clear evidence of fatigue failure, such as beach marks and secondary cracks. Additionally, a failure analysis was performed, not only in terms of the layer in which the wires broke and the type of fracture surface but also according to the position from the clamp mouth where these failures occurred inside the suspension clamp.

Data presented in this study could be used in various non-linear finite-element programs in order to better understand the mechanical behaviour of conductors. Furthermore, the generated information could be helpful for planning the maintenance of power lines. Based on the evaluation of the parameter H/w presented in this work, it emerged that the H/w parameter represents a clear advance in the design of transmission lines against fatigue due to aeolian vibrations when compared to the previously recommended Every Day Stress (EDS). This is supported by the fact that, when using the H/w parameter, the static data are consistent with those predicted using appropriate equations.

Keywords: H/w parameter, Mean stress, Fretting fatigue, Wöhler curve, Overhead conductor.

Contents

Acknowledgements.....	iv
Preface.....	v
Resumo.....	vii
Abstract.....	viii
Contents.....	ix
List of figures.....	xi
List of tables.....	xviii
Nomenclature.....	xix
CHAPTER 1: INTRODUCTION.....	1
1.1. Motivation and originality.....	1
1.2. Overview of studies on conductor fatigue.....	3
1.3. Aim and objectives.....	8
1.4. Structure of the thesis.....	8
CHAPTER 2: FATIGUE OF POWER LINE CONDUCTORS.....	10
2.1. Power line motion.....	10
2.1.1. Wind excitation of power line conductors.....	10
2.1.2. Aeolian vibration.....	12
2.2. Fretting fatigue.....	14
2.3. Mechanism of conductor fatigue.....	16
2.4. Poffenberger-Swart (P-S) equation.....	18
2.5. Endurance limits of power line conductor.....	20
2.5.1. Endurance limit approach for conductors.....	21
2.5.2. Damage cumulative approach for conductor.....	22
2.6. Safe design parameter of overhead conductor.....	24
2.6.1. Every Day Stress (EDS).....	24

2.6.2. H/w parameter.....	26
CHAPTER 3: MATERIALS AND EXPERIMENTAL METHODS.....	33
3.1. Materials	33
3.1.1. Conductors.....	33
3.1.2. Suspension clamps	35
3.1.3. Apparatus and sensors.....	36
3.2. Methodology and experimental procedure	39
3.2.1. Methodology for the evaluation of H/w parameter.....	39
3.2.2. Experimental procedure	42
CHAPTER 4: EXPERIMENTAL RESULTS AND DISCUSSIONS.....	51
4.1. Strain analysis	51
4.1.1. Static test	51
4.1.2. Dynamic test.....	58
4.2. Fatigue test	65
4.2.1. Resistance limits in function of bending amplitude (Y_b)	68
4.2.2. S-N curves generated	72
4.3. Constant fatigue life diagram as a function of H/w	78
4.4. Failure analysis.....	80
4.4.1. Macroscopic analysis	80
4.4.2. Microscopic analysis.....	101
CHAPTER 5: CONCLUSIONS AND RECOMMENDATIONS.....	108
5.1. Conclusions	108
5.2. Recommendations and suggestions	110
References	112
Appendix	119

List of figures

Figure 2.1: Schematic representation of various flow regimes depending on Reynolds number (Lienhard, 1966; Vecchiarelli, 1997)	11
Figure 2.2: Vortex shedding-induced aeolian vibration of power line conductor (Giosan, 2013)	11
Figure 2.3: Distribution of the wind velocity and power in Brazil (CEPEL, 2015)	14
Figure 2.4: Representation of mechanical contact between two cylinders subjected to two loads and the elliptical fretting marks	15
Figure 2.5: Fretting fatigue of conductor: (a) intense surface wear, fracture of some aluminium wires in the outer layer of the ACSR conductor; and (b) elliptical fretting marks and wire break of the inner layer of the ACSR conductor (Azevedo <i>et al.</i> , 2009)	16
Figure 2.6: Powder (aluminium oxide) coming out of the AAC Orchid conductor: (a) during the fatigue test; and (b) after testing	16
Figure 2.7: (a) Cross section of an ACSR conductor; and (b) critical contacts region of the conductor in the suspension clamp (Fadel, 2010)	17
Figure 2.8: Schematic montage of conductor and the suspension clamp showing the standard position to measure the bending amplitude Y_b	19
Figure 2.9: S-N curves compiled by CIGRÉ and the CIGRÉ Safe Border Line, SBL (CIGRÉ, 1979).....	23
Figure 2.10: Recommended safe design tension in terms of H/w vs $L_s D/m$ (L_s , D and m are, respectively, the span length, conductor diameter and the conductor mass per unit) (CIGRÉ, 2005).....	31
Figure 3.1: (a) Drawing; (b) assembly of suspension clamp; and (c) dimensions of suspension clamp (Aida, 2010)	36
Figure 3.2: (a) Shakers; (b) controller; and (c) amplifier used for fretting fatigue bench ..	37
Figure 3.3: Type of accelerometer used (left) and the Laser usb LDS vibration controller and analysis system software (right).....	38
Figure 3.4: (a) The load cell used during the experiment; and (b) the indicator of the conductor stretching load	38
Figure 3.5: (a) Strain gauge of 350 Ohm; (b) the ADS data acquisition unit used to measure strain	39

Figure 3.6: Schematic view for the last point of contact between the conductor and the suspension clamp, the bending displacement (Y_b) and the 89 mm distance from the LPC (Last Point of Contact) (Araújo, 2014)	43
Figure 3.7: The orthogonal position of the accelerometer with respect to the conductor axis	44
Figure 3.8: The assembly of the conductor and the suspension clamp on the bench	45
Figure 3.9: Strain gauges glued on all wires from the external layer of the ACSR Tern conductor for static test	48
Figure 4.1: Polar diagram of axial stress in each external layer wire of the AAAC 900 MCM conductor at different values of (a) $H/w = 1820$ m; (b) $H/w = 2144$ m; and (c) $H/w = 2725$ m.....	52
Figure 4.2: Polar diagram of axial stress in each external layer wire of the ACSR Tern conductor at different values of (a) $H/w = 1820$ m; (b) $H/w = 2144$ m; and (c) $H/w = 2725$ m	53
Figure 4.3: Polar diagram of axial stress in each external layer wire of the AAC Orchid conductor at different values of (a) $H/w = 1820$ m; (b) $H/w = 2144$ m; and (c) $H/w = 2725$ m	54
Figure 4.4: Polar diagram of axial stress in each external layer wire of the ACAR 750 MCM conductor at different values of (a) $H/w = 1820$ m; (b) $H/w = 2144$ m; and (c) $H/w = 2725$ m.....	55
Figure 4.5: Axial average stress (from strain measurements in all wires of the external layer) for different H/w steps during loading and unloading of the AAAC 900 MCM conductor.....	56
Figure 4.6: Axial average stress (from strain measurements in all wires of the external layer) for different H/w steps during loading and unloading of the ACSR Tern conductor.....	57
Figure 4.7: Axial average stress (from strain measurements in all wires of the external layer) for different H/w steps during loading and unloading of the AAC Orchid conductor	57
Figure 4.8: Axial average stress (from strain measurements in all wires of the external layer) for different H/w steps during loading and unloading of the ACAR 750 MCM conductor.....	58

Figure 4.9: Bending stress versus bending amplitude: comparison between measured and predicted using the Poffenberger-Swart (P-S) formula on the AAAC 900 MCM conductor with the $H/w = 1820$ m	59
Figure 4.10: Bending stress versus bending amplitude: comparison between measured and predicted using the Poffenberger-Swart (P-S) formula on the AAAC 900 MCM conductor with the $H/w = 2144$ m.....	59
Figure 4.11: Bending stress versus bending amplitude: comparison between measured and predicted using the Poffenberger-Swart (P-S) formula on the AAAC 900 MCM conductor with the $H/w = 2725$ m.....	60
Figure 4.12: Bending stress versus bending amplitude: comparison between measured and predicted using the Poffenberger-Swart (P-S) formula on the ACSR Tern conductor with the $H/w = 1820$ m.....	60
Figure 4.13: Bending stress versus bending amplitude: comparison between measured and predicted using the Poffenberger-Swart (P-S) formula on the ACSR Tern conductor with the $H/w = 2144$ m.....	61
Figure 4.14: Bending stress versus bending amplitude: comparison between measured and predicted using the Poffenberger-Swart (P-S) formula on the ACSR Tern conductor with the $H/w = 2725$ m.....	61
Figure 4.15: Bending stress versus bending amplitude: comparison between measured and predicted using the Poffenberger-Swart (P-S) formula on the AAC Orchid conductor with the $H/w = 1820$ m.....	62
Figure 4.16: Bending stress versus bending amplitude: comparison between measured and predicted using the Poffenberger-Swart (P-S) formula on the AAC Orchid conductor with the $H/w = 2144$ m.....	62
Figure 4.17: Bending stress versus bending amplitude: comparison between measured and predicted using the Poffenberger-Swart (P-S) formula on the AAC Orchid conductor with the $H/w = 2725$ m.....	63
Figure 4.18: Bending stress versus bending amplitude: comparison between measured and predicted using the Poffenberger-Swart (P-S) formula on the ACAR 750 MCM conductor with the $H/w = 1820$ m	63
Figure 4.19: Bending stress versus bending amplitude: comparison between measured and predicted using the Poffenberger-Swart (P-S) formula on the ACAR 750 MCM conductor with the $H/w = 2144$ m	64

Figure 4.20: Bending stress versus bending amplitude: comparison between measured and predicted using the Poffenberger-Swart (P-S) formula on the ACAR 750 MCM conductor with the $H/w = 2725$ m	64
Figure 4.21: Rotation graph of the ruler mounted at the first node from the suspension clamp versus the number of cycles elapsed as well as the instance of wire break	66
Figure 4.22: (a) Two lines made around the ACSR Tern conductor between the LPC and 89 mm before the fatigue test; (b) two lines move out, indicating three broken wires on the external layer of the ACSR Tern conductor during the fatigue test	67
Figure 4.23: (a) Sample taken from the fretting fatigue test bench; (b) measurement of the distance to wire breaks from the mouth of the suspension clamp which is the reference position	67
Figure 4.24: Curves of bending displacement versus fatigue life for the AAAC 900 MCM conductor at different values of H/w parameter	68
Figure 4.25: Curves of bending displacement versus fatigue life for the ACSR Tern conductor at different values of H/w parameter	69
Figure 4.26: Curves of bending displacement versus fatigue life for the AAC Orchid conductor at different values of H/w parameter	69
Figure 4.27: Curves of bending displacement versus fatigue life for the ACAR 750 MCM conductor at different values of H/w parameter	70
Figure 4.28: Comparison curves of bending displacement versus fatigue life for different conductors tested at $H/w = 1820$ m.....	71
Figure 4.29: Comparison curves of bending displacement versus fatigue life for different conductors at $H/w = 2144$ m.....	71
Figure 4.30: Comparison curves of bending displacement versus fatigue life for different conductors at $H/w = 2725$ m.....	72
Figure 4.31: S-N curves of AAAC 900 MCM conductor for different values of H/w	73
Figure 4.32: S-N curves of the ACSR Tern conductor for different values of H/w	73
Figure 4.33: S-N curves of the AAC Orchid conductor for different values of H/w	74
Figure 4.34: S-N curves of the ACAR 750 MCM conductor for different values of H/w ..	74
Figure 4.35: Comparison of the mean S-N curves of different conductors tested at $H/w = 1820$ m.....	75
Figure 4.36: Comparison of the mean S-N curves of different conductors tested at $H/w = 2144$ m.....	76

Figure 4.37: Comparison of the mean S-N curves of different conductors tested at $H/w = 2725$ m.....	76
Figure 4.38: Conductor's fatigue strength, term of the H/w parameter versus bending stress, considering 10^6 cycles as a reference	79
Figure 4.39: Conductor's fatigue strength, term of the H/w parameter versus bending amplitude, considering 10^6 cycles as a reference	80
Figure 4.40: Scheme of the system conductor/suspension clamp showing: (a) The failure distance (FD) and (b) the position of the broken wire related to the suspension clamp (Represented with a partial cross section).....	81
Figure 4.41: Mean failure distance of wire breaks from the suspension clamp mouth function of bending displacement for the AAAC 900 MCM conductor tested at $H/w = 1820$ m.....	82
Figure 4.42: Mean failure distance of wire breaks from the suspension clamp mouth function of bending displacement for the conductor AAAC 900 MCM tested at $H/w = 2144$ m	83
Figure 4.43: Mean failure distance of wire breaks from the suspension clamp mouth function of bending displacement for the AAAC 900 MCM conductor tested at $H/w = 2725$ m	83
Figure 4.44: Mean failure distance of wire breaks from the suspension clamp mouth function of bending displacement for the ACSR Tern conductor tested at $H/w = 1820$ m	84
Figure 4.45: Mean failure distance of wire breaks from the suspension clamp mouth function of bending displacement for the ACSR Tern conductor tested at $H/w = 2144$ m	84
Figure 4.46: Mean failure distance of wire breaks from the suspension clamp mouth function of bending displacement for the ACSR Tern conductor tested at $H/w = 2725$ m	85
Figure 4.47: Mean failure distance of wire breaks from the suspension clamp mouth function of bending displacement for the AAC Orchid conductor tested at $H/w = 1820$ m.....	85
Figure 4.48: Mean failure distance of wire breaks from the suspension clamp mouth function of bending displacement for the AAC Orchid conductor tested at $H/w = 2144$ m.....	86
Figure 4.49: Mean failure distance of wire breaks from the suspension clamp mouth function of bending displacement for the AAC Orchid conductor tested at $H/w = 2725$ m.....	86
Figure 4.50: Mean failure distance of wire breaks from the suspension clamp mouth function of bending displacement for the ACAR 750 MCM conductor tested at $H/w = 1820$ m	87

Figure 4.51: Mean failure distance of wire breaks from the suspension clamp mouth function of bending displacement for the ACAR 750 MCM conductor tested at $H/w = 2144$ m	87
Figure 4.52: Mean failure distance of wire breaks from the suspension clamp mouth function of bending displacement for the ACAR 750 MCM conductor tested at $H/w = 2725$ m	88
Figure 4.53: Mean failure distance of broken wire measured from the suspension clamp month versus the H/w value for different cables tested	89
Figure 4.54: Scheme of a conductor with its cross section showing wire from the external (E) and the internal (I) layer	89
Figure 4.55: Percentage distribution of wire breaks per layer function of the H/w parameter for the AAAC 900 MCM conductor.....	90
Figure 4.56: Percentage distribution of wire breaks per layer function of the H/w parameter for the ACSR Tern conductor	90
Figure 4.57: Percentage distribution of wire breaks per layer function of the H/w parameter for the AAC Orchid conductor.....	91
Figure 4.58: Percentage distribution of wire breaks per layer function of the H/w parameter for the ACAR 750 MCM conductor.....	91
Figure 4.59: Percentage comparison distribution of wire breaks per layer function of the parameter $H/w = 1820$ m for conductors tested.....	93
Figure 4.60: Percentage comparison distribution of wire breaks per layer function of the parameter $H/w = 2144$ m for conductors tested.....	93
Figure 4.61: Percentage comparison distribution of wire breaks per layer function of the parameter $H/w = 2725$ m for conductors tested.....	94
Figure 4.62: Types of strands fracture surface identified on all conductors (AAAC 900MCM, ACSR Tern, AAC Orchid and ACAR 750MCM) tested: (a) Quasi-planar type, (b) 45° type, (c) L type and (d) V type.....	96
Figure 4.63: Types of fracture surface in function of the different values of the H/w parameter for the AAAC 900 MCM conductor.....	97
Figure 4.64: Types of fracture surface in function of the different values of the parameter H/w for the ACSR Tern conductor	98
Figure 4.65: Types of fracture surface in function of the different values of the parameter H/w for Orchid conductor	98

Figure 4.66: Types of fracture surface in function of the different values of the parameter H/w for the ACAR 750 MCM conductor.....	99
Figure 4.67: Comparison of the types of fracture surfaces for different conductors tested with $H/w = 1820$ m (AAAC 900 MCM, ACSR Tern, AAC Orchid and ACAR 750 MCM)	100
Figure 4.68: Comparison of the types of fracture surfaces for different conductors tested with $H/w = 2144$ m (AAAC 900 MCM, ACSR Tern, AAC Orchid and ACAR 750 MCM)	100
Figure 4.69: Comparison of the types of fracture surfaces for different conductors tested with $H/w = 2725$ m (AAAC 900 MCM, ACSR Tern, AAC Orchid and ACAR 750 MCM)	101
Figure 4.70: Fracture surface of AAAC 900 MCM wire (arrow indicating the quasi-planar area).....	102
Figure 4.71: SEM of the fracture surface of an AAAC 900 MCM strand: (a) crack initiated in the fretted region and beach marks; (b) zoom of the crack initiation point; (c) dimples and (d) the striations mark.....	103
Figure 4.72: Elliptical contact zone in an Aluminum wire (AAAC 900 MCM) from the external layer showing mixed stick/slip fretting regime	103
Figure 4.73: Fractured surface of Aluminum 1350-H19 wire, obtained from ACSR Tern conductor after fatigue test, with crack propagation at an oblique angle. Massive clamp indentation is shown at the right edge (arrow)	104
Figure 4.74: SEM of the fracture surface of an ACSR Tern conductor showing the fretting scar and a small quasi-planar zone	104
Figure 4.75: Fracture surface of an AAC Orchid conductor showing the fretting mark (a) and (b) the dimples.....	105
Figure 4.76: Fracture surface of an ACSR Tern conductor showing (a) the fretting mark, (b) the micro crack and (c) the striations mark.....	105

List of tables

Table 2.1: Brief comparison of power line motion according to the frequency, the amplitude vibration and the wind velocity (EPRI, 2006)	13
Table 2.2: EPRI recommendation of endurance limits as functions of the aluminium wire layers (Braga <i>et al.</i> , 2004; EPRI, 2006)	22
Table 2.3: Value of A and b for the CIGRÉ's safe border line (SBL).....	24
Table 2.4: Values of EDS recommend by CIGRÉ for safe design tensions (Zetterholm, 1960)	25
Table 2.5: Summary of the damage on power lines made by CIGRÉ (2005)	26
Table 2.6: Turbulence intensity of wind function of terrain type (CIGRÉ, 2005)	29
Table 2.7: Recommended safe design tension in terms of H/w value function of terrain for single conductor undamped and unarmoured (CIGRÉ, 2005; EPRI, 2006)	30
Table 3.1: Geometrical configuration of different conductors investigated in this study ...	34
Table 3.2: Geometrical and mechanical proprieties of different cables used in this study .	35
Table 3.3: Mechanical properties of aluminium AA 1350-H19 and AA 6201-T81.....	35
Table 3.4: EDS (% UTS) values of each cable for various values of H/w parameterised ..	41
Table 3.5: Calculated values of the Poffenberger-Swart constant (K) and the bending amplitude at 89 mm from the LPC between the suspension clamp and the conductor (Y_b)	41

Nomenclature

σ_a	Dynamic bending stress
β	Angle through which the conductor is bent at the suspension clamp
ε	Dynamic strain in the outer layer wire in the vicinity of the clamp
μ	kinematic viscosity of air
A	Basquin constant
A_a	Area of aluminum wires
AAAC	All Aluminium Alloy Conductor
AAC	All Aluminium Conductor
ACAR	Aluminium Conductor Alloy Reinforced
ACSR	Aluminium Conductor Steel Reinforced
Al	Aluminium
a_n	Amplitude at the node
A_s	Area of steel wires
b	Basquin constant
CIGRÉ	<i>Conseil International des Grands Réseaux Electriques</i> (International Council on Large electric Systems)
C_s	Strouhal number
D	Conductor diameter
d_a	Diameter of aluminium wire

d_s	Diameter of steel wire
E	External
E_a	Young's modulus of aluminum wires
EDS	Every Day Stress
EI	Flexural stiffness
EI_{min}	Minimal flexural stiffness
EPRI	Electric Power Research Institute
E_s	Young's modulus of steel wires
F_{crit}	Limit value for the Chow test
FD	Failure distance
F_{obs}	Value of the Chow test
f_{vs}	frequency of vortex-shedding
H	Horizontal tensile load
I	Internal
IEEE	Institute of Electrical and Electronics Engineers
K	Poffenberger_Swart constant
LPC	Last point of Contact
L_s	Span length
m	Conductor mass per unit length
MFD	Mean failure distance
N	Number of cycles
n_a	Number of aluminium wires

N_f	Number of cycles to failure
n_i	Number of cycles at a specific stress level
n_s	Number of steel wires
p	Descriptive level of Chow test
P_{max}	Maximum power
QP	Quasi planar
Re	Reynolds number
RTS	Rate Tensile Strength
s	Sag
SBL	Safe border line
S_s	Static stress
$S_{s,a}$	Static stress in the aluminium wire
$S_{s,s}$	Static stress in the steel wire
St	Steel
T	Static conductor tension
UTS	Ultimate tensile Strength
V_a	Maximum loop velocity
V_w	Wind velocity
w	Conductor weight per unit length
x	Distance on the conductor from the LPC between the conductor and clamp and the vertical displacement measuring point
Y	Amplitude at the antinode
Y_b	Vertical displacement (Bending amplitude)

y_{max} free-loop amplitude of vibration

ρ_a Density of aluminium wires

ρ_s Density of steel wires

CHAPTER 1

INTRODUCTION

1.1. Motivation and originality

The most common form of damage occurring in overhead conductors is fatigue failure of conductor wires, especially at points where the conductor motion is constrained (at suspension clamps or support locations, for example). While fatigue failures of conductors have occurred in all types of power line conductors, this type of damage results mainly from aeolian vibration.

The power line conductor is essential for much electrical power transmission. As such, the conductor cost is always quite significant in projects and in maintenance of power line transmission. For example, in 2001, approximately 67 million people in Brazil's southern regions, south-east and middle-west were left without electric energy for several hours due to a blackout caused by fatigue damage of power line transmission from aeolian vibration. This blackout, extending for nearly ten hours, was significantly financially detrimental to the Brazilian market system. Unfortunately, there are other detrimental instances of failure sequences on power line transmission globally, such as the one in South Africa five years ago.

Today, as the Brazilian population is growing, there is a visible concomitant surge in demand for electrical energy. The Energy Research Company of Brazil shows a growth of the core network, potentially reaching around 40000 km, in hope of assuaging the electrical energy demands of the population. Without a doubt, this demonstrates that the Brazilian electrical system is booming and will therefore require investments in research and development to maximise the quality and stabilise the reliability of supplied energy. Due to this extension to the Brazilian electricity distribution network, occurrences of conductor failure are likely to increase in number.

One design parameter of power line conductors which influences the fatigue life of a conductor is the *conductor tension*. It has been firmly established that any power line conductor grows increasingly vulnerable to aeolian vibration and thereafter, to fatigue

damage when its tensile load is increased (EPRI, 2006; Fadel, 2012). This load is controlled at the design stage in order to reduce the harmful effects of the aeolian vibration while at the same time, not violating power line clearance. Therefore, the determination of accurate guidance for the safe tension of power line conductors is vitally important for both design and maintenance purposes.

This much needed guidance, initially proposed by the CIGRÉ panel in 1960, is *Every Day Stress* (EDS). The EDS is the safe design parameter of overhead conductors with respect to aeolian vibration (CIGRÉ, 2005). The EDS, expressed as a percentage of the conductor-rated tensile strength (RTS), is defined as the maximum tensile load to which the conductor can be subjected, at the temperature which will occur for the longest period of the time, without any risk of damage due to aeolian vibration.

However, despite the intentions of the EDS parameter, field observations have reported fatigue of power lines after the application of the recommended safe tension proposed by CIGRÉ. As a result of this observation, and after field observations for reaching the goal fixed by the EDS parameter, a second parameter, called H/w or *catenary parameter*, was proposed by CIGRÉ. The H/w parameter is defined as the ratio between the initial horizontal tensile load H prior to any significant wind or ice loading and before creep at the average temperature of the coldest month on the site of the power line.

As mentioned previously, the H/w parameter has been proposed by CIGRÉ as a new design parameter for power line conductors. It has established a value limit of the parameter H/w below which the vibration regime of the conductor does not represent risks of fatigue damage due to aeolian vibration for its structural entirety (CIGRÉ, 2005). This project methodology against conductor fatigue is inherently empirical in origin, and has been applied with increasing frequency for the project of new lines of transmission in Brazil and other countries, in spite of the fact that there is an inadvisably limited quantity of field and laboratory data for its validation as well as explicit criticisms levied by some investigators prominent in this research area (Barrett, 2001).

Moreover, there have been no experimental comparative studies from a conductor fatigue laboratory that ensure the effectiveness of this parameter under the aspect of power line conductor fatigue resistance. Even though the conductor selection for the new transmission lines must apparently be adapted to the parameter H/w as criterion of a project against fatigue due to the aeolian vibration, it is essentially an untested parameter. This research,

then, intends to realise more systematic ways of applying the parameter H/w for various conductor types, studying aspects of mechanical and material characterisation that influence dynamic solicitation and fatigue resistance.

1.2. Overview of studies on conductor fatigue

The first study concerning aeolian vibration of overhead conductors was documented at the beginning of last century, with the first cases of damaged conductor power lines reported by Stockbridge (1925), Varney (1926) and Nefzger (1933). At that point, no criterion or experimental investigation was available to evaluate the fatigue behaviour of conductors related to fatigue properties of materials used in constructing the conductor. Therefore, a fatigue test is clearly necessary for determining fatigue characteristics of conductors, using some measurement of vibration intensity.

Four measurements have been employed as laboratory experimental work: 1) the free-loop amplitude of vibration, y_{\max} ; 2) angle through which the conductor is bent at the suspension clamp, β ; 3) relative bending amplitude of the conductor to the clamp, Y_b ; and 4) the dynamic strain in the outer layer wire in the vicinity of the clamp, ε . Among the four, the relative bending amplitude, Y_b , and the free-loop amplitude, y_{\max} , are nowadays widely used because of their practicability in the laboratory (EPRI, 2006).

The measurement of the differential displacement of the conductor was introduced for the first time by Tebo (1941) and further pursued by Edwards & Boyd (1963) who used the technique with success for about 25 years at Ontario Hydro. This differential displacement, Y_b , was defined as the total displacement peak to peak of the conductor at 3.5 in (89 mm) from the last point of the contact (LPC) between the conductor and the suspension clamp. Poffenberger & Swart (1965) formulated the mathematical relation between the bending amplitude and the bending stress on the outer layer wires of the conductor at the LPC between the conductor and the suspension clamp: good correlation has been found for the conductor deflection measured at 3.5 in (89 mm) from the last point of contact (LPC).

The following year, in 1966, the Institute of Electrical and Electronic Engineers (IEEE) recommended the method of *bending amplitude* as a practical method for assessing the severity of conductor fatigue (IEEE, 1966), suggesting an equation to convert the bending amplitude of the conductor at 3.5 in (89 mm) to the bending stress using the Poffenberger-

Swart formula (Poffenberger and Swart, 1965) and subsequently derived an evaluation criterion for conductor fatigue based on the maximum allowable bending stress or strain (IEEE, 1966).

In order for laboratory test conditions to emulate field conditions, test methodologies have been developed by researchers like Ramey & Silva (1981), Brunair *et al.* (1988), Gopalan (1993), Zhou *et al.* (1995), Henriques (2006) and Fadel *et al.* (2012). Analytical or numerical models, in an attempt to portray the dynamic problem, were then constructed, especially in the work of Papailiou (1995, 1997), Dastous (2005) and Hong *et al.* (2005). Langlois *et al.* (2014) developed a numerical tool for predicting the deformed shape of a conductor near the suspension clamp.

Ramey & Silva (1981) evaluated the reduction effects of the amplitude on the fatigue life of conductors by mechanically reproducing aeolian vibration in the laboratory. The tests started with high amplitude to cause rapid damage, and thereafter the tests were run at low amplitude. From experimental fatigue data on different ACSR conductors, Ramey and Silva concluded that amplitude reduction can significantly extend the fatigue life of conductors.

The work of Ramey & Silva (1981) has been continued by Brunair *et al.* (1988) who used the same approach with an experiment on the ACSR (Aluminium Conductor Steel Reinforced) Drake conductor. Using the same EDS as the ACSR Ibis conductor, they generated an S-N curve of the ACSR Drake and validated the cumulative damage hypothesis formulated by Miner. Furthermore, they confirmed the large variation of fatigue life of conductors.

Heics & Harvard (1994) conducted a study to verify the influence of four vibration recording devices, all of which were commercially available in 1986. Most devices induced a significant influence on the vibration if the antinode amplitudes of the adjacent spans were significantly different.

Zhou *et al.* (1995) developed an experimental apparatus for fretting fatigue testing of conductor wire, observing that larger amplitude fatigue load caused an increase in the slip zone and reduction in the fatigue life of the wire.

In 2002, Cardou presented a review of fatigue on power line conductors and fatigue under spectrum loading. At that time, according to Cardou (2002), the only information available was a paper published by Brunair *et al.* (1988) who made the S-N curves for the first and fifth strand break of the ACSR conductor with a tension equal to 25% of RTS.

Great efforts were undertaken by researchers at the University of Brasilia (UnB) in performing interesting advanced studies regarding fatigue of power line conductors. They started with the construction of the conductor fretting fatigue bench made by Henriques (2006). After designing the new fatigue test rig for power line conductors, fatigue tests were undertaken on the cable to have access to the exploratory S-N curve for the ACSR Grosbeak conductor, and thereafter, the resulting failure analysis. The fatigue tests were run at constant displacements of 0.9 and 1.3 mm with the tensile load of 20% of the RTS by controlling the resonance frequency. It was observed that the S-N curve for Grosbeak was located significantly higher than the CIGRÉ limit. Concerning the failure, it has been noticed that the rupture was initiated by fatigue cracking; shearing followed after for the fatigue test at $Y_b = 0.9$ mm. However, for the 1.3 mm displacement, V-types fracture surfaces have been observed with 45° on more than one wire.

Raj & Parthasarathy (2007) reviewed the existing mathematical models related to conductor damping and friction used to predict the mechanical behaviour under torsion, bending and tension loading, concluding that the Raoof and Huang (RH) model is preferred for the torsion and tensile loading of conductors because of its simplicity. However, they admitted that this aspect has not yet been studied extensively, as revealed by this review.

In 2010, in her thesis at UnB on the fatigue life of the ACSR Ibis conductor, Fadel (2010) analysed the impact on fatigue behaviour of the application of higher stretching loads or every day stress (EDS) for an ACSR conductor. In addition, Fadel (2010) made an experimental validation of the use of the Poffenberger-Swart formula, and thereafter the S-N curves were generated. The fatigue test has been carried out on the ACSR Ibis conductor at 20% and 30% UTS (Ultimate Tensile Strength) to evaluate the effect of high mean stress on the conductor fatigue life. Fadel experimentally observed the reduction of fatigue life by an average of 50% when the conductor tension was increased from 20% to 30% UTS. Furthermore, failure analyses were undertaken and three types of fractures were observed, along with changes in the distribution of broken wire.

Goudreau *et al.* (2010) (Tests I to III) carried out experimental work on the measurement of bending strains for two types of Aluminium Conductor Steel Reinforced (ACSR) conductors (Drake and Bersfort) loaded with 25% rated tensile strength (RTS), which were reported in a series of three papers (Goudreau *et al.*, 2010a, b, c). During measurements, the bending and the traction mode were isolated from the bending and the traction stress to clarify the fretting fatigue of conductors. By controlling the frequency and the bending amplitude during a fatigue test, Goudreau *et al.* (2010) undertook the test on two types of ACSR conductors (Drake and Bersfort) with 25% rated tensile strength (RTS) as tension.

The fatigue strength of power line conductors is often presented using an S-N diagram which involves the bending stress. This must be used accordingly. In relation to this, Goudreau *et al.* (2010) compared conductor fatigue data and found some inherent limits. Goudreau and colleagues used two approaches: P-S (Poffenberger-Swart) σ_a and $\sigma_a(fy_{\max})$. Doubling the conductor tension from 20% to 40% of RTS resulted in $\sigma_a(fy_{\max})$ becoming $\sqrt{2}$ times greater than its initial value. On the other hand, P-S σ_a was found to vary as the square root of the applied tension.

P-S, σ_a and $\sigma_a(fy_{\max})$ do not take into account the geometry of the suspension clamp which has an impact on the stress measurement of the conductor. The third paper by Goudreau *et al.* (2010) reported an improvement in strain measurement. In their work, Goudreau and colleagues observed that the top and the bottom wires do not bend cyclically about their own neutral axis, as it had been assumed by P-S σ_a and the $\sigma_a(fy_{\max})$. The presented model is greatly influenced by the length of the contact circular arc as well as by the rotation of the wire axis.

Zhao *et al.* (2011) investigated the fretting fatigue of aluminium single wires from ACSR conductors by testing them on a fretting fatigue wear machine which they themselves constructed. The tension wires of 5% and 10% of conductor RTS with different angles between wires were used at different excitation amplitudes. Zhao *et al.* (2011) concluded that the fretting fatigue varied in respect of the angle, the amplitude and the tensile force. In 2011, Lévesque *et al.* established a finite element model for the contact between the conductor and the clamp at the LPC. Data from fatigue tests on ACSR conductors (Drake

and Bersfort) at a constant frequency and displacement with 25% UTS tension were used to derive the finite element model.

As recently as 2013, Rolim *et al.* presented strain analysis for a cable by carrying out the test on the conductor built on the spans of 9 m and 12 m using transmission elements such as towers, suspension clamps and isolators. The set-up used in this work was chosen to simulate, as accurately as possible, the Brazilian configuration line. Strain data were collected at last point of contact (LPC) considering five different displacements (i.e. 0.05, 0.1, 0.2, 0.3 and 0.4 mm) at 89 mm from the LPC. Meanwhile, the excitation frequencies of the conductor were 10, 20, 30, 40 and 50 Hz with the tension cable equal to 20% and 30% UTS. It was observed by Rolim *et al.* (2013) that 20 Hz recorded the best agreement between the theoretical and the measured strains. Conversely, at 30 Hz and 40 Hz, there clearly was *not good agreement* between these two sets of values.

Most of the fretting fatigue occurrences, as well as the lives of power line conductors, were analysed using the everyday stress constant (EDS). Since 1960, guidelines have been provided by CIGRÉ (2005) on the safe design tension of the power line conductors subject to aeolian vibration. Though the 18% UTS as an EDS value was proposed for ACSR conductors, many years of investigation revealed that this safe design value actually led to fatigue failure even at the lowest levels of EDS. Thus, difficulty in generalising the fatigue behaviour of power line conductors naturally arose.

So, in order to generalise the fatigue analysis of conductors, CIGRÉ subsequently proposed the use of the H/w , ratio between the tensile load (H) and the conductor weight per meter (w). The parameter fatigue ranking (H/w) chosen by CIGRÉ (2005) presumes the minimum and maximum values between 1000 m and 1400 m respectively after field observations on different lines. According to CIGRÉ, the fatigue failure of conductors could not happen in this range of H/w value; however, not a single experiment was conducted to confirm this range or to determine where within this range the limit could fall. Moreover, no experiments have been conducted regarding rank, or to generalise the fretting fatigue of conductors by using the H/w parameter, or for the determination of fatigue life.

An extensive survey of the literature reveals a serious scarcity of studies concerning H/w as a parameter for conductors. The aim of the present work is therefore an effort to fill this

gap, to investigate fretting fatigue life expectancy related to H/w parameters via experiments on four different types of conductors: AAAC 900 MCM, ACSR Tern, AAC Orchid and ACAR 750 MCM.

1.3. Aim and objectives

This research presents experimental work on the fatigue of power line conductors, with the aim of establishing the accuracy of H/w parameter as a quantitative indicator of the fatigue life of conductors. A series of static and fatigue tests were conducted on four types of the most widely known conductors – 1) the AAAC (All Aluminium Alloy Conductor); 2) the ACSR (Aluminium Conductor Steel Reinforced); 3) the AAC (All Aluminium Conductor); and 4) the ACAR (Aluminium Conductor Alloy Reinforced) – with the objective of supplying necessary information to accurately test and evaluate the application of the parameter H/w for fatigue resistance of overhead conductors. This will contribute two fold to the project design of power: for controlling the conductor tension, and for maintenance assessment of power line conductors. An integral part of comparative study of the fatigue resistance of conductors in terms of the H/w parameter is presented in this work. Furthermore, it will seek to explain the related fatigue behaviour to propose the evaluation of the state of power lines at operation. Additionally, it will aid the maintenance sector in the inspection process against fatigue resulting from aeolian vibration.

1.4. Structure of the thesis

This thesis is structured into five chapters:

Chapter 1 presents the aim and objectives, the motivation and the originality of this work. It also explores issues related to power line fatigue and its impact on economy and population. Thereafter, an overview of the study of conductor fatigue is presented in the final section, highlighting the contributions of this present work. Finally, the aim and objectives of this work are showing out.

Chapter 2 focuses on the power line conductor by presenting the motion of power lines, the problem of fatigue in cables and design methodologies applied to assess the fatigue life of conductor fatigue. Emphases are placed on fretting fatigue of conductors. The safe design parameters of overhead conductors are explored, as well as inconveniences and advantages of each parameter.

Chapter 3 presents the materials used for this work and the experimental methods established to reach the objectives defined above.

Chapter 4 presents the results of the experimental work and related discussions. It divided into three sections, i.e. strain analysis, fatigue test and fatigue analysis.

Chapter 5 summarises the research based on the obtained results and makes suggestions and recommendations for important future work.

CHAPTER 2

FATIGUE OF POWER LINE CONDUCTORS

2.1. Power line motion

Overhead power lines are exposed to nature's dynamic forces of wind, rain, snow or earthquakes. These and other dynamic forces of nature set power line conductors into cyclic motions, including aeolian vibration, conductor galloping and wake-induced vibration. Wind-induced conductor vibration can cause damage and failure on overhead conductors, dampers, insulators, and several overhead line fittings (Loredo-Souza *et al.*, 1998; Kiessling *et al.*, 2003; EPRI, 2006)

2.1.1. Wind excitation of power line conductors

Aeolian vibration results from vortex-shedding associated with wind blowing through conductors. Various flow regimes can be determined by the Reynolds number (Re), calculated by Equation 2.1:

$$Re = \frac{vD}{\nu} \quad (2.1)$$

in which v (m/s), D (m) and ν (Ns/m²) are, respectively, the wind velocity, the conductor diameter and the kinematic viscosity of air. Figure 2.1 shows the various flow regimes related to the Reynolds number:

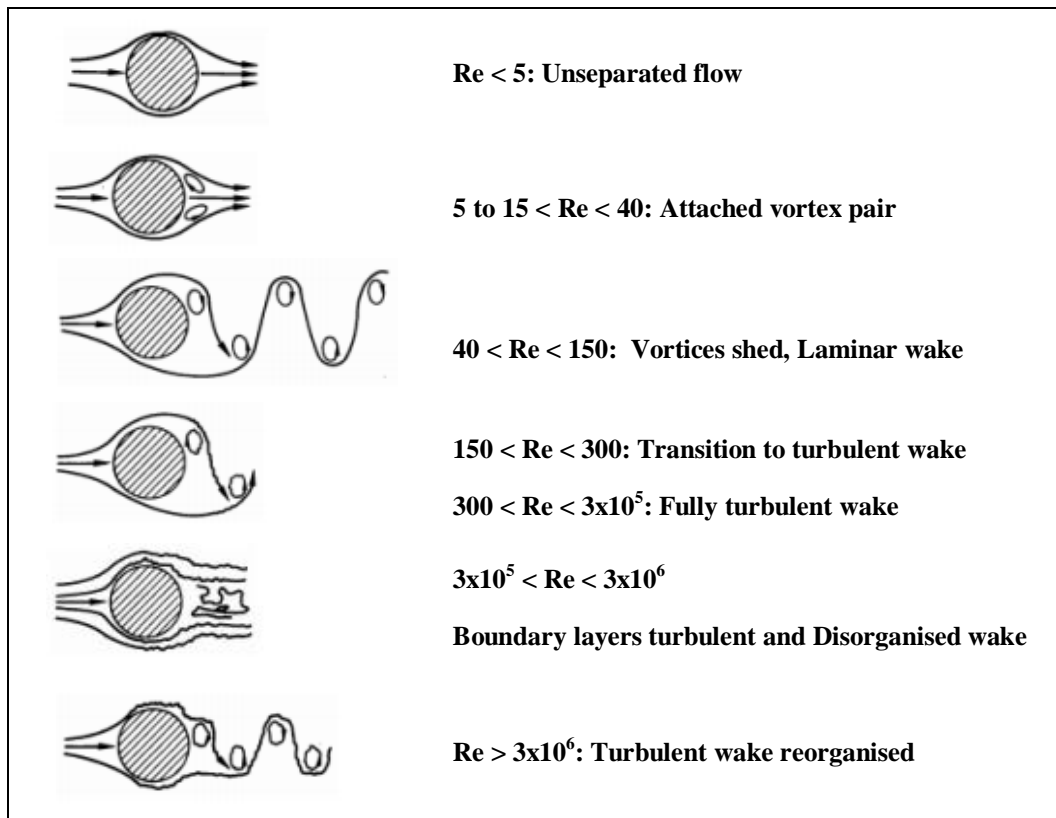


Figure 2.1: Schematic representation of various flow regimes depending on Reynolds number (Lienhard, 1966; Vecchiarelli, 1997)

As mentioned, vortex-shedding is responsible for aeolian vibration. The pressure fluctuation from vortex-shedding generates an oscillation force, making the conductor to fluctuate up and down (Figure 2.2).

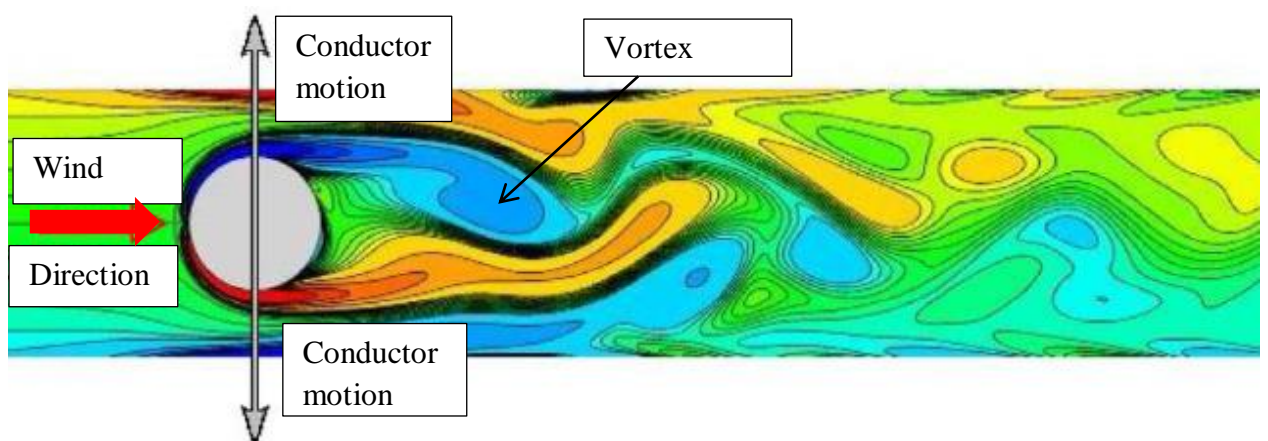


Figure 2.2: Vortex shedding-induced aeolian vibration of power line conductor (Giosan, 2013)

The frequency of vortex-shedding (f_{vs} , Hz) can be calculated using the following expression (Equation 2.2):

$$f_{vs} = \frac{C_s V_w}{D} \quad (2.2)$$

where C_s is the Strouhal number; V_w (m/s) is the wind velocity; and D (mm) is the conductor diameter.

The Strouhal number C_s is considered to be in the range of 0.18 up to 0.22 (EPRI, 2006) as aeolian vibration occurs around this value of the Strouhal number for the power line conductor. The IEEE 664 standard (2007) used the Strouhal number $C_s = 0.185$ to describe wind induced frequency for various cases of power line conductors.

2.1.2. Aeolian vibration

As early as the 1920s, it has been observed that power lines vibrate because of winds with a velocity ranging between 1 m/s and 7 m/s (EPRI, 2006). The major cause of fatigue failure of cable strands is aeolian vibration. The vibration frequency of the conductor during aeolian vibration depends on the tensile load and the conductor frequency ranging between 3 and 150 Hz. During aeolian vibration, the conductor can reach an amplitude which equates with the conductor's diameter.

Other types of conductor motion (i.e galloping and wake-induced vibrations) may also cause fatigue of a conductor strand. However, this is not the main problem associated with those motions. Table 2.1 shows a brief comparison between three types of conductor motion, referring to the frequency range as well as the amplitude of vibration as a function of the conductor diameter (EPRI, 2006). Wind velocity (i.e. weather conditions) is also presented in the table.

Table 2.1: Brief comparison of power line motion according to the frequency, the amplitude vibration and the wind velocity (EPRI, 2006)

	Aeolian vibration	Galloping vibration	Wake-induced vibration
Type of power line affected	All	All	All
Approximate amplitude range function of conductor diameter (D)	0.01 to 1xD	5 to 300xD	0.5 to 80xD
Approximate range of frequency	3 to 150 Hz	0.08 to 3 Hz	0.15 to 10 Hz
Wind velocity	1 to 7 m/s	7 to 18 m/s	4 to 18 m/s

In Brazil, the most predominant climates are equatorial and tropical, with snow occurring only occasionally, especially in the southern part of the country. Brazilian transmission power lines are therefore affected by motions of wind or ice. In fact, wind velocities higher than 7 m/s are observed in Brazil however this can cause damage on the powerline transmission. Figure 2.3 shows the average speed of wind in this country. However, on the basis of the classification of power line motions (Table 2.1) and wind velocity distribution data in Brazil (Figure 2.3), a higher incidence of wind motion for transmission lines can be expected. According to Fuchs *et al.* (1992), this power line motion is caused by moderate winds with constant speeds between 0.5 and 9.7 m/s occurring at very large spans in the region where the transmission power line crosses a large river, valley or level ground without high trees or plantation. After many years in operation, the power line conductor could failure by fatigue. This kind of fatigue is characterised as a fretting fatigue.

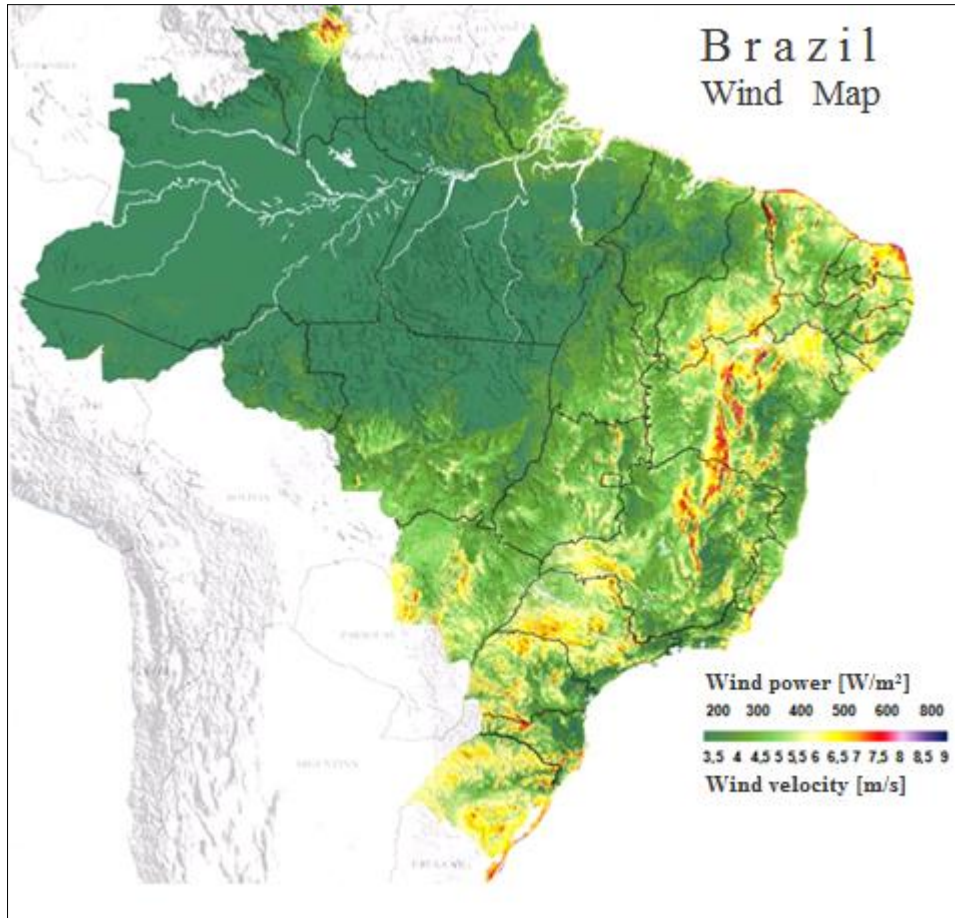


Figure 2.3: Distribution of the wind velocity and power in Brazil (CEPEL, 2015)

2.2. Fretting fatigue

The nature of fretting fatigue is a complex phenomenon, so much so that the terms used to describe this phenomenon are not yet standardised. There is not yet even a unified definition of *fretting*. As numerous terms can be found in the literature whose commonality is fretting – fretting fatigue, fretting wear, fretting corrosion, impact-slide fretting – the general term *fretting* loosely covers all related aspects of this phenomenon (Smith, 1998). Despite the definition multiformity, the fundamental characteristics of *fretting* are as follows (Hills & Nowell, 1994):

- induced by the small relative movement between two mechanical components; and
- occurring most frequently when two or more tight fitting surfaces undergo a small relative movement produced by oscillating forces.

The history of fretting fatigue can be traced back to 1911 with Eden *et al.* (1911) who initiated a study on fretting. Some years later, Tomlinson (1927) investigated fretting wear processes. However, the first review of fretting was by Campbell (1969). Following Campbell's publication, several review papers were published summarising *fretting* as knowledge status at various periods (Waterhouse *et al.*, 1969, 1984, 1992). As an illustration of the importance of fretting research, several international symposia have been organised over the past 30 years by the American Society for Testing and Materials (ASTM) (Waterhouse *et al.*, 1981, 1984; Hoepfner *et al.*, 1994, 1996).

Fretting is a complex phenomenon as it involves a variety of aspects such as tribology, mechanics of contact and the science of material. Figure 2.4 shows the schematic configuration of mechanical contact between two cylinders subjected to two loads (P radial load and Q axial cyclic load) with the ellipse marks demonstrating consequences of fretting.

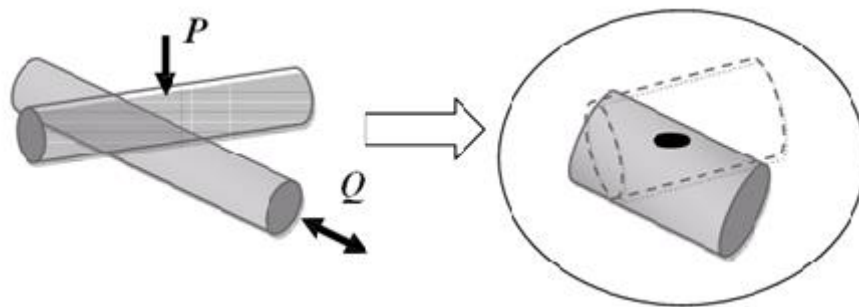


Figure 2.4: Representation of mechanical contact between two cylinders subjected to two loads and the elliptical fretting marks

Referring to the power line conductor and depending on the loading conditions, there are three different modes of contact which lead to fatigue by fretting:

- the small relative movement at the conductor area between the suspension clamp and the outer layer wires of the conductor;
- the contact between aluminium wire from the inner layer of the conductor; and
- the contact between the aluminium wire and the steel wire from different layers of the conductor, in the case of Aluminium Steel Conductor Reinforced (ASCR).

The wear between surfaces leads to dust accumulation in all three modes of contact. In contact with the air, the dust particles oxidize and turn black as aluminium oxide (Al_2O_3) is formed. Al_2O_3 is the hard material associated with the fretting phenomenon which accelerates the fatigue of the cable (Figure 2.6).

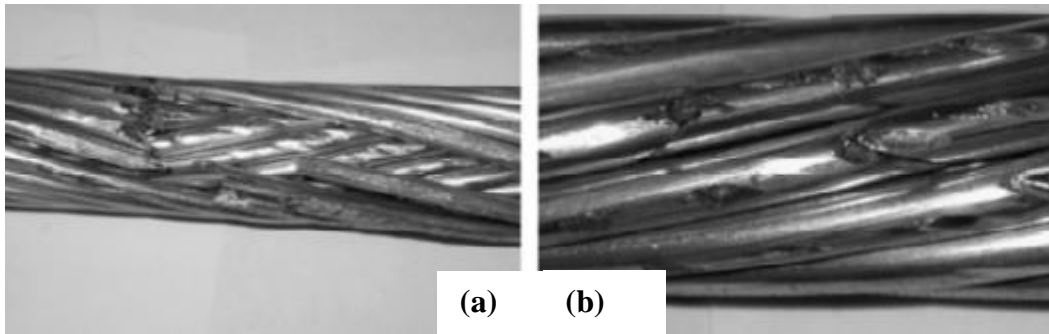


Figure 2.5: Fretting fatigue of conductor: (a) intense surface wear, fracture of some aluminium wires in the outer layer of the ACSR conductor; and (b) elliptical fretting marks and wire break of the inner layer of the ACSR conductor (Azevedo *et al.*, 2009)

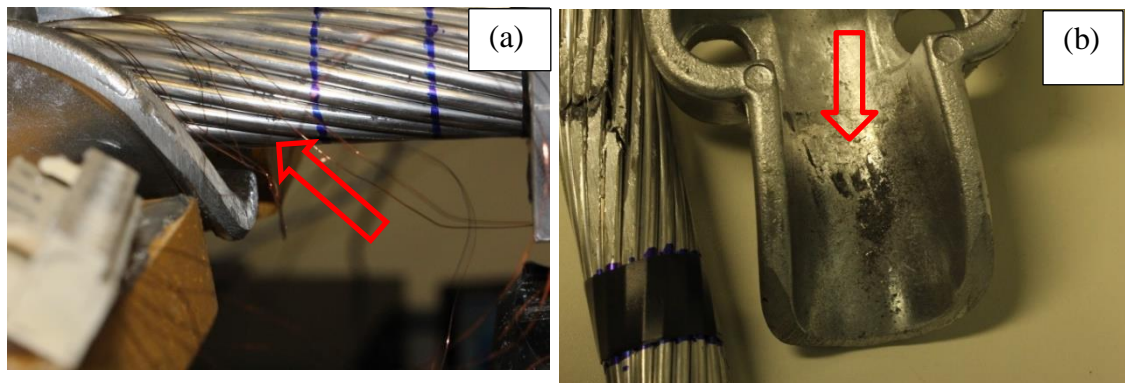


Figure 2.6: Powder (aluminium oxide) coming out of the AAC Orchid conductor: (a) during the fatigue test; and (b) after testing

2.3. Mechanism of conductor fatigue

The main cause of fatigue failure of strands in overhead conductors is the aeolian vibration, a fatigue which generally occurs at points where conductor motion is constrained against transverse vibration such as suspension clamps. Overhead conductors consist of concentric layers of helically-laid wires. When the conductor is tightened, the tensions of

the conductor wires of each layer cause them to permeate the layer with a certain amount of pressure. The restriction of movement and the pressure between layers restricts the wires constituting the cable from slipping, which then causes fretting between the wires, and thereafter generates cable contact with the suspension clamp, for example. Within the suspension clamp, the conductor establishes a series of contacts, either between wires or between the wires and the suspension clamp in the outermost layer of the cable. Figure 2.7 shows a cross sectional view of the ASCR conductor with various localised contact points.

Generally in the cable, depending on the loading conditions, three different contact modes lead to fatigue fretting:

- the contact between suspension clamp and wires from the outermost layer of the cable (point A below);
- the contact between two aluminium wires (points B and C below); and
- the contact between the aluminium wire and steel wire (point D below).

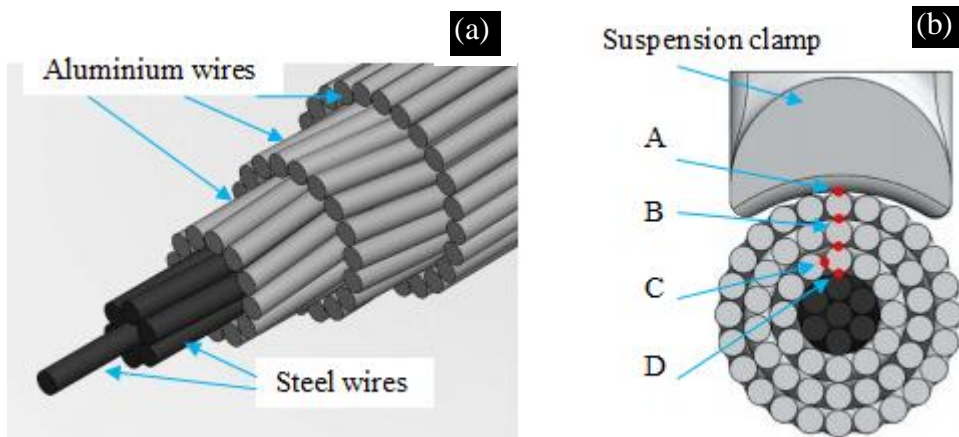


Figure 2.7: (a) Cross section of an ASCR conductor; and (b) critical contacts region of the conductor in the suspension clamp

These three region types are critical areas of the conductor fretting fatigue process. These contact points, once the fretting-induced crack is formed, can propagate fatigue leading to wire break, or in extreme cases, the complete breakdown of the conductor. The failure most frequently occurs at cable attachment points such as suspension clamps, dampers, spacers and other power line hardware (Dulhunty, 1971; CIGRÉ, 1985).

2.4. Poffenberger-Swart (P-S) equation

In 1966, the Institute of Electrical and Electronics Engineers (IEEE) Transmission and Distribution Committee standardised the method of conductor vibration measurement (IEEE, 1966) primarily recommended in the evaluation of overhead conductor fatigue risk due to the aeolian vibration. This standard, called the ‘bending amplitude method’, is recommended by many organisations related to power line transmission, such as CIGRÉ (*Conseil International des Grands Réseaux Electriques*) and IEC (International Electrotechnical Commission). The IEEE standard defines the location for measuring the bending amplitude at 89 mm (3.5 in) on the conductor from the last point of contact (LPC) between the conductor and the suspension clamp, as primary measured parameters for the aeolian vibration of the conductor on the field, as well as in the fatigue laboratory of conductors. The use of 89 mm (3.5 in) was initially proposed by Tebo (1941) with the objective of being close to the suspension clamp where the aeolian vibration shape of the conductor is governed only by the conductor stiffness effect. Since the standardisation, many researchers, such as Josiki *et al.* (1976) and Cloutier *et al.* (1999), have relied on bending amplitude as the measurement of conductor vibration.

Most fatigue failures in strands of conductor occur at inner-layer wires and wires to suspension clamp contact points (Fricke & Rawlins, 1968; EPRI, 2006). Because of difficulty of accurate measurement of mechanical strain or stress at these points, the reliance on some assumptions is vital. Poffenberger & Swart (1965) presented a mathematical model for calculating the bending strain at the conductor surface from bending amplitude of the conductor in the field or laboratory. This mathematical model considers the portion of the cable near the suspension clamp as an Euler beam (Figure 2.8).

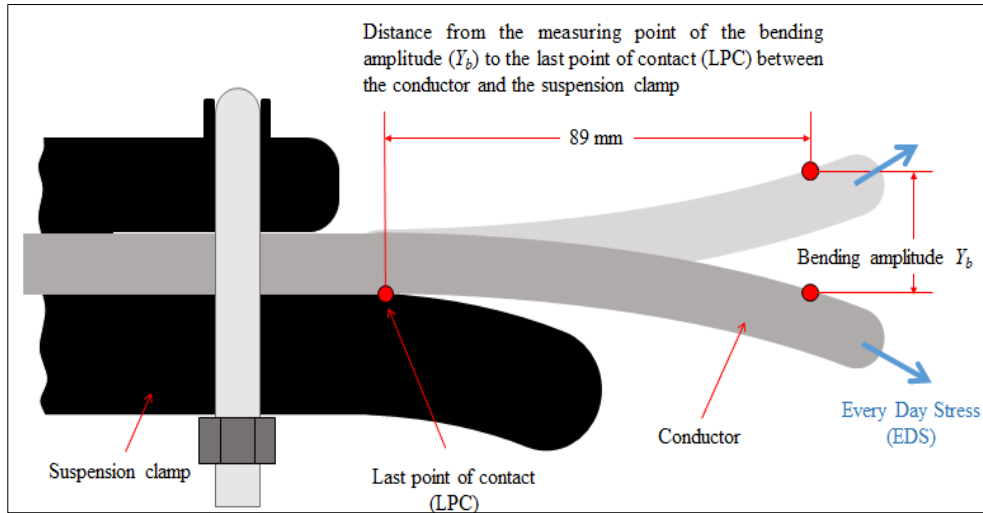


Figure 2.8: Schematic montage of conductor and the suspension clamp showing the standard position to measure the bending amplitude Y_b

Thus, the vertical displacement, measured peak to peak at 89 mm (3.5 in), can be converted to the bending strain in the outer layer of the aluminium wire conductor using Equation 2.3. More specifically, the Poffenberger-Swart Equation (1965) can be written as follows:

$$\sigma_a = KY_b \quad (2.3)$$

where σ_a (MPa) is the dynamic bending stress amplitude (zero to peak); Y_b (mm) is the conductor's vertical displacement range (peak to peak) measured at 89 mm from the last point of contact (LPC) between conductor and clamp; and

$$K = \frac{E_a d p^2}{4(e^{-px} - 1 + px)} \left[N / mm^3 \right] \quad (2.4)$$

where E_a (MPa) and d (mm) are the Young's modulus and the diameter of wire in the outer layer, respectively; x is the distance on the conductor from the LPC between conductor and clamp and the vertical displacement measuring point (usually = 89 mm) (see Figure 2.8); and:

$$p = \sqrt{\frac{T}{EI}} \quad (2.5)$$

where T (N) is the static conductor tension at average ambient temperature during test period; and EI (N.mm²) is the flexural stiffness of the conductor, whose minimum value is as follows:

$$EI_{\min} = n_a E_a \frac{\pi d_a^4}{64} + n_s E_s \frac{\pi d_s^4}{64} \quad (2.6)$$

where n_a, E_a, d_a are the number, individual diameter and Young's modulus of the aluminium wires; and n_s, E_s, d_s are the respective values for the steel wires. In this approach, the conductor is considered a bundle of individual wires free to move relative to each other; the flexural stiffness takes its minimum value EI_{\min} . For smaller bending amplitudes, the individual wires would stick together; thus the conductor would behave as a solid rod, increasing the flexural stiffness to its maximum. Formulae that consider the stick-slip theory to compute EI and hence the dynamic bending stress were proposed by Papailiou (1995, 1997).

2.5. Endurance limits of power line conductor

The *endurance limit* of a conductor has significant importance in the design of new lines and the monitoring of the power lines in operation. It is, in fact, one of the most important parameters of conductor vibration levels to a value, or set of values, below which the conductor could operate normally with an infinite lifespan, without risk of fatigue induced damage. The average lifespan, though, is estimated by CIGRÉ (1985) as approximately 30 years in terms of technical and economic satisfaction. Two approaches are used in the determination of the limits of fatigue tolerance for conductors: the endurance limit approach and the cumulative damage approach

2.5.1. Endurance limit approach for conductors

The *endurance limit approach*, recommended by IEEE (1996) and EPRI (2006), assumes that the conductor will have an infinite lifespan when its vibration levels are maintained under certain limits.

The IEEE began recommending this approach following the conductor vibration study over the subsequent decades; its standard is widespread in the overhead power line technique. The methodology is based on the measurement of the conductor bending amplitude near the suspension clamp, preferably at 89 mm from LPC. This bending amplitude is related to the bending stress of the conductor near the suspension clamp. Following a previous study, the IEEE adopted the limit of the bending strain as 150 microstrains peak to peak on the conductor at the LPC. At the time this limit was established, it had been observed that an ACSR (Aluminium Conductor Steel Reinforced) conductor 750 MCM (54/7), already operating for almost 30 years with a conventional suspension clamp, had not been affected by fatigue damage. Therefore, the 150 microstrain limit considered by the IEEE is very conservative and could be used for orientation purposes. Thus the value of 200 microstrains has been regarded as valid for meeting the criteria of limit endurance of conductors, even though it is also quite conservative (IEEE 1996).

The EPRI analysis for this approach looks similar to the one made by the IEEE, confirming the standards established by the IEEE (i.e. the measurement of the bending amplitude at 89 mm and the importance of the outermost layer in the calculation of the conductor stress). Thus, the EPRI presented the Poffenberger-Swart formula, relating the bending amplitude and the stress (strain) of the cable (section 2.4). After various fatigue tests undertaken on different ACSR conductors, the EPRI concluded that the number of wires does not influence the fatigue life of conductors. Furthermore, tests revealed that conductors with one aluminium layer are more resistant to fatigue than those with more than one aluminium layer. The EPRI recommended the following endurance limits based on the experimental results in function of the number of aluminium wire layers (Table 2.2).

Table 2.2: EPRI recommendation of endurance limits as functions of the aluminium wire layers (Braga *et al.*, 2004; EPRI, 2006)

Number of aluminium wire layers	Endurance limit (MPa)
1	22.5
> 1	8.5

2.5.2. Damage cumulative approach for conductor

The *damage cumulative approach* has been recommended by CIGRÉ (1979, 1988) for applying the S-N curves as an endurance limit. This approach is based on Miner's theory (Miner, 1945) and on the accumulation damage method. CIGRÉ proposes the S-N graph called 'Safe Border Line' (SBL) obtained from a compilation of multiple fatigue test results on conductors in several laboratories globally. The SBL is a more conservative S-N curve estimated from fatigue life of AAAC and AAC conductors. Figure 2.9 shows the basic S-N curve of different conductors compiled by CIGRÉ, as well as the SBL curve.

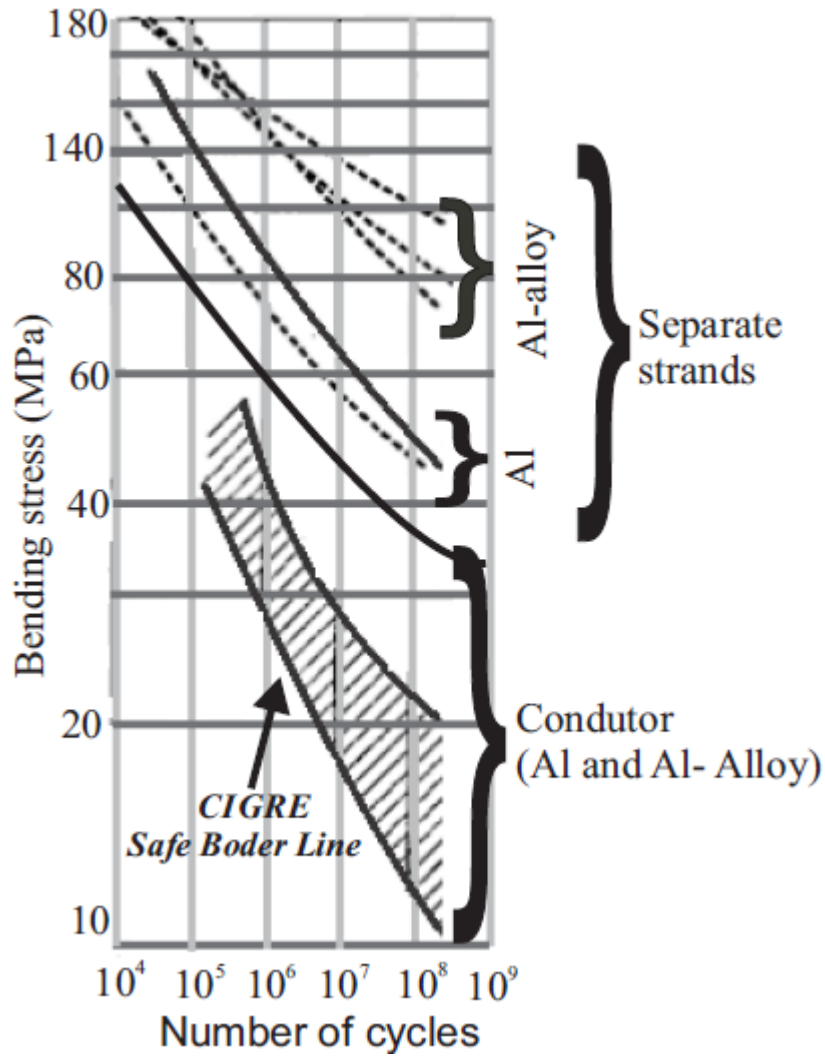


Figure 2.9: S-N curves compiled by CIGRÉ and the CIGRÉ Safe Border Line, SBL (CIGRÉ, 1979)

The SBL can be approximated by this exponential equation (2.7):

$$\sigma_a = AN^b \quad (2.7)$$

where σ_a is the bending stress; N is the fatigue (number of cycles to failure); and A and b are Basquin constants, determined according to the fatigue life (Table 2.3).

Table 2.3: Value of A and b for the CIGRÉ’s safe border line (SBL)

Number of aluminium wire layers on the conductor	$N < 2 \times 10^7$		$N > 2 \times 10^7$	
	A	b	A	b
1	730	-0.2	430	-0.168
>1	450	-0.2	263	-0.168

2.6. Safe design parameter of overhead conductor

The design of overhead power lines has been guided by the control of the conductor *tension*. Many reasons have justified this option: among them is the objective of ensuring that the maximum tension of the conductor corresponding to the assumed most severe climatic loading does not exceed a predefined load, to allow the conductor susceptibility against the detrimental effects of aeolian vibration. Another reason is related to the maximum temperature operation of the conductor which could allow the conductor to work in respect to the conduct clearance. It is well known that when the tension of the overhead conductor increases, the conductor becomes increasingly vulnerable to aeolian vibration. Therefore, some organisations related to the power line conductor have deemed it necessary to establish an upper limit for conductor tension that can prevail for a significant period of time. The EDS (Every Day Stress) panel was created by CIGRÉ to investigate the safe parameter design of power line conductors. Many parameters have been proposed for the purpose of safe design of overhead conductors, but two – Every Day Stress and the catenary parameter H/w – are the most prevalent in the literature.

2.6.1. Every Day Stress (EDS)

Every Day Stress (EDS) is the safe design parameter of overhead conductors, with respect to aeolian vibration, initially proposed by CIGRÉ in 1960 (CIGRÉ, 2005). The EDS, expressed as a percentage of the conductor rated tensile stress (RTS), is defined as the maximum tensile load to which the conductor can be subjected, at the temperature which will occur for the longest period of the time without any risk of damage due to aeolian

vibrations. CIGRÉ recommends different values of EDS for overhead conductors and for conductors with dampers only, armour rods only, as well as for conductors with both dampers and armour rods (Table 2.4).

Table 2.4: Values of EDS recommend by CIGRÉ for safe design tensions (Zetterholm, 1960)

	Unprotected lines	Dampers	Armour rods	Armour rods and dampers
Copper conductors	26			
ACSR	18	24	22	24
Aluminium conductors	17			
Aldrey conductors	18	26		

Observations from the field, though, have reported fatigue of power lines after the application of the recommended EDS values by CIGRÉ. Consequently, the EDS parameter appears to be insufficient for explaining the recent damage found on lines. Table 2.5 summarises the investigation results from the EDS panel in situ on the damage of power line conductors. It has been observed by the EDS panel that lines are damaged, even they were designed with EDS less than 18%. Clearly, the requirement for a new parameter is evident.

Table 2.5: Summary of the damage on power lines made by CIGRÉ (2005)

Service life (years)	% of lines damaged	
	$EDS < 18\%$	$EDS \geq 18.5\%$
≤ 5	5.26	25
$< 5 \geq 10$	20.93	35.29
$< 10 \geq 20$	45	78
> 20	58.93	91.67

2.6.2. H/w parameter

The H/w parameter, also called the *catenary parameter*, another parameter adopted by CIGRÉ, is defined as the ratio between the initial horizontal tensile load (H) and the conductor weight (w) per unit length. The tensile load (H) is the initial horizontal tension before any significant wind and ice loading and before creep at the average temperature of the coldest month at the site of the power line (CIGRÉ, 2005; EPRI, 2006).

Compared to the EDS, the H/w presents several advantages, as it affects several parameters involved in the fatigue characteristic of conductors. A few of these are presented below.

First, the H/w takes into account the conductor diameter which influences the energy induced by the wind and the frequency vortex. The maximum power, P_{\max} , that can be transmitted by the conductor is given by the following expression:

$$P_{\max} = \frac{1}{2} \sqrt{\frac{H}{w}} m V_w \quad (2.8)$$

where V_w is the wind velocity and m is the conductor mass per unit length.

Secondly, the H/w takes into account the ratio between aluminium and steel of a conductor expressed as a ratio of the areas (A_a, A_s), static stress ($S_{a,a}, S_{a,s}$) and density (ρ_a, ρ_s) of the aluminium and steel wires respectively, as follows:

$$\frac{H}{w} = \frac{A_a S_{s,a} + A_s S_{s,s}}{g(A_a \rho_a + A_s \rho_s)} \quad (2.9)$$

where g is the gravitational acceleration.

This allows for making the following approximations that the ratio between the aluminium and steel Young's modulus (E_a and E_s) is almost equal to 3 (Equation 2.10) and the ratio between the steel and the aluminium density (ρ_a and ρ_s) is also equal to 3 (Equation 2.11):

$$E_a \cong 3E_s \quad (2.10)$$

and

$$3\rho_a \cong \rho_s \quad (2.11)$$

Using Hooke's law in Equation 2.10 and by assuming the same deformation in aluminium and in steel:

$$\frac{S_{s,s}}{E_s} = \frac{S_{s,a}}{E_a} \quad (2.12)$$

$$S_{s,s} \cong 3S_{s,a} \quad (2.13)$$

Equation 2.14 results from the substitution of Equations 2.11 and 2.13, in Equation 2.9:

$$S_{s,a} \cong k \frac{H}{w} \quad (2.14)$$

Where

$$k = g\rho_a \quad (2.15)$$

It can be observed that the static stress (S_s) in the aluminium wires can be approximated by a constant function, directly proportional to the H/w parameters independent of the amount of steel in the conductor. Therefore, the H/w parameter takes into account the ratio of aluminium steel in the conductor. The static tensile stress is also taken into account by the parameter H/w as the tensile stress influences the life of a conductor, as proven by Fadel *et al.* (2012).

The self-damping of the conductor is a function of the tension (H), the loop length, the frequency of the vibration and the node velocity. The conductor self-damping can be a major source of energy dissipation during the aeolian vibration but by increasing the tension in the conductor (H), strand slipping is reduced, resulting in a decrease of the self-damping of the conductor, and thereafter, the reduction of the fatigue life of conductor.

$$P_n = \sqrt{\frac{H}{m}} m \frac{V_a^2}{2} \left(\frac{a_n}{Y} \right) \quad (2.15)$$

Finally, the H/w parameter also takes into account the sag of conductor, as it is the catenary constant. It has been proven theoretically that all conductors will have the same sag for a constant H/w (Barrett *et al.*, 2001). The expression of the sag (s) for the span length (L_s) using the catenary formula is given by the following Equation 2.16:

$$s = \frac{H}{w} \left(\cosh \frac{w \frac{L_s}{2}}{H} - 1 \right) \quad (2.16)$$

The H/w parameter is clearly more advantageous than EDS. Apart from taking into account the several parameters involved in the fatigue of conductors, the H/w parameter has the further advantage of being easy to use.

As mentioned previously, the aeolian vibration is a harmful phenomenon of power line transmission as it is the main cause of conductor fatigue. Wind power reaches its maximum vibration displacement when the Strouhal frequency becomes almost equal to the natural frequency of the conductor (Rawlins, 1983). Turbulence due to aeolian vibration arises from the interaction between wind and the conductor. The local terrain and the nature of the ground strongly influence turbulence intensity. On the basis of wind turbulence to which intensity values are attributed, the CIGRÉ has proposed the classification of terrains presented in Table 2.6.

Table 2.6: Turbulence intensity of wind function of terrain type (CIGRÉ, 2005)

Terrain	Turbulence Intensity
Open sea; large stretches of open water	0.11
Rural areas; open country with few, low obstacles	0.18
Low density built-up areas; small towns; suburbs; open woodland with small trees	0.25
Town and city centres with a high density of buildings; broken country with tall trees	0.35

The CIGRÉ recommends a maximum safe design tension value of H/w in relation to aeolian vibration of undamped and unarmoured conductors. Table 2.7 shows the safe design tension value of H/w , and the function of the terrain characteristics at the average temperature of the coldest month on site of the line. The CIGRÉ classifies terrains in four categories and recommends the application of category 1 if there is any doubt on the terrain.

Table 2.7: Recommended safe design tension in terms of H/w value function of terrain for single conductor undamped and unarmoured (CIGRÉ, 2005; EPRI, 2006)

Terrain Category	Terrain Characteristics	H/w (m)
1	Open, flat, no stress, no obstruction, with snow cover, or near/across large bodies of water, flat desert	1000
2	Open, flat, no obstruction, no snow (e.g. farmland without any obstruction), summer time	1125
3	Open, flat, or undulating with very few obstacles (e.g. open grass or farmland with few trees, hedgerows and other barriers), prairie or tundra	1225
4	Built-up with some trees and building (e.g. residential suburbs), small towns, woodlands and shrubs, small fields with bushes, trees and hedges	1425

However, all the lines are not undamped and unarmoured, and span lengths are not always equivalent. Therefore, two parameters have been suggested by CIGRÉ to provide guidance for the safe design tension with respect to aeolian vibration: 1) the H/w and 2) $L_s D/m$, with L_s , D and m being the span length, the conductor diameter and the conductor mass per unit length, respectively. Figure 2.10 shows the safe design tension (H/w vs LD/m) for the four terrain categories.

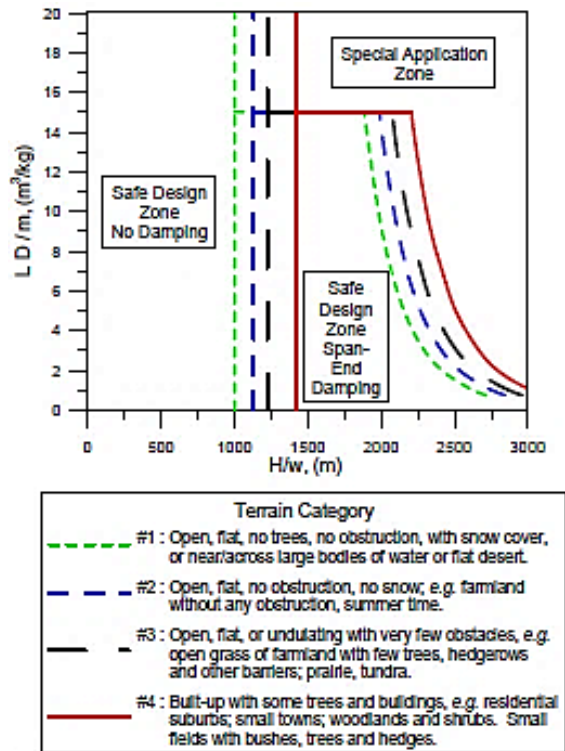


Figure 2.10: Recommended safe design tension in terms of H/w vs $L_s D/m$ (L_s , D and m are, respectively, the span length, conductor diameter and the conductor mass per unit) (CIGRÉ, 2005)

The graph of Figure 2.10 has been divided in three zones:

No damping zone: for this zone, where the H/w is less than 1000 m, the line will be safe without the damper to dissipate the aeolian vibration for terrain category 1. Theoretically this means that the conductor will have an infinite life for all types of span lengths. The values of H/w recommended by CIGRÉ in this region are 1125, 1225 and 1425 for the terrain categories 2, 3 and 4 respectively. The no damping zone is defined by the H/w value only.

Span end damping zone: the need for the production of conductors against aeolian vibration is undeniable. Usually the protection is made by means of a Stockbridge damper set at the end of the span.

Special application zone: aeolian vibration may or may not be a design constraint for any parameters (H/w and $L_s D/m$) falling in this zone. For this zone, the CIGRÉ

recommends the availability of adequate protection of the transmission line before launching.

CHAPTER 3

MATERIALS AND EXPERIMENTAL METHODS

3.1. Materials

3.1.1. Conductors

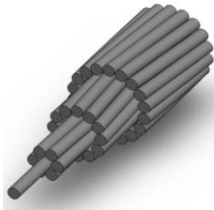
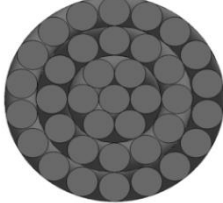

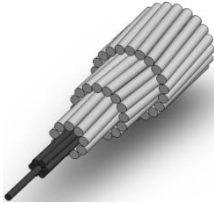
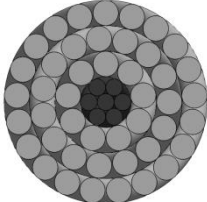


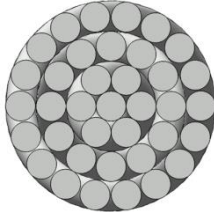

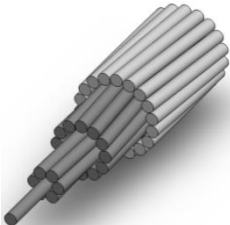
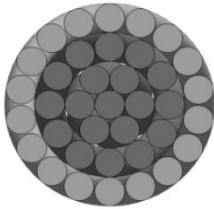

The following four types of conductors were selected for the series of tests required for this research with the objective of covering the large types of conductor used in power line transmission:

- All Aluminium Alloy Conductor (AAAC)
- Aluminium Conductor Steel Reinforced Conductor (ACSR)
- All Aluminium Conductor (AAC)
- Aluminium Conductor Alloy Reinforced (ACAR)

The AAAC 900 MCM, ACSR Tern, AAC Orchid and ACAR 750 MCM conductors were chosen for experimentation. The AAAC 900 MCM conductor has a nominal diameter of 27.74 mm and consists of one aluminium core surrounded by four layers of aluminium wires. All wires have a diameter of 3.962 mm and are made of 6201-T81 aluminium alloy (AA 6201-T81). The Tern (ACSR conductor), the second conductor chosen, has a core conductor in steel surrounded by four layers, of which one consists of steel wires. The nominal diameter of ACSR Tern conductor is 27.03 mm with all steel wires having a diameter of 2.25 mm. The rest of the wires are in 1350-H19 aluminium (AA 1350-H19), each with a diameter of 3.38 mm. All the wires of the AAC Orchid, the third conductor in this work, are made of AA 1350-H19 aluminium, each with a diameter of 3.33 mm. This AAC conductor has 23.30 mm of nominal diameter. The last conductor is the ACAR 750 MCM 18/19 conductor which has the outer layer (18 wires) in pure aluminium (AA 1350-H19) and the inner layer (19 wires) in aluminium alloy (AA 6201-T81). The ACAR 750 MCM conductor has a nominal diameter of 25.32 mm and each wire has a diameter of 3.617 mm. Table 3.1 shows the geometrical configuration of each conductor described above, as well as the cross sectional view of each conductor investigated. The geometrical

and mechanical proprieties are presented in Table 3.2. The mechanical properties of the AA 1350-H19 and the AA 6201-T81 are gathered in Table 3.3.

Table 3.1: Geometrical configuration of different conductors investigated in this study

Conductor	Drawing	Drawing of cross section	Picture of cross section
AAAC 900 MCM			
ACSR Tern			
AAC Orchid			
ACAR 750 MCM			

Aluminium Alloy
 Aluminium
 Steel

Table 3.2: Geometrical and mechanical proprieties of different cables used in this study

Conductor		AAAC 900 MCM	ACSR Tern	AAC Orchid	ACAR 750 MCM
Diameter (mm)		27.74	27.03	23.3	25.32
Number of wires on each layer	<i>Aluminium</i>	18-12-6-1	21-15-9	18-12-6-1	18-12-6-1
	<i>Steel</i>	-	6-1	-	-
Diameter of wires (mm)	<i>Aluminium</i>	3.962	3.38	3.33	3.617
	<i>Steel</i>	-	2.25	-	-
Linear mass (kg/m)		1.252	1.339	0.889	1.046
Rated tensile strength, RTS (kgf)		13421	10010	5143	8635

Table 3.3: Mechanical properties of aluminium AA 1350-H19 and AA 6201-T81

All alloy	Young's modulus (GPa)	Limit of Resistance			Hardness (HBn)	Strain Deformation at rupture (%)
		Yield strength	Ultimate strength	Fatigue strength		
		σ_{rt} (MPa)	σ_y (MPa)	σ_e (MPa)		
AA 1350 H19	68.9	165	186	48.3*	50	≥ 1.7
AA 6201T81	69	310	330	105*	88	6

*at 50 megacycles

3.1.2. Suspension clamps

Suspension clamps are used to connect the conductor to a suspension tower. In this work, the mono articulated suspension clamp is used. This suspension clamp has a weight of 1.28 kg, and a conductor diameter range between 14 and 29 mm.

The suspension clamps are made of high mechanical strength aluminium alloy, with a smooth even surface, showing no sharp edges, and the mouth output having a maximum angle of 20°, thus avoiding damage to the cables. Figure 3.1(a) shows a technical drawing of the geometry of the mono articulated suspension clamp and its specifications. Figure 3.1(b) and Figure 3.1(c) illustrate respectively the assembling process and the dimensions of the suspension clamp.

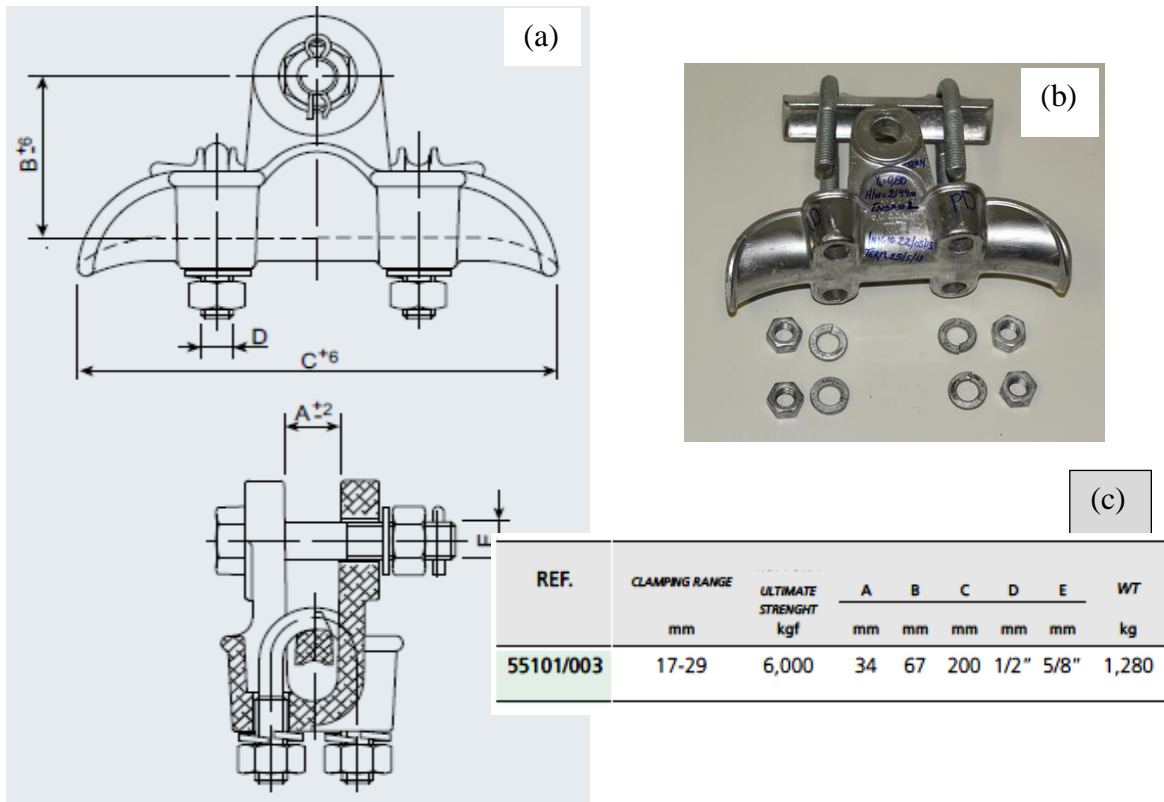


Figure 3.1: (a) Drawing; (b) assembly of suspension clamp; and (c) dimensions of suspension clamp (Aida, 2010)

3.1.3. Apparatus and sensors

The four main apparatus and sensors used in this work are the electrodynamic shaker, the load cells, the accelerometer and the laser. The lines below present the apparatus and sensors for one of the three conductor fretting fatigue benches in the laboratory (*Grupo de Fadiga, Fratura e Materiais; GFFM*) at University of Brasília.

A Data Physic Electrodynamic Shaker was used. In principle, the electrodynamic shaker operates like a speaker where the armature movement is created by an electrical current in the coil. The coil produces a magnetic field opposite to the static magnetic field produced

by the electromagnet in the shaker. Electrical current (electrical power) is provided to the shaker armature through the amplifier (Figure 3.2) which also provides the necessary power for the cooling fan. It has the role of monitoring the system interlock signal, shutting down and halting the test when abnormality is observed in the vibration closed loop system. The controller role is to ensure that what has been programmed is the same as the output signals from the controller sensor, in this case the accelerometer.

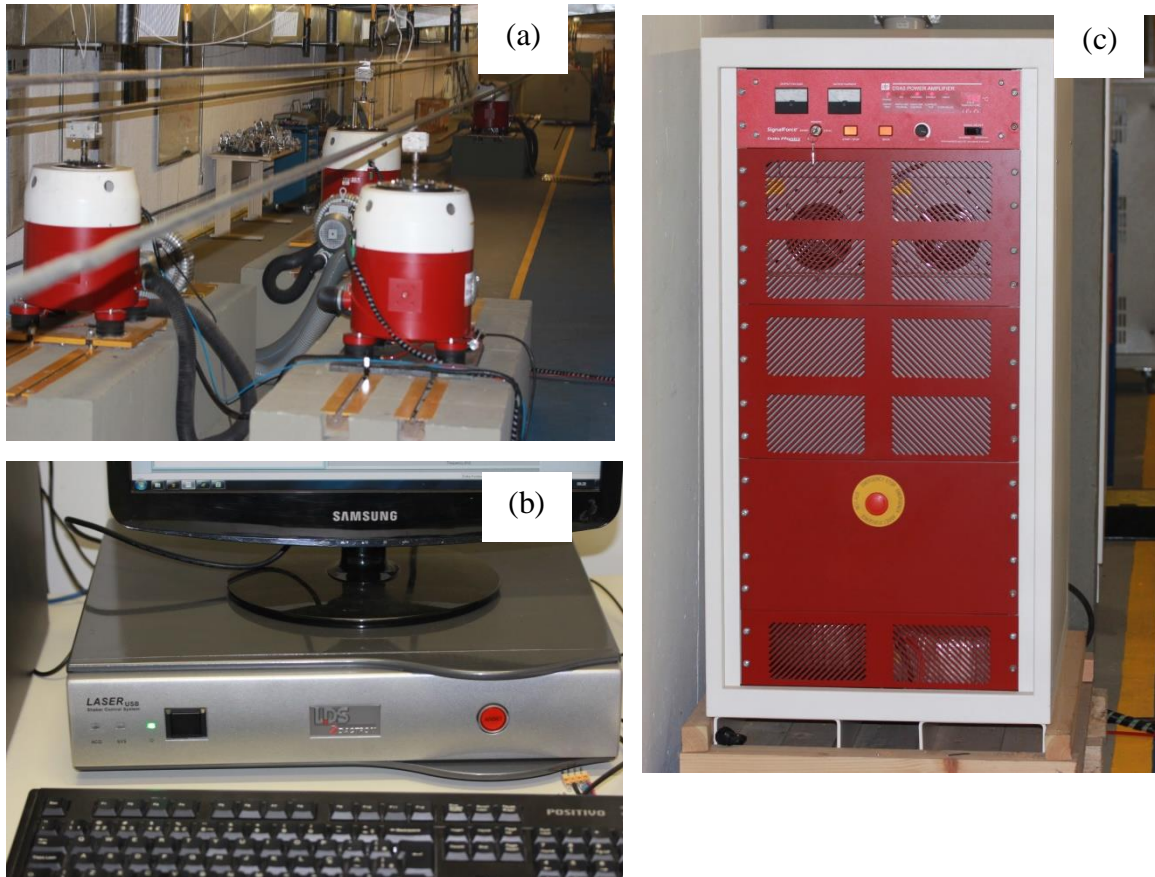


Figure 3.2: (a) Shakers; (b) controller; and (c) amplifier used for fretting fatigue bench

An accelerometer is a device which senses the motion of a component or object to which it is attached and produces an electrical signal (voltage or current) proportional to the component or object motion. The signal produced by the accelerometer passes through four typical steps: amplification, filtration, differentiation and integration. In this research, the piezoelectric accelerometers were used, with measurements captured by a Laser USB LDS vibration control and analysis system software (Figure 3.3).



Figure 3.3: Type of accelerometer used (left) and the Laser usb LDS vibration controller and analysis system software (right)

The load cell, comprised of the main metallic body accommodating strain gauges connected in Wheatstone bridge, is used to measure the stretching load of the conductor. When a load is applied, the load cell experiences a change in strain resulting in the unbalance of the Wheatstone bridge. The load value is displayed by the indicator which is connected to the load cell and supplied with electrical current (Figure 3.4).



Figure 3.4: (a) The load cell used during the experiment; and (b) the indicator of the conductor stretching load

The strain gauge is a sensor used to measure the strain of objects during experimentation. The most widely used type is the *metallic strain gauge* whose main part consists of very fine resistance wire. The electrical resistance, changing when the object or sample is deformed, cannot be measured with an ordinary ohmmeter. Therefore, the use of the Wheatstone bridge is necessary to measure the miniscule changes of resistance. In this work, the strain gauges of 350 Ohms with 2.08 as the gauge factor were used. These strain gauges have been connected in quarter bridge to make the strain measurement through the

data acquisition system ADS 2000 (Lynx Technology). Figure 3.5 shows the picture of the strain gauges and the ADS 2000 data acquisition unit used during this experimental work.

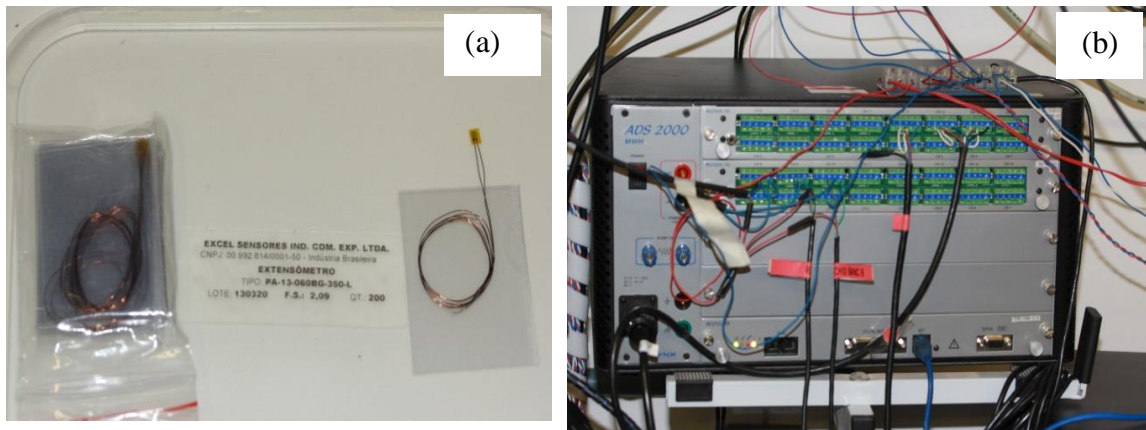


Figure 3.5: (a) Strain gauge of 350 Ohm; (b) the ADS data acquisition unit used to measure strain

3.2. Methodology and experimental procedure

3.2.1. Methodology for the evaluation of H/w parameter

The fatigue resistance of the conductor is generally obtained with the same methodology as for fatigue of the specimen on the MTS (Mechanical Test Systems) fatigue machine. The S-N curve is generated by maintaining the strain or the stress of the conductor- at a LPC between the conductor and the suspension clamp - constant, monitoring the conductor wire break and recording the number of cycles. The test in the laboratory to generate the S-N curve of conductors (fatigue tests) focuses on the suspension clamp, as this is the critical zone of the assembly system conductor/suspension clamp (EPRI, 2006). In these tests, the fatigue life of the conductors is determined as a function of vibration intensity measurements, since the stresses responsible for fatigue failure at the specific failure point - critical point - are impossible, or at least difficult, to assess for the conductor. However, this vibration intensity is correlated to the stress by means of the Poffenberger-Swart formula (presented in section 3.4). The S-N curve has been established by repeating the test for various stress amplitudes expressed in terms of vibration amplitude at 89 mm from the last point of contact (LPC) between the conductor and the suspension clamp, Y_b .

All fatigue tests in this work were strictly conducted according to CIGRÉ (1985), EPRI (2006) and IEEE (1966) specifications. The fatigue life of the assembly conductor/suspension clamp was obtained using the criterion associated with the breaking of 10% of the number of aluminium wires, as recommended by CIGRÉ (1985). S-N curves have been generated for each conductor (cited in section 4.1.1) using three different values of H/w : 1820, 2144 and 2725 m. These upper and the lower values of H/w were parameterised to allow the use of preliminary tests realised at the University of Brasilia on ACSR Ibis conductor. This increases the database for comparative purposes. Moreover, these values are reported within a range that enables the execution of tests within a feasible period in terms of laboratory testing time, but which are still relevant in terms of data for the design against fatigue (or residual life calculation) of real lines.

It is worth noting that a value of H/w less than 1820 m could create difficulties for obtaining breaks in the cables thus increasing the duration of the test. Meanwhile, a value of H/w greater than 2725 m could make the control test difficult for an AAC Orchid cable as it will present a very high EDS value (Table 3.4). The H/w of 2144 m was defined to generate fatigue data for 20% UTS of the AAAC 900MCM. From the calculation of the Poffenberger-Swart constant (K) for each H/w value, three displacement amplitudes (Y_b) were used in this study to generate the bending stress at the LPC of 23.70, 26.80, 28.22 and 31.35 MPa depending on the cable (Table 3.4). Thereafter, these calculated bending stresses were compared with those measured during tests using strain gauges glued at the diametrically opposite point of LPC. Table 3.5 shows the calculated values (as part of this work) of the Poffenberger-Swart constant (K) and the bending amplitude at 89 mm from the LPC between the suspension clamp and the conductor (Y_b).

Table 3.4: EDS (% UTS) values of each cable for various values of H/w parameterised

Conductor	EDS (% UTS, kgf)		
	H/w	H/w	H/w
	1820 m	2144 m	2725 m
AAAC 900 MCM	17	20	25
ACSR Tern	24	29	36
AAC Orchid	31	37	47
ACAR 750 MCM	22	26	33

Table 3.5: Calculated values of the Poffenberger-Swart constant (K) and the bending amplitude at 89 mm from the LPC between the suspension clamp and the conductor (Y_b)

Conductor	Bending amplitude, Y_b (mm)							
	H/w	K (MPa/mm)	H (kgf)	m kgf/m	Stress (MPa)			
	(m)				23.7	26.8	28.22	31.35
AAAC 900 MCM	1820	33.3	2282		0.71	-	0.85	0.94
	2144	34.83	2684	1.25	0.68	-	0.81	0.9
	2725	37.35	3409		0.63	-	0.76	0.84
ACSR Tern	1820	32	2432		-	0.84	0.88	0.98
	2144	33.66	2873	1.34	-	0.8	0.84	0.93
	2725	36.38	3644		-	0.74	0.78	0.86
AAC Orchid	1820	30.91	1615		-	0.87	0.91	1.01
	2144	32.49	1903	0.89	-	0.82	0.87	0.96
	2725	35.07	2422		-	0.76	0.8	0.89
ACAR 750 MCM	1820	31.98	1903		-	0.84	0.88	0.98
	2144	33.53	2242	1.05	-	0.8	0.84	0.93
	2725	36.09	2849		-	0.74	0.78	0.87

The mark (-) indicates that the test will not be conducted at the corresponding defined condition

3.2.2. Experimental procedure

3.2.2.1. Parameters used for conductor fatigue test

The parameters below should be taken into account before carrying out the fatigue test on power line conductors:

➤ Stretching load

The stretching load is associated with the average mechanical stress (Every Day Stress, EDS) to which the conductor is subjected throughout its life. In this work, all tests have been conducted with the stretching load corresponding to the different values of H/w (defined in section 3.2.1) for evaluating the H/w parameter on the fatigue life of conductors.

➤ Tightening torque of the suspension clamp bolts

The tightening torque, independent of the conductor diameter, is normally supplied by the manufacturing company of suspension clamps. The tightening torque, applied to the nuts securing the bolts to the suspension clamp, inserts a compressive load on the conductor/suspension clamp assembly, reducing slippage of the conductor on the suspension clamp. In all tests presented below, we used a mono articulated suspension clamp enabling the mounting of cables with diameters ranging from 14 to 29 mm. For these tests, a torque of 50 Nm was used, as suggested by Fadel (2010).

➤ Bending amplitude

The bending displacement amplitude measured on the conductor at the 89 mm distance point from the last point of contact (LPC) between the conductor and the suspension clamp is also one of the control parameters. The bending amplitude is correlated to the nominal stress in the conductor wire at the LPC by the Poffenberger-Swart formula (section 2.4). It is important to underline that the bending displacement at 89 mm is measured at peak to peak (Figure 3.6). Table 3.5 shows various values of Y_b used during the experimental work.

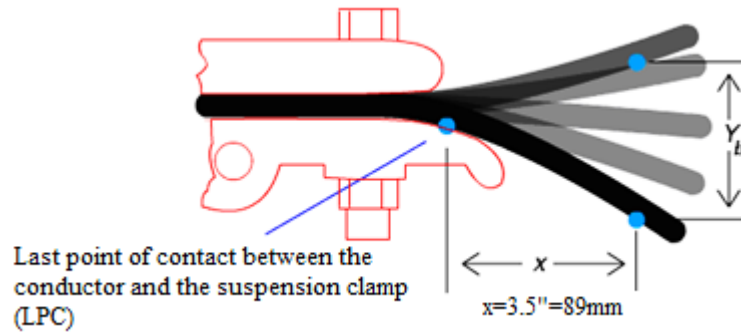


Figure 3.6: Schematic view for the last point of contact between the conductor and the suspension clamp, the bending displacement (Y_b) and the 89 mm distance from the LPC (Last Point of Contact) (Araújo, 2014)

3.2.2.2. Preparation and mounting of sample on the conductor fatigue bench

Sample preparation started by removing the conductor from the drum and stretching it on suspended pulleys within the tested active span at a length of 40 m. To avoid contact between the conductor and the laboratory floor, the sample was positioned on the fretting fatigue bench (Appendix A) at the same time special care was taken to avoid any contact between the conductor (sample) and any component which could create some micro crack on the conductor's wires. After positioning and stretching, the sample was subjected to a sequence of procedures that led to the preparation of the assembly as described below:

First, the pistol grip clamp (fixed clamp) was fixed at one end at the side of the fixed block 1 and the other at the side of the adjustable block (Figure A.3; Appendix A).

The specimen was then placed into the suspension clamp (mounted on the adjustable block). Care was taken to avoid any damage to the conductor region which was in contact with the suspension clamp. Suspension clamps were installed, but their mounting nuts not tightened to accommodate the stretching of the conductor (sample).

The other end of the sample was fixed to another pistol grip (fixed clamp) located in the range liabilities between the fixed block 3 and the adjustable block (Figure A.1; Appendix A).

The specimen was then stretched using the winch lever. With the addition of counter weights to the lever arm, the sample was stretched until it reached the traction load which corresponded to 10% more than the H/w value required to run the test. After stretching the sample, the suspended pulleys positioned along the span test were removed.

The conductor was then left for at least six hours to accommodate the load through the conductor. After this accommodation, the counter weights were removed until the tensile load value reached the H/w value required to run the fatigue test of the sample. The conductor was stretched at the required H/w value for running tests, and thereafter the suspension clamp nuts were tightened with the controlled torque (50 Nm). The conductor was then attached to the electromechanical shaker by a fixing table that was provided with an accelerometer positioned orthogonally to the conductor (sample) axis (Figure 3.7).

Near the suspension clamp, the bracket was fixed on the conductor to allow the mounting of the accelerometer at 89 mm from the LPC between the conductor and the suspension clamp. Moreover, this allowed the mounting of the laser sensor for the cycle counting during the test, as shown in Figure 3.8.

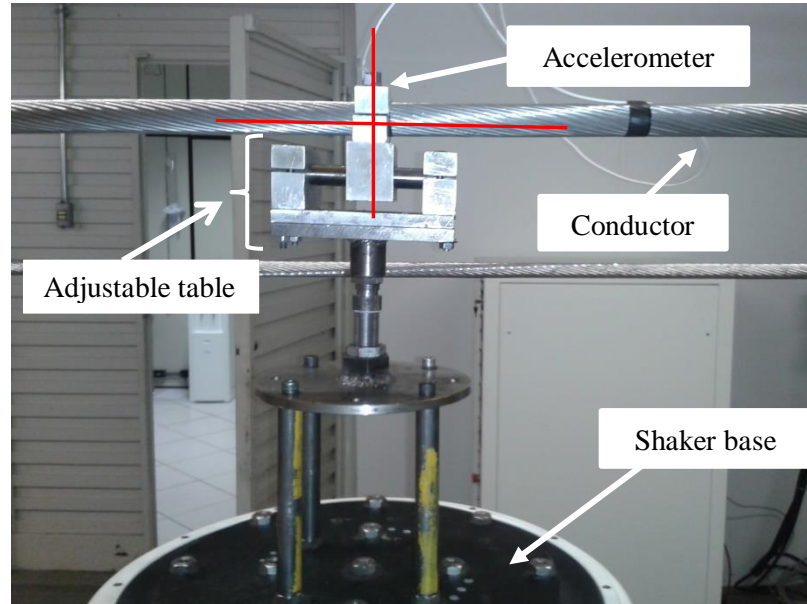


Figure 3.7: The orthogonal position of the accelerometer with respect to the conductor axis

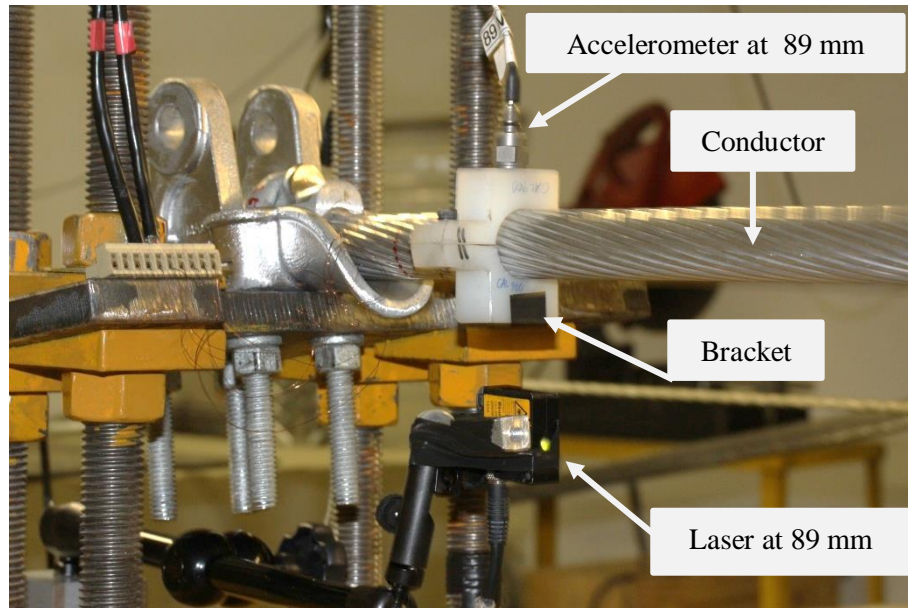


Figure 3.8: The assembly of the conductor and the suspension clamp on the bench

The preparation and mounting procedure of the sample on the bench can be delineated into the following steps:

- a) placing the sample on the bench, avoiding damage to the sample through crack formation;
- b) fixing the two pistol grips on the conductor – one at each end of the conductor – and positioning the suspension clamp on the adjustable block;
- c) stretching the sample using the winch lever and the counterweight;
- d) removing the suspended pulleys positioned along the span test (Figure A.2; Appendix A);
- e) removing part of the counter weight after the accommodation of the load until the tensile load value in the cable reaches the value of H/w required to run the test;
- f) tightening the suspension clamp nuts using a controller torque equal to 50 Nm;
- g) fixing the conductor on the shaker using the adjustable table as well as the bracket, with the accelerometer mounted on the bracket orthogonally to the conductor axis (Figure 3.7);
- h) putting the acceleration at 89 mm from the LPC between the conductor and the suspension clamp; and finally (Figure 3.8)

- i) mounting the laser sensor at 89 mm to count the cycles, in the end verifying that all sensors are well-connected.

3.2.2.3. Operation on the bench

Two types of control software were used to carry out all operations on the bench in this work: 1) the conductors in fatigue test (*Test de Fadiga em Conductores*, TFC-Fatigue Test of conductor) developed by Lynx Technology Laboratory; and 2) the Laser vibration control software from Brüel and Kjær.

The performance of the fatigue tests consisted of two main procedures: 1) the sweep frequencies to determine the driver's frequency (Usually near one of the resonance frequencies); and 2) the dwell programme at a certain frequency (chosen after the sweep) with controlled displacement amplitude of the conductor at 89 mm from LPC. During the sweep, the frequency range and the shaker base displacement were controlled. Likewise, the driver's frequency (near the resonance frequency) and the bending displacement at 89 mm were controlled for the dwell programme during the fatigue test. The practical steps used in tests for the operation of the bench monitoring system are delineated below:

- i) Make a sweep frequency in a certain range (generally between 15 to 25 Hz) to detect the natural frequencies.
- ii) After the natural frequency was detected, the system was excited with the frequency slightly less than the natural frequency (Driver's frequency), and the bending amplitude at 89 mm is required to run the test. At this step (ii), the programme used was a dwell.
- iii) After stabilising the system, the first node on the sample from the suspension was visually detected and marked with a tape.
- iv) Thereafter, the system was turned off to allow the installation of the rotation sensor for the strand failure detection at the marked point (Figure A.6; Appendix A).
- v) The test began by monitoring the recorded data from the rotation sensor through the TFC software; the test was stopped when the number of broken wires was equal to 10% of the total number of aluminium wires of the conductor.
- vi) After completing the test, the cable part, including the suspension clamp, was cut off and extracted for further fatigue analysis.
- vii) This procedure was repeated for subsequent tests.

3.2.2.4. Taking out the sample from the bench

After 10% of the total number of aluminium strands of the conductor were considered broken (Failure by fatigue), the fatigue test was stopped and the sample removed from the bench using the following procedure:

- i) First, all sensors were removed (sensors at 89 mm point, the rotation sensor for the strand failure detection, the acceleration on the shaker) as well as their related devices on the conductor.
- ii) The mouth of the suspension clamp was marked with insulation tape.
- iii) The suspension clamp was referenced to indicate the passive and active side, and right and left, to allow further analysis after withdrawing the sample from the bench.
- iv) Four steel screw clamps were mounted, two each side of the suspension clamp, at a distance of about 10 cm from the mouth of the suspension clamp. These steel screw clamps keep the conductor strands together during the cutting process and minimise the disturbance of the failure region under the suspension clamp.
- v) Suspended pulleys were situated along the span of the test, securing the cage counterweight to the manual hoist, raising it to lighten the load applied to the sample.
- vi) The load applied to the conductor was lightened by means of the winch lever.
- vii) When there was no load in the conductor, the sample was cut between the two steel screw clamp regions at each side, passive and active span.
- viii) The suspension clamp and part of the conductor were removed from the bench for analysis.
- ix) The sample was opened by checking the amount and location of breaks (external or internal, top or base) and break away distance from the mouth of the suspension clamp.

3.2.2.5. Conductor static test

The tensile stress acting on each external wire of the conductor can be determined through the static test. The tensile stress of the conductor is important to know as it is one of the categories of the stress in the suspension clamp and it affects the conductor fatigue life.

Furthermore, the static tension has an effect on the bending stiffness which characterises the deformation shape of conductor during its vibration. In this work, the purpose of the static test was to follow the trend of the function developed in section 2.6.2.

The static tests were undertaken by gluing strain gauges on all wires from the external conductor layer (Figure 3.9). For these test campaigns, four types of conductors, cited in section 3.1.1, have been used.

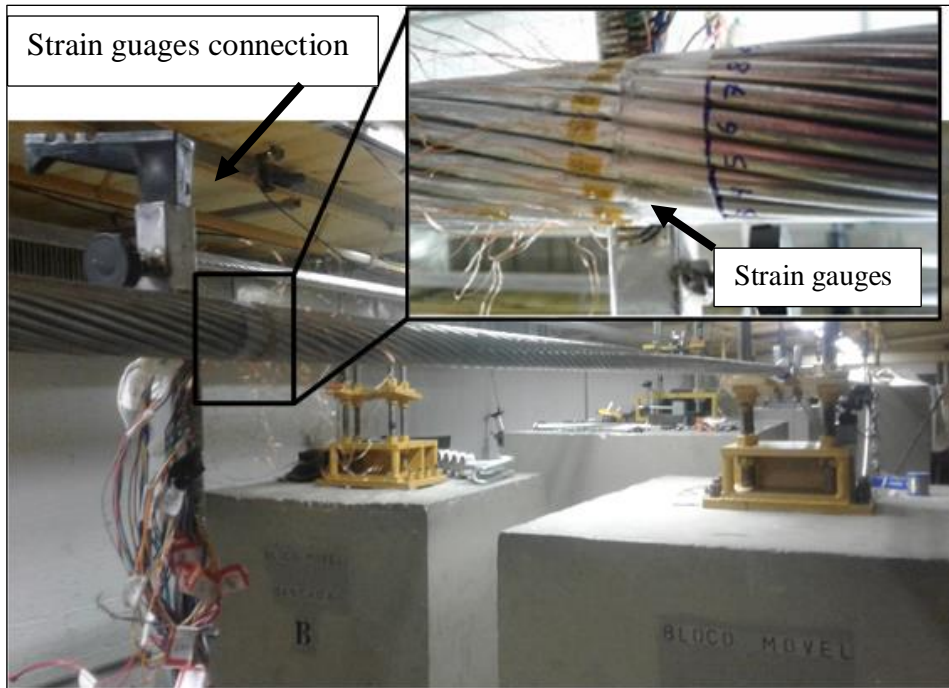


Figure 3.9: Strain gauges glued on all wires from the external layer of the ACSR Tern conductor for static test

The static test began by stretching the conductor with the H/w value 10% greater than 2725 m and leaving it for at least six hours to accommodate the tension on the conductor. Thereafter, the H/w value was reduced to 2725 m and the strain gauges glued on all wires from the external conductor layer. To avoid the impact of the suspension clamp, the strain gauges were glued far from the suspension clamp (at 3 m) rather than at the middle of the span. The strain gauges were calibrated and zeroed at a load corresponding to 5% of the RTS for the AAAC 900 MCM, ACSR Tern and ACAR 750 MCM conductors, and 10% of RTS for the Orchid conductor. It is important to underline that these values were selected taking into account the practical limitations of the fretting fatigue benches in the laboratory and also the conductor weight of the span length. The static stress, S_s , was obtained by

adding the value read from the data aqisitor with the one calculated at the stretching value where the strain gauges were zeroed.

The axial load in the conductor was gradually increased from the reference axial load up to $H/w = 2725$ m passing through the two H/w values selected for this study (1820 and 2144 m). After reaching the value of $H/w = 2725$ m, the conductor was gradually unloaded in the same manner (with the same pitch variation) as it was loaded, with the purpose of determining the creep of the conductor. At both stages (loading and unloading), a 30 minute interval was maintained between consecutive variation steps to ensure the conductor *tension* accommodation and the reading stability thought the strain gauges. The UnB (*Universidade de Brasília*) laboratory has a temperature control facility; therefore, all tests were conducted by maintaining a constant temperature in the laboratory (18° C) to avoid temperature variation effects on the conductor.

The chronology adhered for conducting the static test is as follows:

1. Stretch the conductor with the tensile load greater that the one for the $H/w = 2725$ m.
2. Leave the conductor for at least 6 hours to accommodate the conductor tensile load.
3. Mark the conductor cross section where the strain gauges will be glued (far from the suspension clamp) and glue the strain gauges by following all recommended processes.
4. Connect the strain gauges to the data aqisitor.
5. Verify if all strain gauges are working by calibrating and zeroing them.
6. Reduce the tensile load up to the references value (5% of RTS for the AAAC 900 MCM, ACSR Tern and ACAR 750 MCM, and 10% of RTS for the AAC Orchid).
7. Again calibrate and zero the strain gauges to start collecting data (make a continuous reading during the entire test period).
8. Apply the new load stretching. Remember that only the height of the lever arm should be loaded, since the use of a winch can cause loss of strain gauges due to sudden movements of the sample.

9. Wait 30 minutes for the conductor tension to stabilise. The reading stability of the strain gauges must be checked at the end of this range to ensure that the reading stability has been achieved.
10. Repeat steps 8 and 9 until the load value of $H/w = 2725$ m is reached.
11. Restart the variation, decreasing load charging according steps 8 and 9, through the same steps presented above up, to the reference value.
12. End the test.

CHAPTER 4

EXPERIMENTAL RESULTS AND DISCUSSIONS

Chapter 4, presenting and discussing the results of the experiments described in Chapter 3, is structured as follows: the strain analysis, the conductor S-N graphs generated from the fatigue tests, and the failure analysis of broken conductor wires.

The first part presents the results and discussions from strain gauge measurements to experimentally evaluate Equation 2.14. Additionally, the evaluation of the Poffenberger-Swart (P-S) formula, the correlation between the bending amplitude at 89 mm (Y_b) and the bending stress in the three top conductor wires at the diametrically opposed point of the last point of contact (LPC) between the conductor and the suspension clamp are presented. Thereafter, S-N graphs from conductor fatigue tests are presented for different values of the H/w parameter. In addition, the fatigue life in terms of the H/w parameter is evaluated for the various conductors tested.

The following part presents failure analysis in terms of the types of broken wires and the distance of occurrence from the mouth of the suspension clamp. Moreover, this part also presents failure analysis of the area of broken wires from microscopic observations.

4.1. Strain analysis

4.1.1. Static test

The results of the static test, Appendix B, are presented using polar diagrams which show the stress values obtained from strain measurements in each wire from the external layer for the AAAC 900 MCM, ACSR Tern, AAC Orchid, and ACAR 750MCM conductor at $H/w = 1820, 2144$ and 2725 m. **Erro! Fonte de referência não encontrada.** shows the polar diagram for the stress values of the AAAC 900 MCM conductor at different values of H/w parameter.

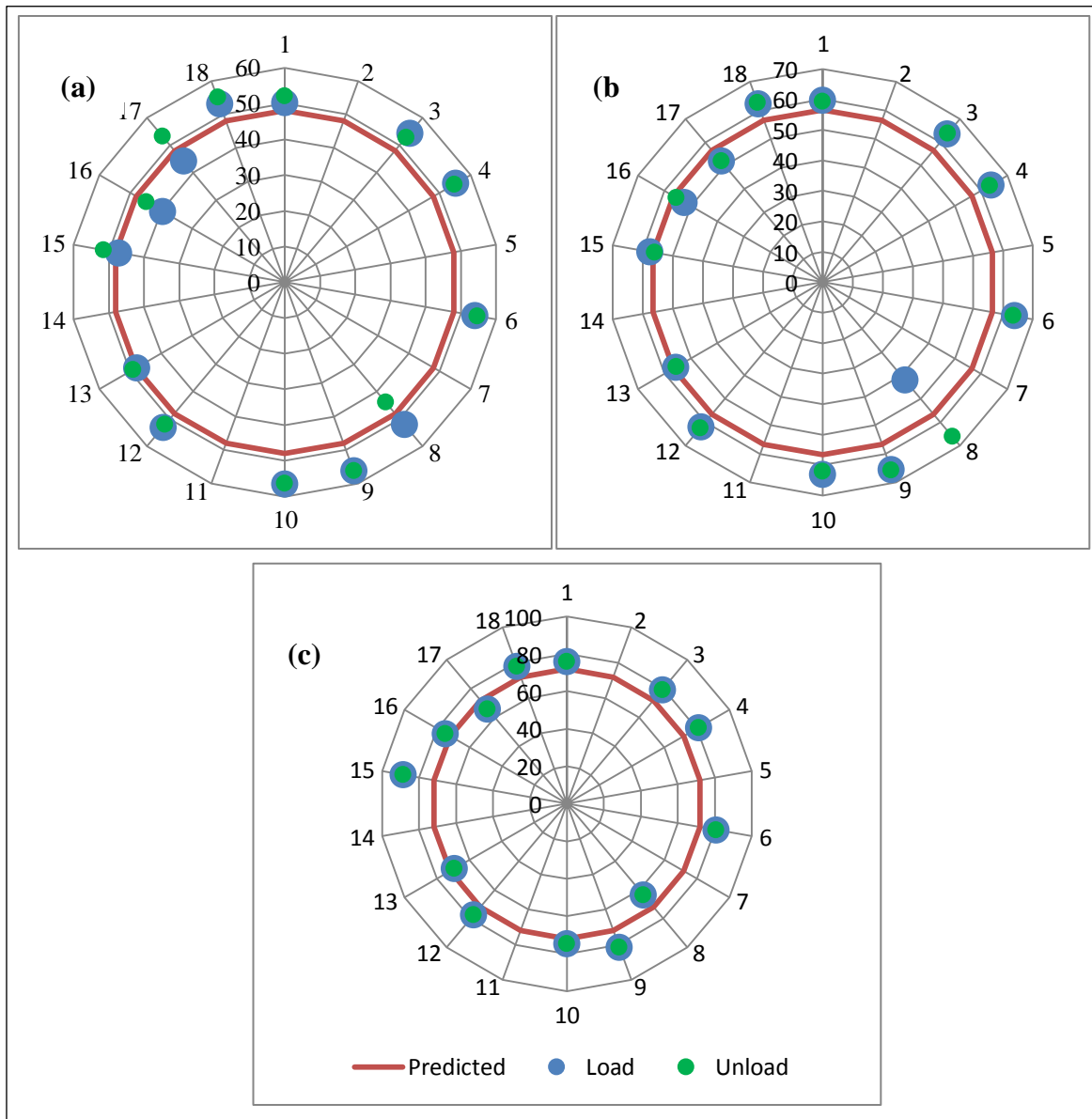


Figure 4.1: Polar diagram of axial stress in each external layer wire of the AAAC 900 MCM conductor at different values of (a) $H/w = 1820$ m; (b) $H/w = 2144$ m; and (c) $H/w = 2725$ m

Similar results were obtained for the ACSR Tern, AAC Orchid, and ACAR 750 MCM conductors at the same H/w values (Figure 4.2 to Figure 4.4). The higher relative average differences between estimated and measured values were of 11% and 9% respectively for the AAAC 900 MCM and ACSR Tern conductor. This difference was even lower for the, AAC Orchid conductor and ACAR 750 MCM conductors. We should notice that some strain gauges, for example strain gauges 2 and 5, failure during the AAAC 900 MCM static test therefore theirs measurements were not considered for this analysis.

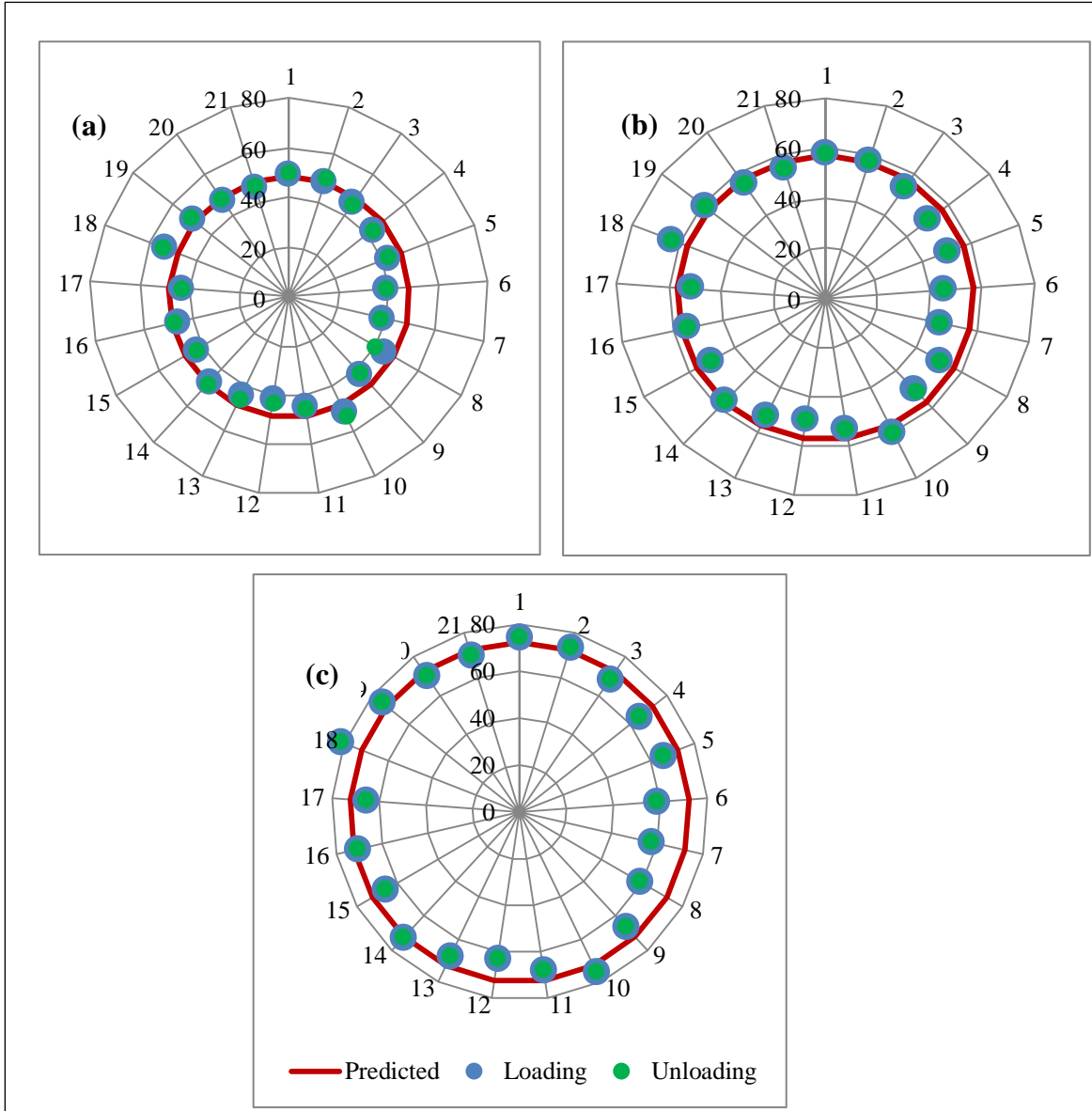


Figure 4.2: Polar diagram of axial stress in each external layer wire of the ACSR Tern conductor at different values of (a) $H/w = 1820$ m; (b) $H/w = 2144$ m; and (c) $H/w = 2725$ m

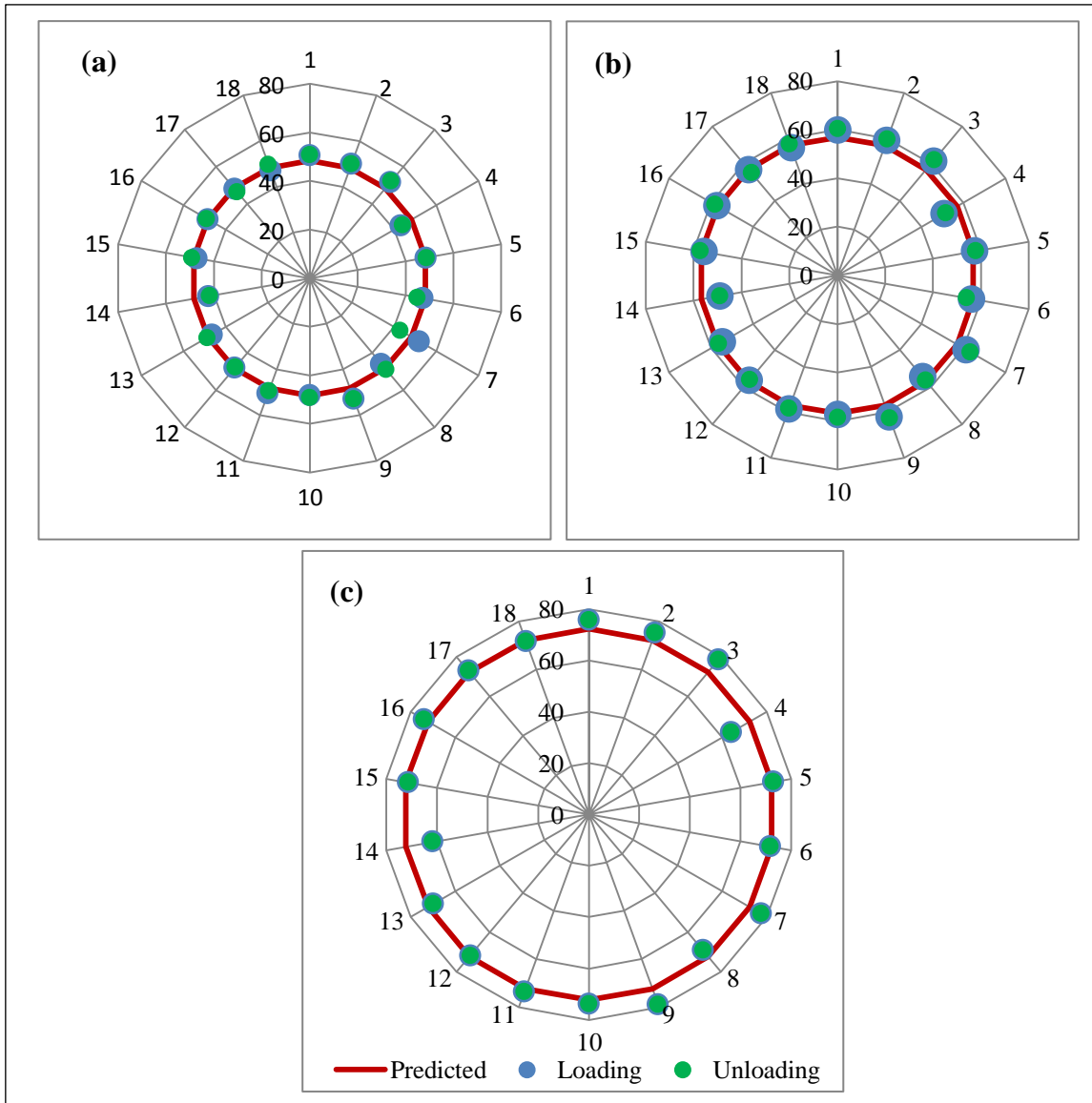


Figure 4.3: Polar diagram of axial stress in each external layer wire of the AAC Orchid conductor at different values of (a) $H/w = 1820$ m; (b) $H/w = 2144$ m; and (c) $H/w = 2725$ m

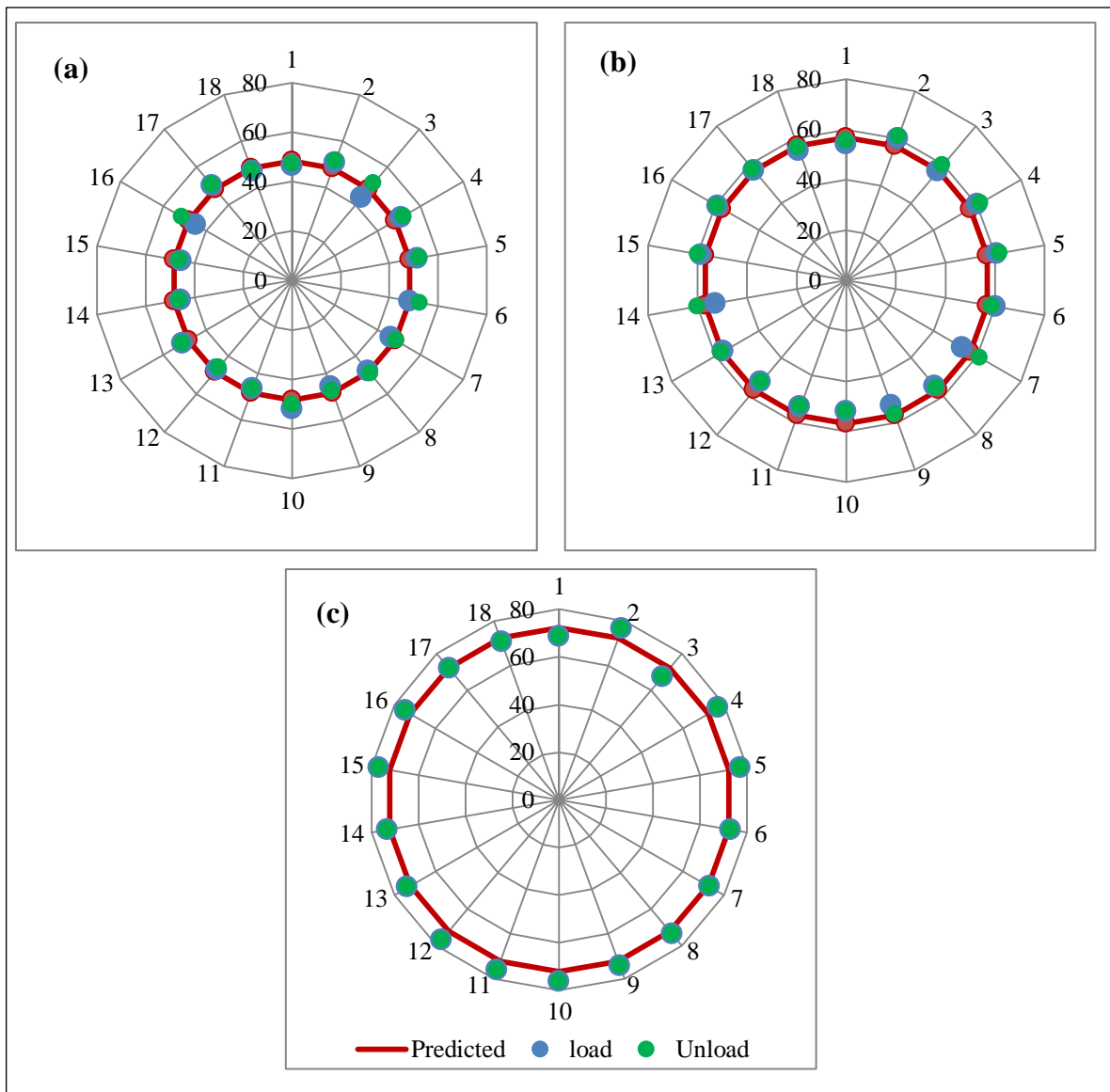


Figure 4.4: Polar diagram of axial stress in each external layer wire of the ACAR 750 MCM conductor at different values of (a) $H/w = 1820$ m; (b) $H/w = 2144$ m; and (c) $H/w = 2725$ m

An alternative way to compare the actual stress values with the theoretical ones is depicted in Figure 4.5 to Figure 4.8 respectively for the AAAC 900 MCM, ACSR Tern, AAC Orchid and the ACAR 750 MCM. In these cases, the mean static stress, S_s , of all wires was plotted for a series of different H/w values obtained by loading and unloading the conductors according to the procedure described in section 3.2.2.5. As seen from these figures, the variation of the mean stress with respect to H/w follows a linear relationship, as modelled by Equation 2.14. The vertical red bars on the experimental data in the graphs represent the standard deviation of the stress measure. It can be observed that the experimental data agree quite well with the theoretical values estimated by Equation 2.14 for different values of H/w used during experiments.

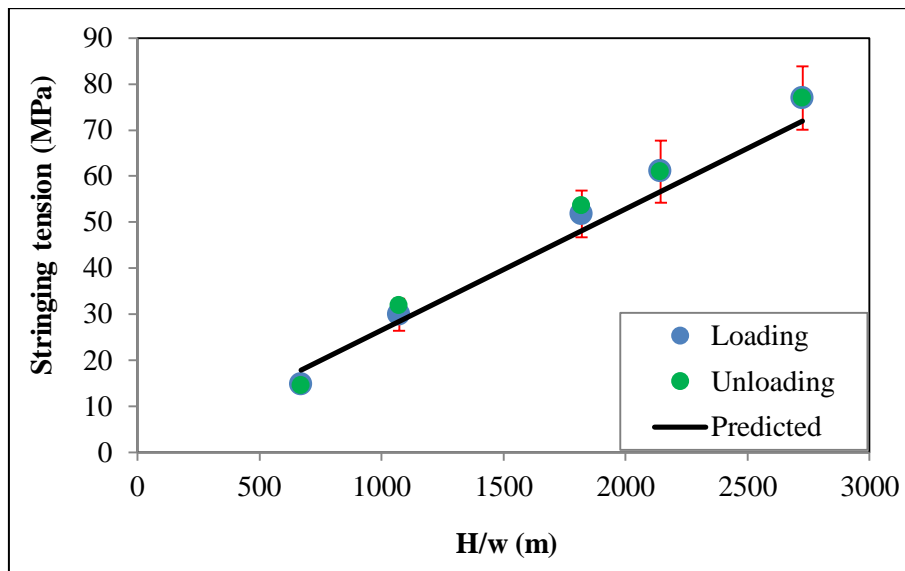


Figure 4.5: Axial average stress (from strain measurements in all wires of the external layer) for different H/w steps during loading and unloading of the AAAC 900 MCM conductor

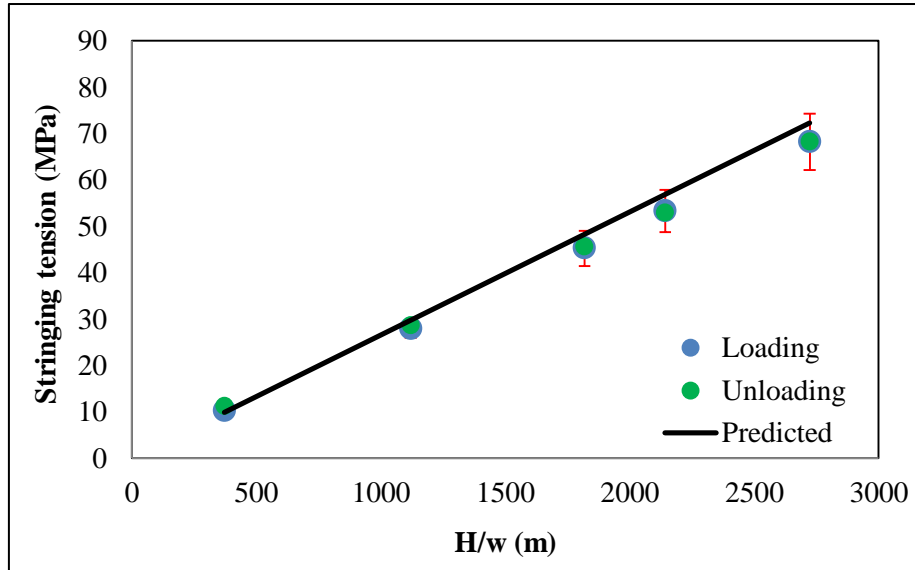


Figure 4.6: Axial average stress (from strain measurements in all wires of the external layer) for different H/w steps during loading and unloading of the ACSR Tern conductor

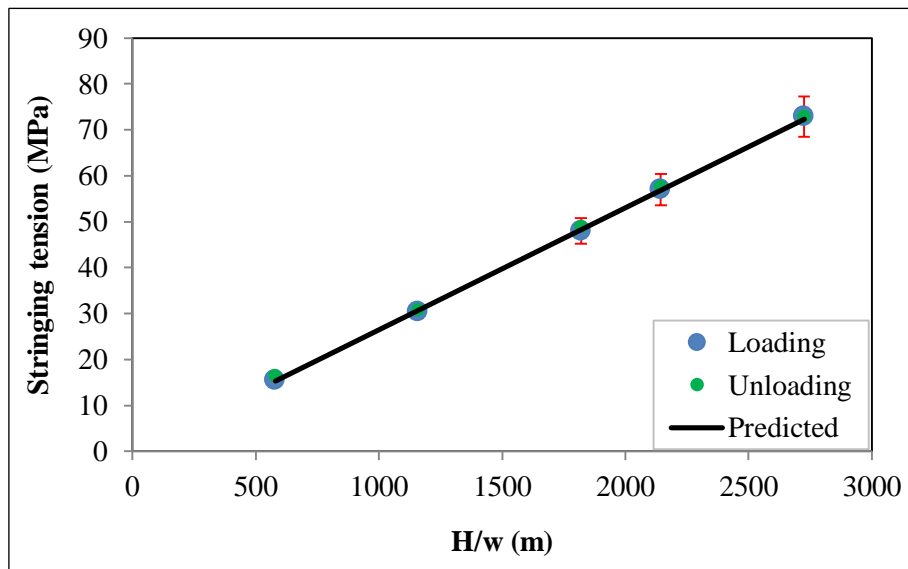


Figure 4.7: Axial average stress (from strain measurements in all wires of the external layer) for different H/w steps during loading and unloading of the AAC Orchid conductor

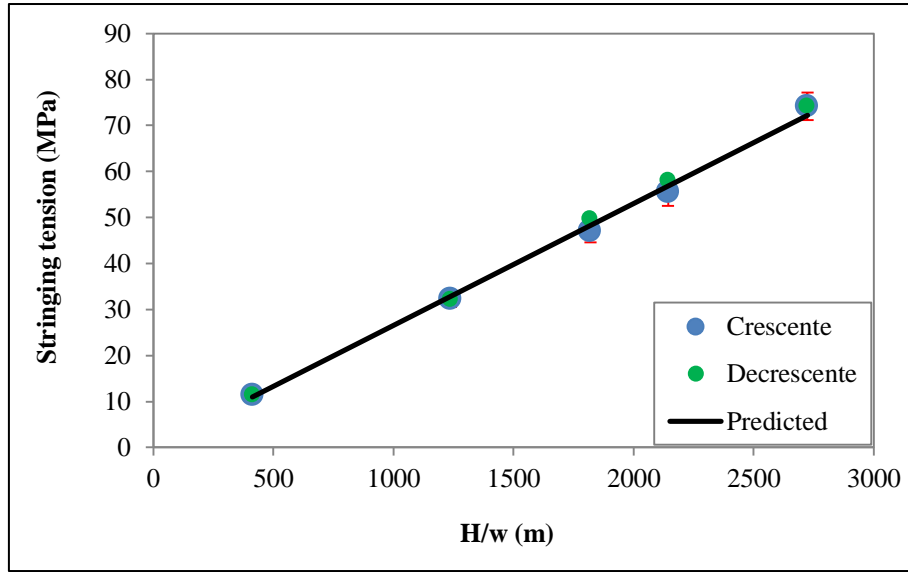


Figure 4.8: Axial average stress (from strain measurements in all wires of the external layer) for different H/w steps during loading and unloading of the ACAR 750 MCM conductor

4.1.2. Dynamic test

The strain gauge results are presented under the dynamic load of conductors. The Poffenberger-Swart (P-S) formula in terms of the H/w parameter and the bending amplitude of conductors measured at 89 mm from LPC between the conductor and the suspension clamp (Y_b) has been evaluated on AAAC 900 MCM, ACSR Tern, AAC Orchid and ACAR 750 MCM conductors, with the bending displacements (Y_b) from Table 3.5 applied during experiments.

Figure 4.9 to Figure 4.20 show the dynamic responses obtained from the conductors tested (AAAC 900 MCM, ACSR Tern, AAC Orchid and ACAR 750 MCM) using the H/w parameter for the defined bending displacement at 89 mm from the LPC between the conductor and the suspension clamp, Y_b . The average of the three strains measured has been taken into account for the evaluation of the P-S stress calculated using Equation 2.3. Three values of H/w (1820 m, 2144 m and 2725 m) have been used for the four conductors which are the AAAC 900 MCM, ACSR Tern, AAC Orchid and ACAR 750 MCM. Detailed experimental data used to plot graphs presented in Figure 4.9 through Figure 4.20 can be found in Appendix C.

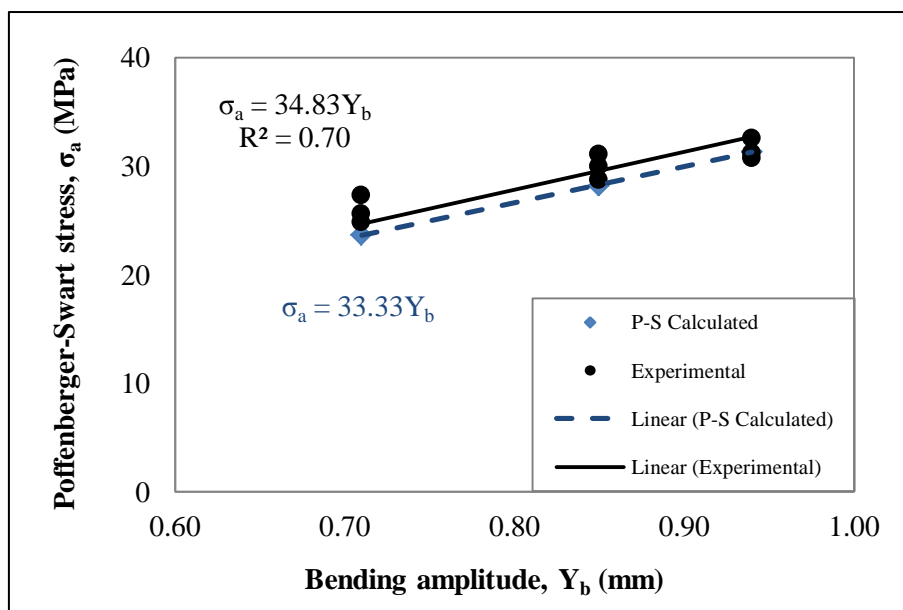


Figure 4.9: Bending stress versus bending amplitude: comparison between measured and predicted using the Poffenberger-Swart (P-S) formula on the AAAC 900 MCM conductor with the $H/w = 1820$ m

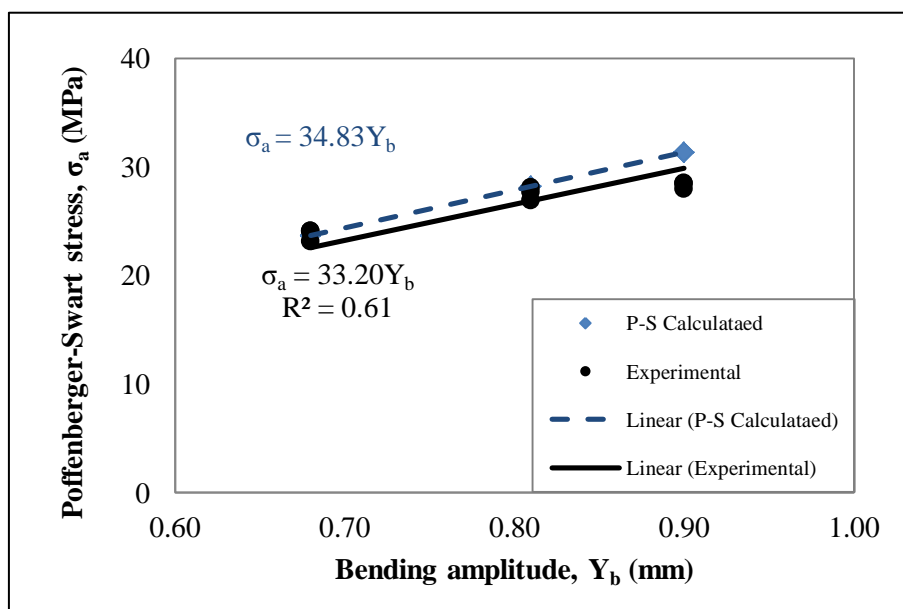


Figure 4.10: Bending stress versus bending amplitude: comparison between measured and predicted using the Poffenberger-Swart (P-S) formula on the AAAC 900 MCM conductor with the $H/w = 2144$ m

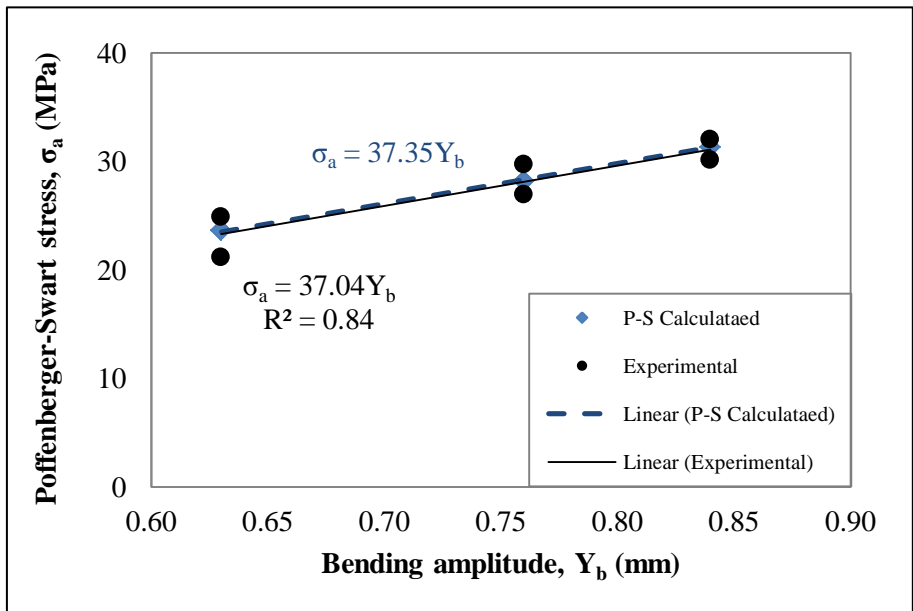


Figure 4.11: Bending stress versus bending amplitude: comparison between measured and predicted using the Poffenberger-Swart (P-S) formula on the AAAC 900 MCM conductor with the $H/w = 2725$ m

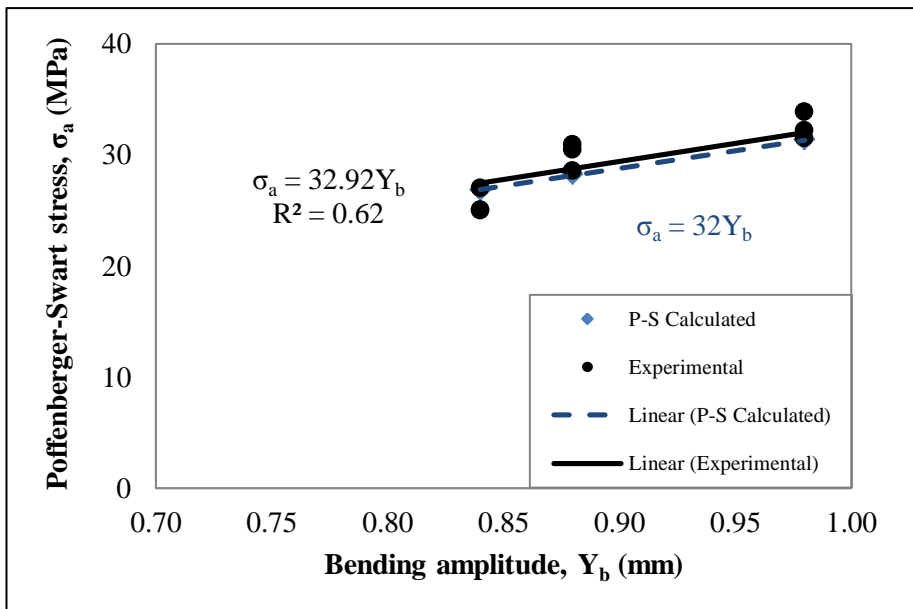


Figure 4.12: Bending stress versus bending amplitude: comparison between measured and predicted using the Poffenberger-Swart (P-S) formula on the ACSR Tern conductor with the $H/w = 1820$ m

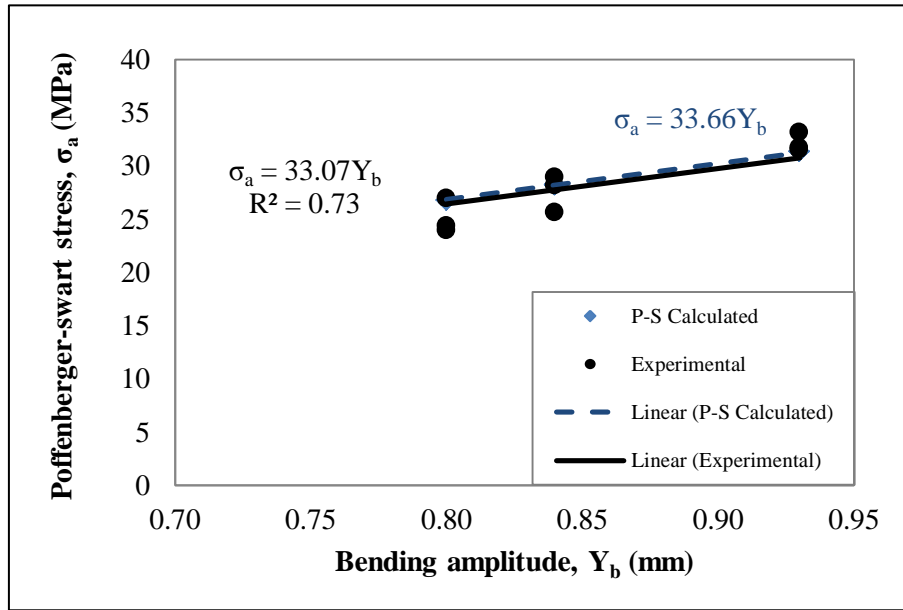


Figure 4.13: Bending stress versus bending amplitude: comparison between measured and predicted using the Poffenberger-Swart (P-S) formula on the ACSR Tern conductor with the $H/w = 2144$ m

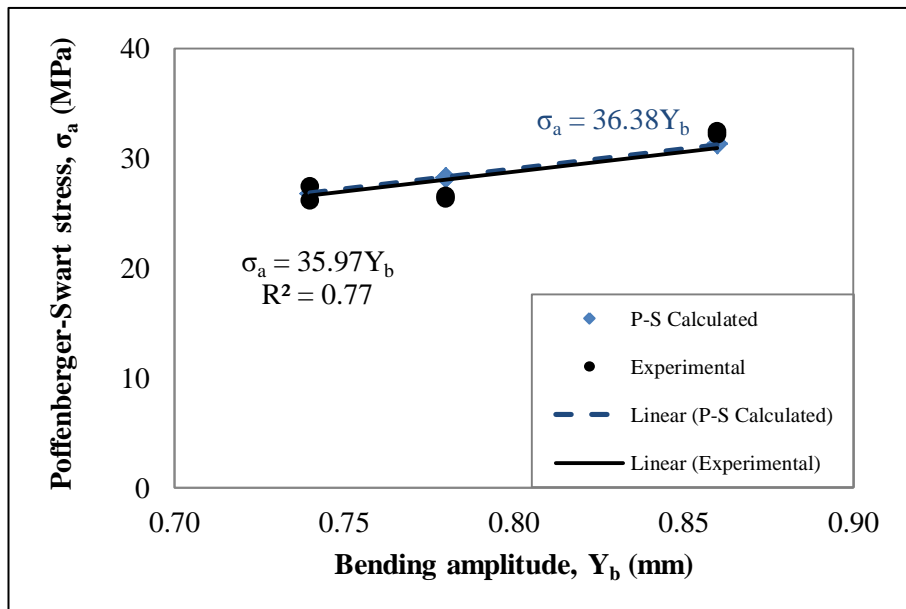


Figure 4.14: Bending stress versus bending amplitude: comparison between measured and predicted using the Poffenberger-Swart (P-S) formula on the ACSR Tern conductor with the $H/w = 2725$ m

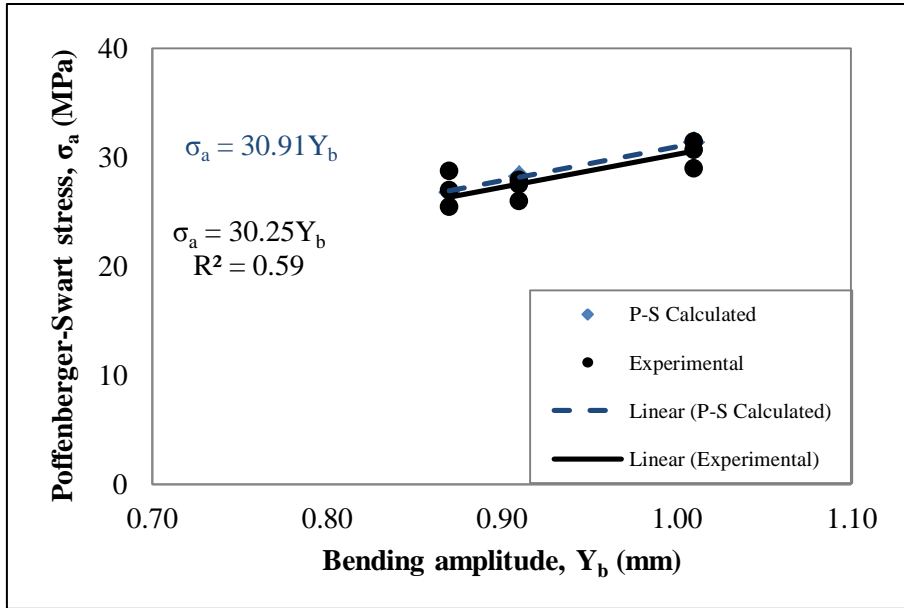


Figure 4.15: Bending stress versus bending amplitude: comparison between measured and predicted using the Poffenberger-Swart (P-S) formula on the AAC Orchid conductor with the $H/w = 1820$ m

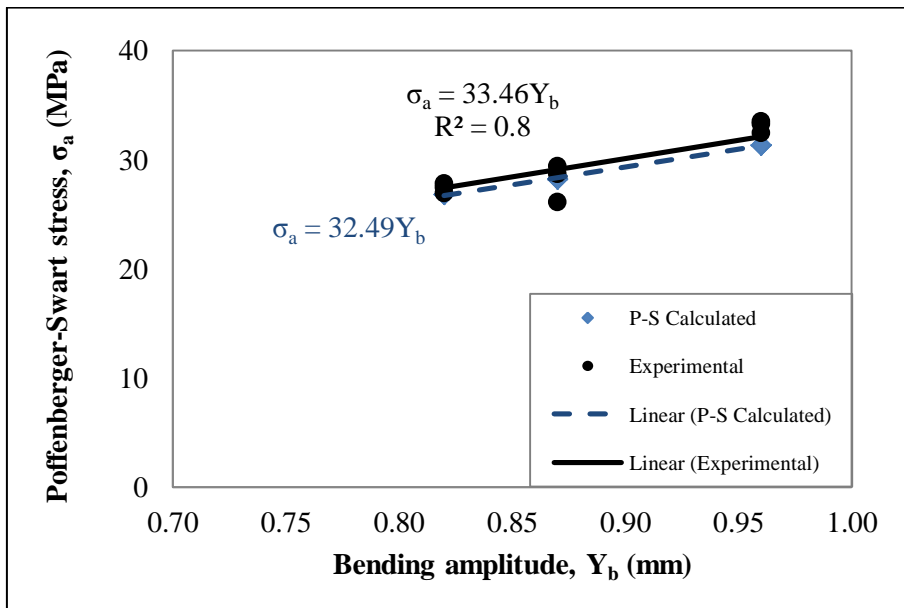


Figure 4.16: Bending stress versus bending amplitude: comparison between measured and predicted using the Poffenberger-Swart (P-S) formula on the AAC Orchid conductor with the $H/w = 2144$ m

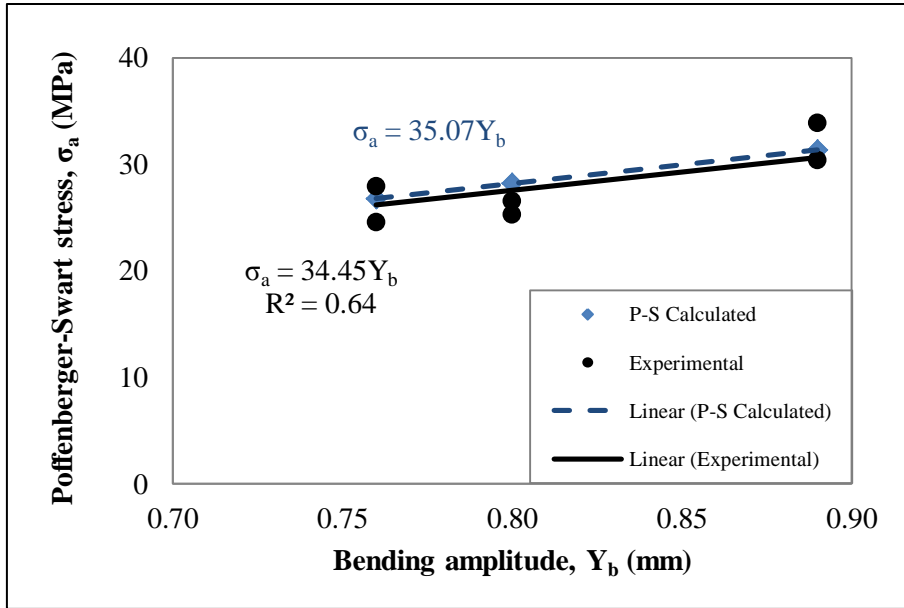


Figure 4.17: Bending stress versus bending amplitude: comparison between measured and predicted using the Poffenberger-Swart (P-S) formula on the AAC Orchid conductor with the $H/w = 2725$ m

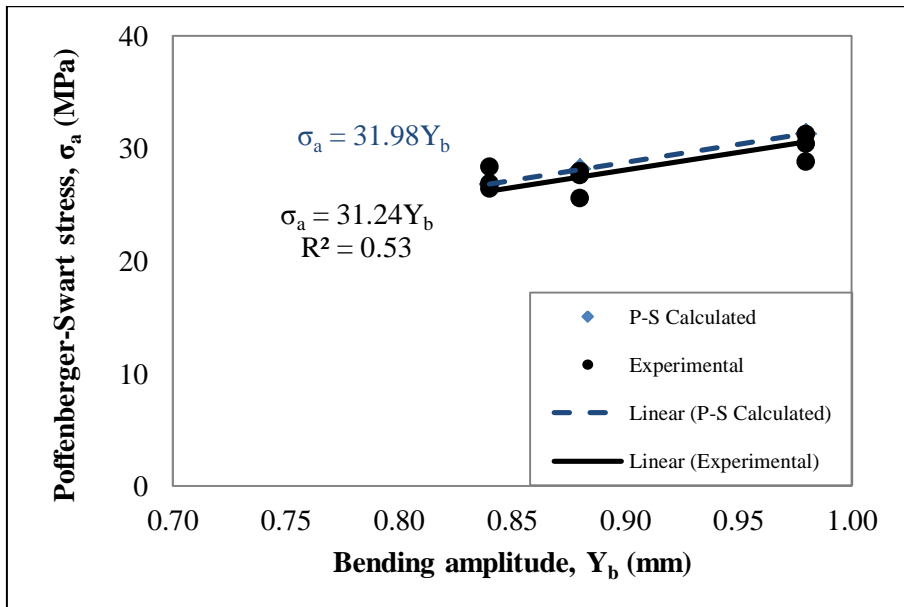


Figure 4.18: Bending stress versus bending amplitude: comparison between measured and predicted using the Poffenberger-Swart (P-S) formula on the ACAR 750 MCM conductor with the $H/w = 1820$ m

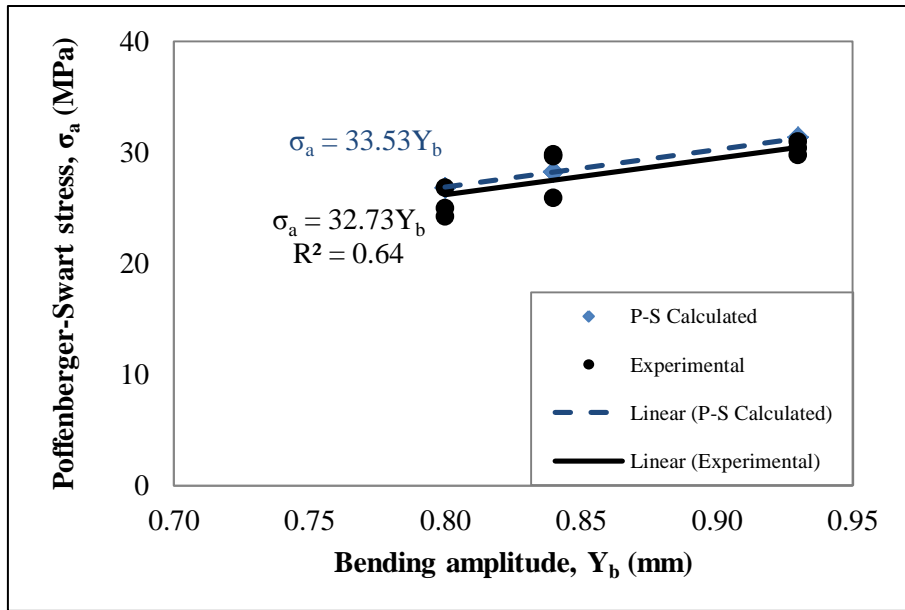


Figure 4.19: Bending stress versus bending amplitude: comparison between measured and predicted using the Poffenberger-Swart (P-S) formula on the ACAR 750 MCM conductor with the $H/w = 2144$ m

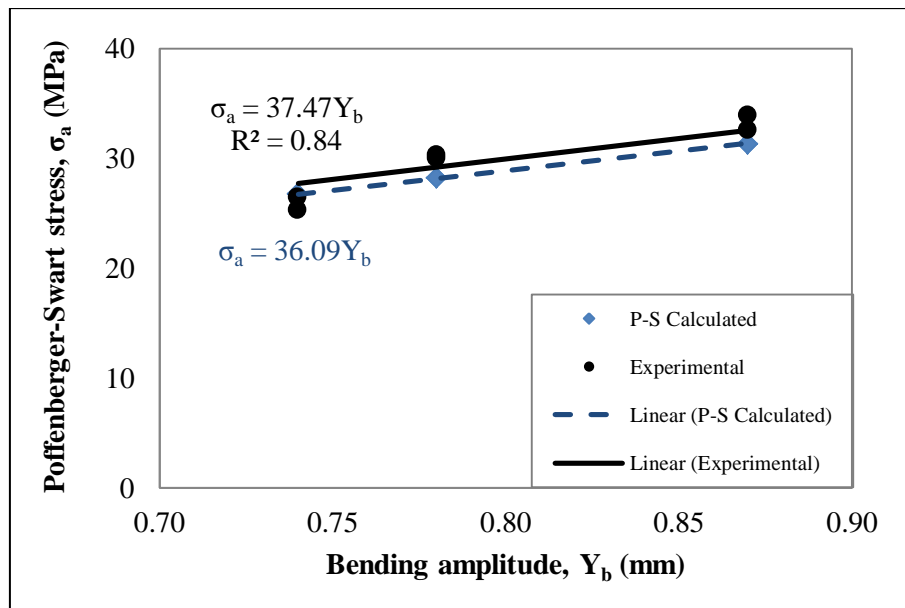


Figure 4.20: Bending stress versus bending amplitude: comparison between measured and predicted using the Poffenberger-Swart (P-S) formula on the ACAR 750 MCM conductor with the $H/w = 2725$ m

Data shown in Figure 4.9 to Figure 4.20 reveals that bending stress (0 to peak) measured using strain gauges is in good agreement related to the bending displacement (peak to peak) imposed at a distance of 89 mm from LPC, between the conductor and the suspension clamp in this range of bending displacement for H/w values considered. For all measurements of bending stress, the bending displacement (Y_b) increased proportionally with the bending stress. The data from these experiments are consistent with the predicted values for all conductors tested, with good correlation coefficients ranging from 0.53 to 0.84 and constants of Poffenberger-Swart that are close enough to the one calculated (Figure 4.9 to Figure 4.20).

The AAAC 900 MCM conductor presents the highest relative deviations for the two separate measurements equal to 15.40% for the $H/w = 1820$ m, $Y_b = 0.71$ mm and test 2 (Appendix C, Table C1). The other conductors tested – the ACSR Tern, AAC Orchid and ACAR 750 MCM – present, respectively, the highest relative error equal to 10.75%, 10.38% and 9.66%. Even though the correlation coefficient seems not to look good (0.53), the regression line appears to be close to the line corresponding to calculated values (Figure 4.18). The Poffenberger-Swart formula correlated well with the conductor tested for the bending displacement used. The four conductors (AAAC 900 MCM, ACSR Tern, AAC Orchid and ACAR 750 MCM) behaved as a cantilever beam near the suspension clamp; however, this point could be better analysed with more details considering a large range of bending displacement with low increments.

4.2. Fatigue test

The fatigue test on each conductor followed each dynamic test. For this experimental campaign, a series of 24 fatigue tests were conducted for each conductor, nine tests with H/w value of 1820 m; nine tests with $H/w = 2144$ m; and six tests with $H/w = 2725$ m. In total, 72 fatigue tests on overhead power line conductors were conducted for this study. During the fatigue test, the rotation graph of the ruler versus the elapsed cycle number was generated. When there is breaking of one conductor wire, the ruler rotates due to the distribution of the stress in the conductor and as the conductor is an assembly of wires which are twisted. The cycle number for each wire break was considered when there was a sudden variation of the rotation angle of the ruler mounted at the first node from the suspension clamp. Figure 4.21 shows the graph of the rotation ruler generated for a third fatigue test on an AAC Orchid conductor which has been loaded with $H/w = 2144$ m and

vibrated at the bending amplitude $Y_b = 0.82$ mm (Appendix D). For this test (Figure 4.21), four wires broke at, respectively, 1.42 ; 1.62 ; 1.78 and 2.05×10^6 cycles.

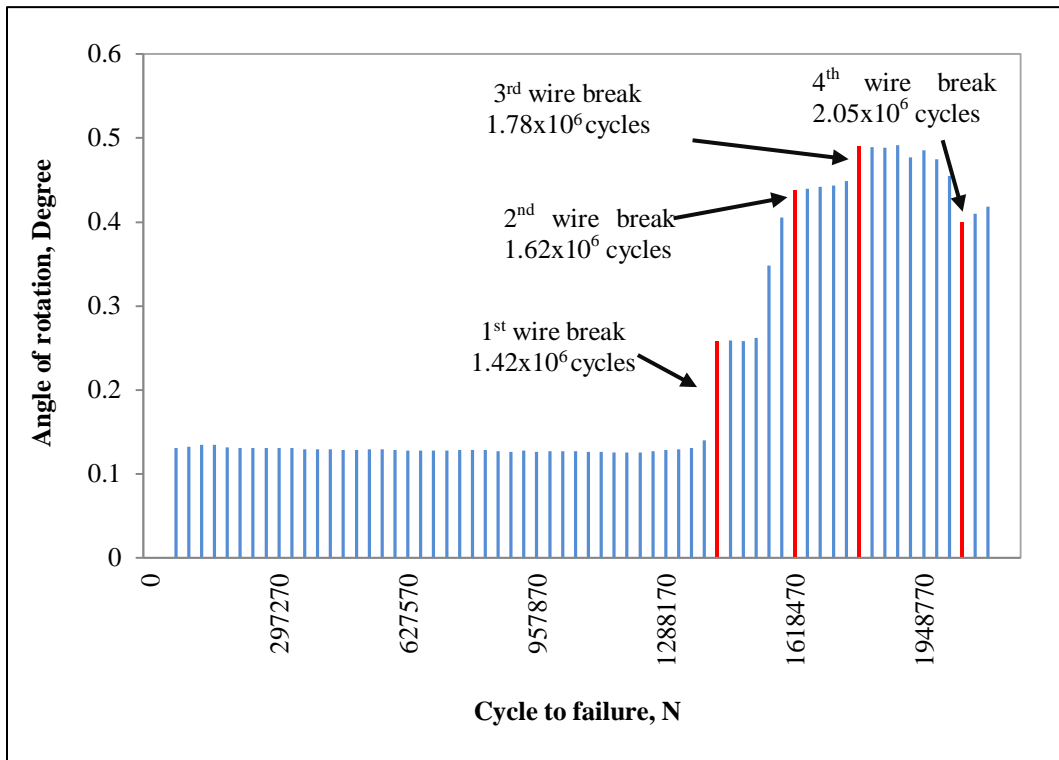


Figure 4.21: Rotation graph of the ruler mounted at the first node from the suspension clamp versus the number of cycles elapsed as well as the instance of wire break

The fatigue test is stopped when 10% of the total number of aluminium wires were broken, or whichever is greater, as recommended by CIGRÉ (1985) (section 3.2.2.4). During the fatigue test, the broken wires for the conductor's first layer were also monitored by observing the two red lines made around the conductor between the accelerometer at 89 mm and the suspension clamp (Figure 4.22a) before the fatigue test. When there was a wire break, the two red lines on the broken wire moved forward to the accelerometer due to the tensile load in the conductor (Figure 4.22b). At the end of the fatigue test, the assembly conductor/suspension clamp were redraw from the bench and the suspension clamp was opened for fatigue analysis. Initially, the broken wires were numbered and located in relation to the clamp (upper or lower part of the cable), the layer number (External layer and internal layer, for example) and the failure distance relative to the mouth of the suspension clamp (Figure 4.23). Thereafter, the fatigue life of each broken wire was determined using the rotation graph of the ruler.

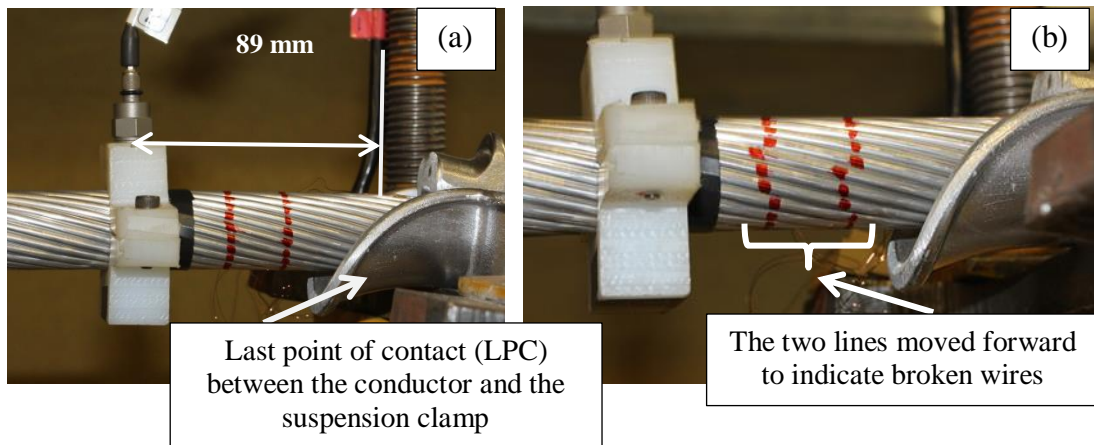


Figure 4.22: (a) Two lines made around the ACSR Tern conductor between the LPC and 89 mm before the fatigue test; (b) two lines move out, indicating three broken wires on the external layer of the ACSR Tern conductor during the fatigue test

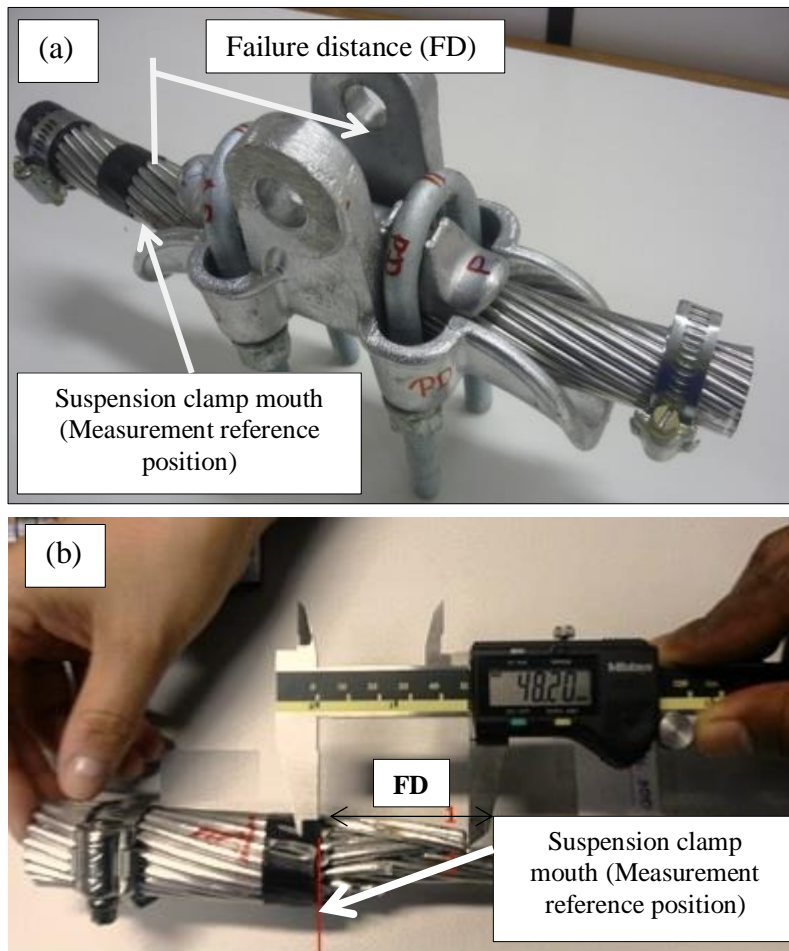


Figure 4.23: (a) Sample taken from the fretting fatigue test bench; (b) measurement of the distance to wire breaks from the mouth of the suspension clamp which is the reference position

4.2.1. Resistance limits in function of bending amplitude (Y_b)

The peak to peak bending displacement at 89 mm from the last point of contact (LPC) between the conductor and the suspension clamp used during the experiment is shown in Appendix D, as well as bending stress generated for each conductor tested: AAAC 900 MCM, ACSR Tern, AAC Orchid and ACAR 750 MCM. These tables also reveal the number of cycles elapsed for each wire break as well as the statistics (mean cycles) related to the number of cycles per bending stress level.

Based on Appendix D, the curve of resistance limits of conductors tested in function of the bending displacement (Y_b) are shown in Figure 4.24 to Figure 4.27.

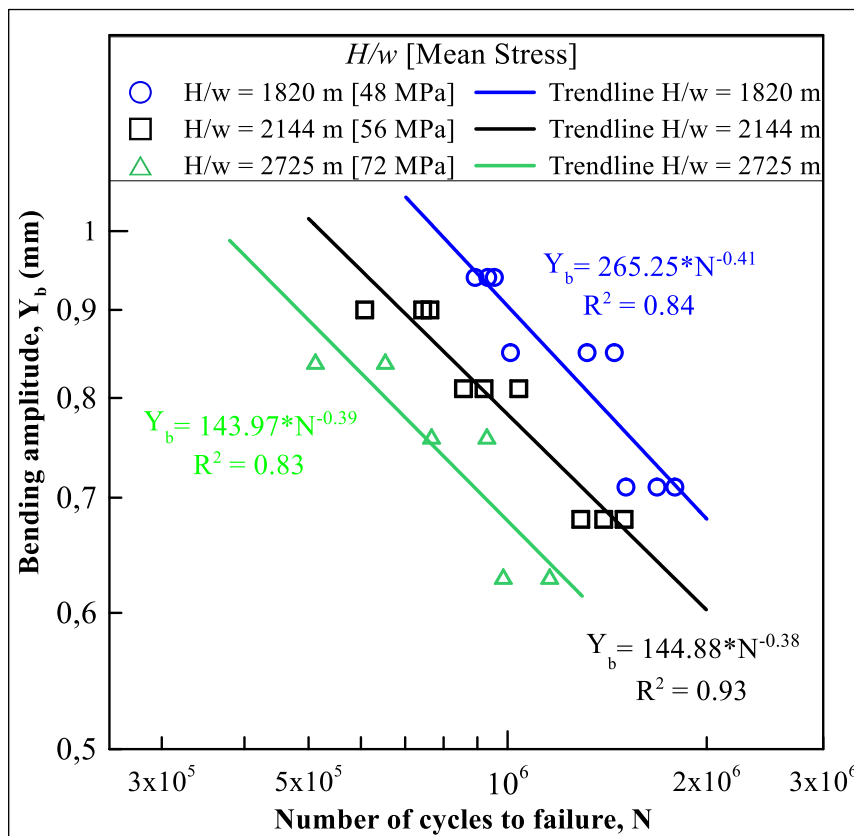


Figure 4.24: Curves of bending displacement versus fatigue life for the AAAC 900 MCM conductor at different values of H/w parameter

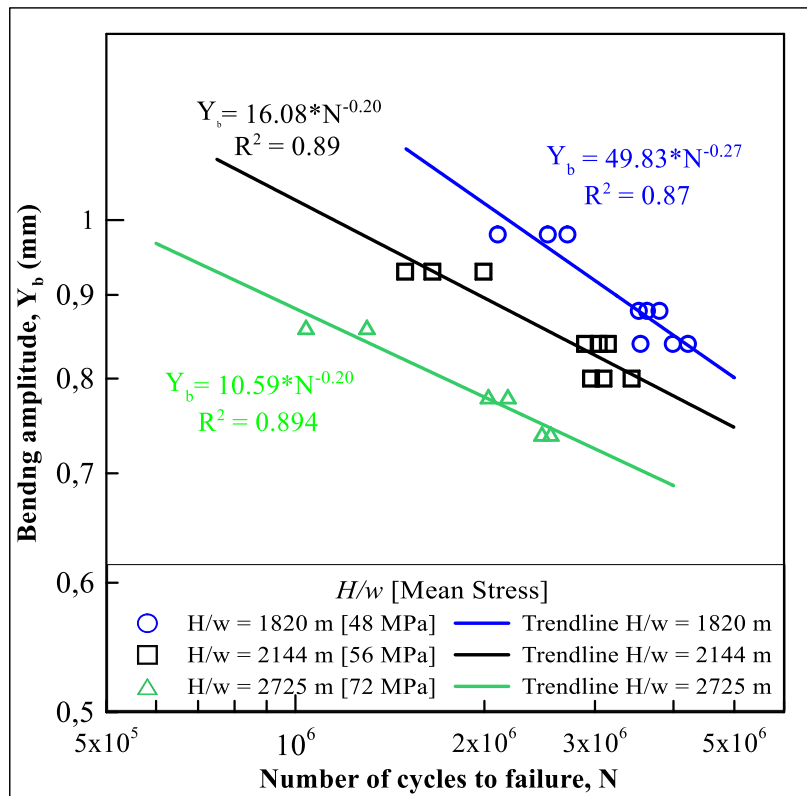


Figure 4.25: Curves of bending displacement versus fatigue life for the ACSR Tern conductor at different values of H/w parameter

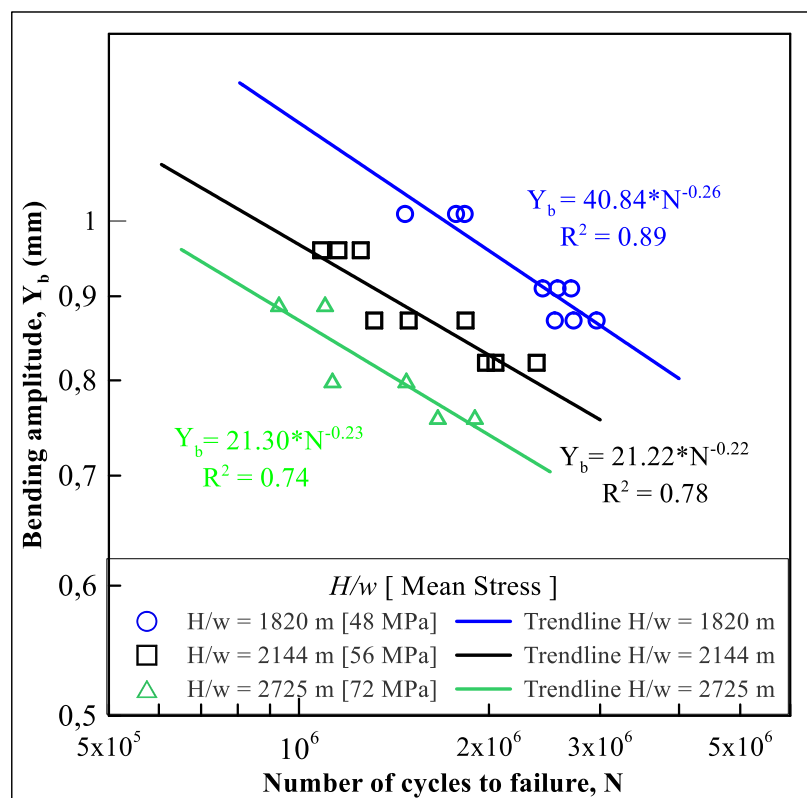


Figure 4.26: Curves of bending displacement versus fatigue life for the AAC Orchid conductor at different values of H/w parameter

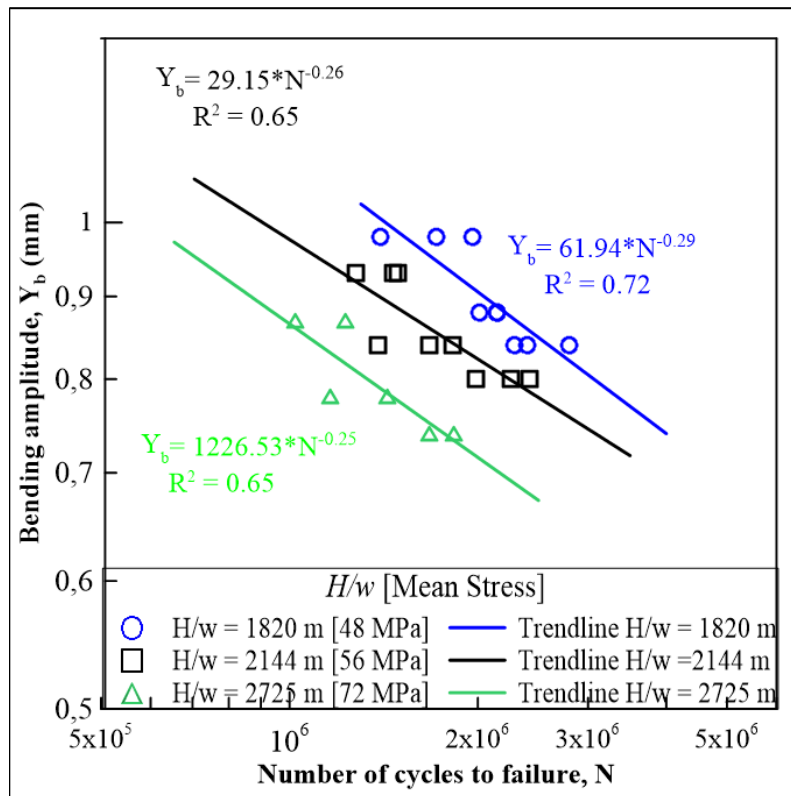


Figure 4.27: Curves of bending displacement versus fatigue life for the ACAR 750 MCM conductor at different values of H/w parameter

The H/w parameter was evaluated for the data presented in Appendix D by using the mean fatigue life for the four conductors. Figure 4.28 to Figure 4.30 show the resistance limits in function of bending amplitude for the AAAC 900 MCM, ACSR Tern, AAC Orchid and ACAR 750 MCM conductors at various values of H/w . The mean fatigue life for each bending amplitude level was considered to plot these graphs.

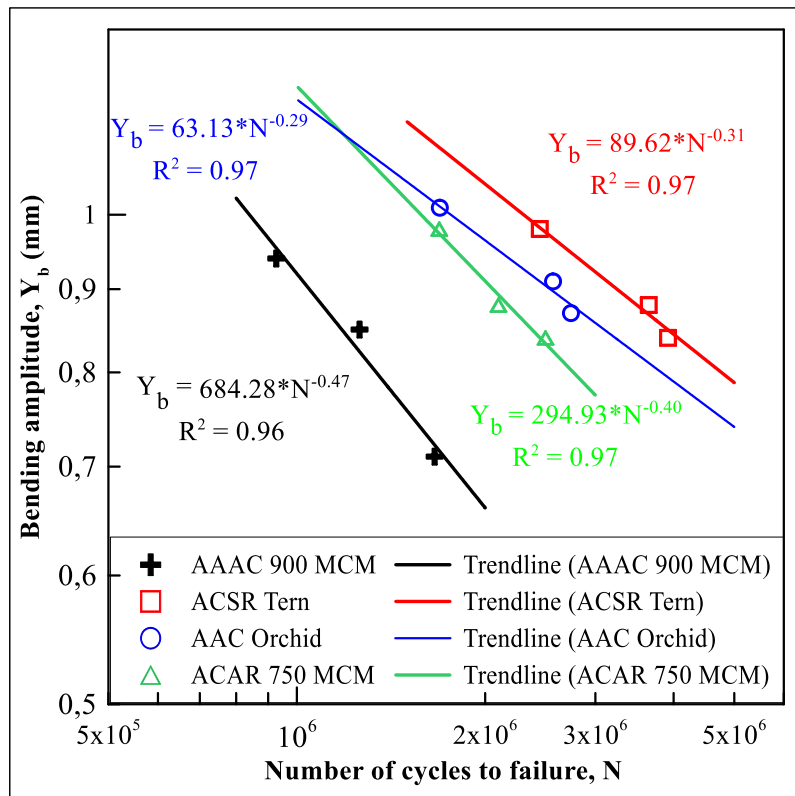


Figure 4.28: Comparison curves of bending displacement versus fatigue life for different conductors tested at $H/w = 1820$ m.

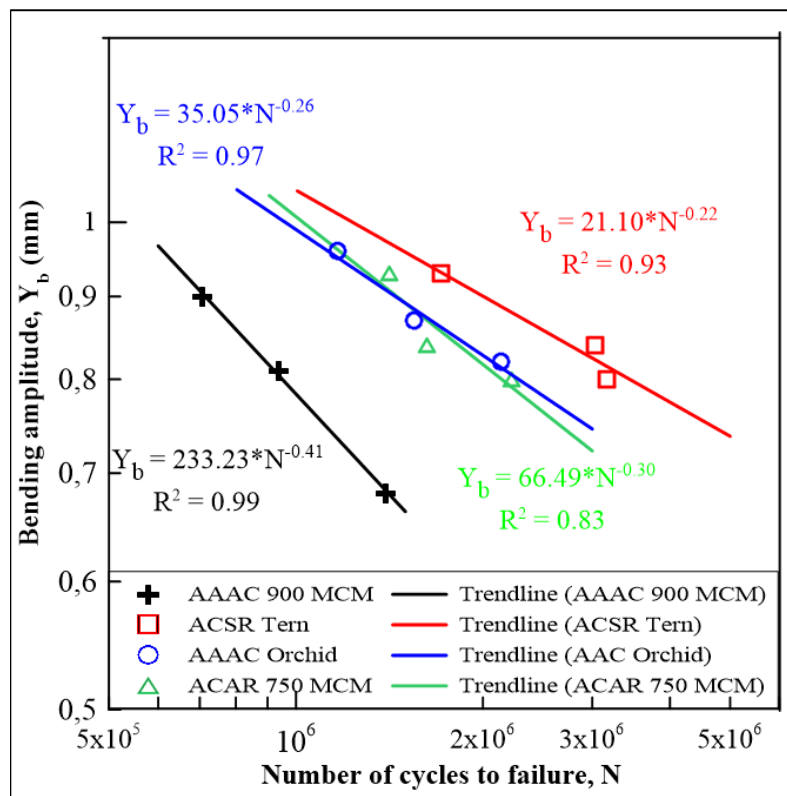


Figure 4.29: Comparison curves of bending displacement versus fatigue life for different conductors at $H/w = 2144$ m

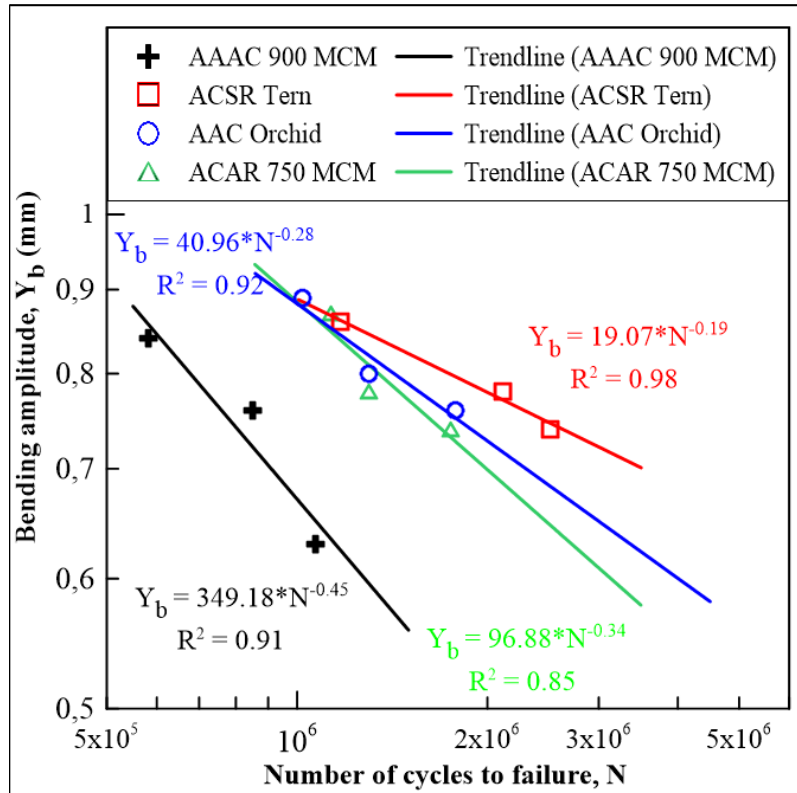


Figure 4.30: Comparison curves of bending displacement versus fatigue life for different conductors at $H/w = 2725$ m

4.2.2. S-N curves generated

The S-N curves were generated from the experimental data presented in Appendix D. Figure 4.31 to Figure 4.34 show the S-N curves generated after the fatigue test for the four conductors tested (AAAC 900 MCM, ACSR Tern, AAC Orchid and ACAR 750 MCM). For each figures below, the value of mean stress related to the H/w value is put in the legend.

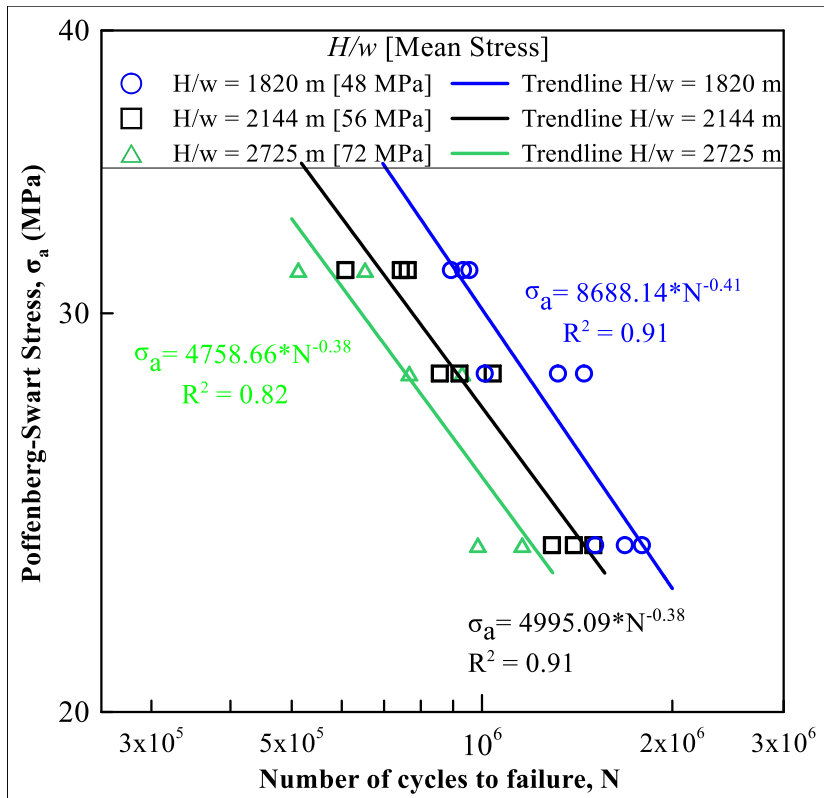


Figure 4.31: S-N curves of AAAC 900 MCM conductor for different values of H/w

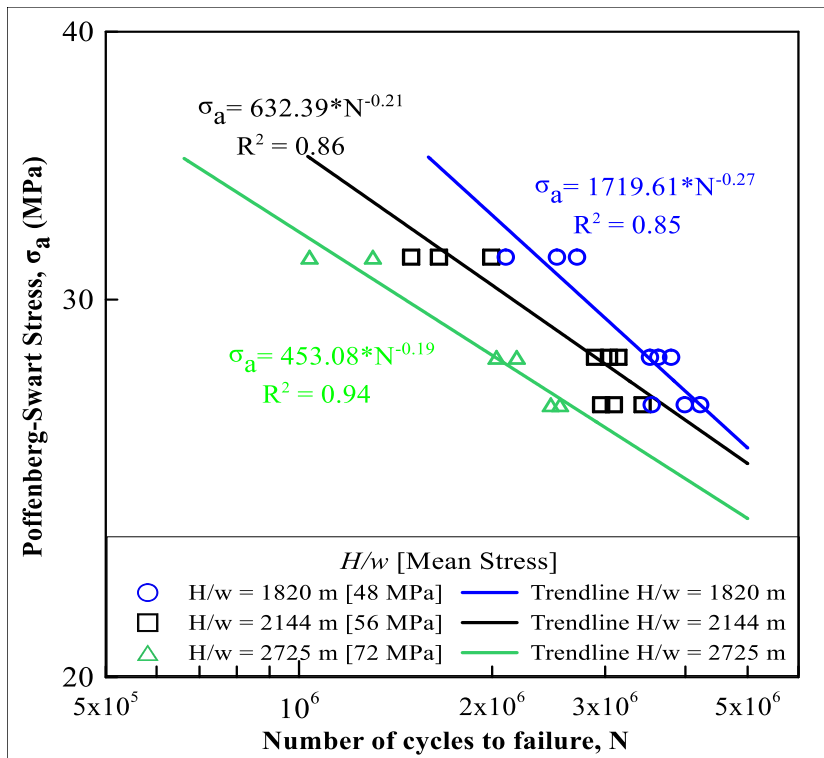


Figure 4.32: S-N curves of the ACSR Tern conductor for different values of H/w

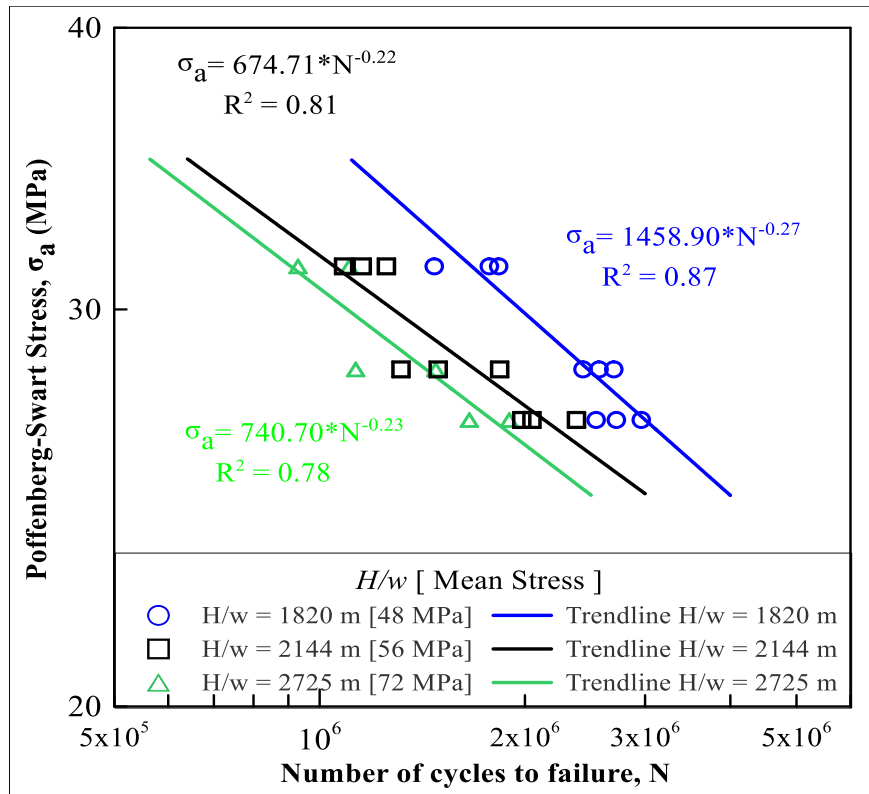


Figure 4.33: S-N curves of the AAC Orchid conductor for different values of H/w

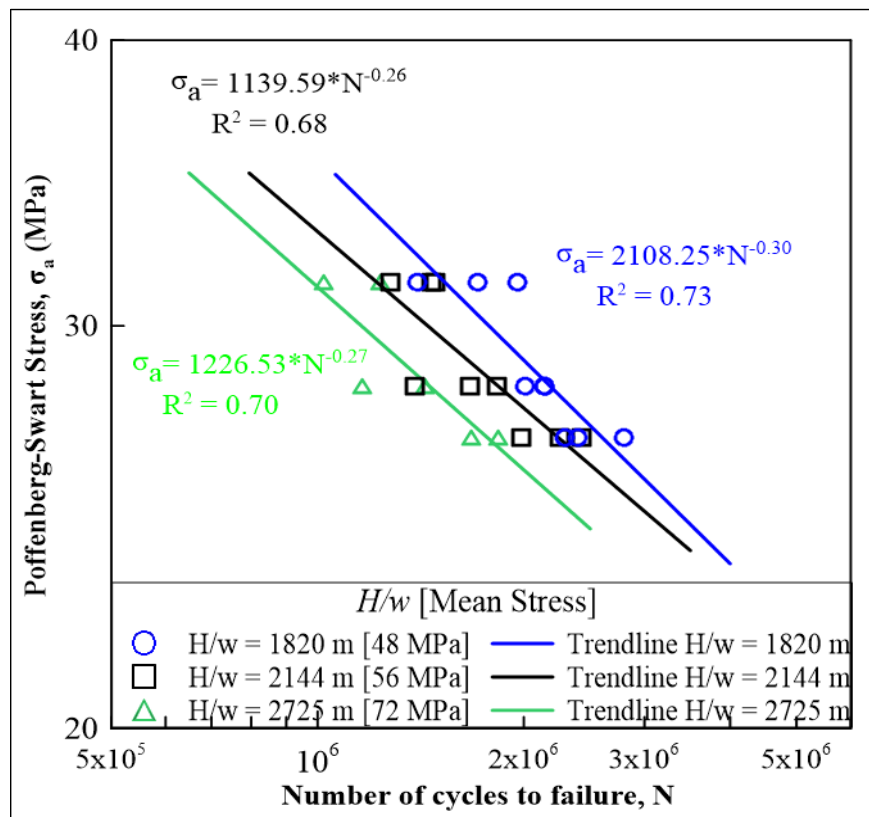


Figure 4.34: S-N curves of the ACAR 750 MCM conductor for different values of H/w

In this study, the effect of H/w was investigated by comparing the fatigue life of the conductors under examination. The correlations presented in Figure 4.35 to Figure 4.37 were derived to facilitate the analysis related to the H/w parameter for the AAAC 900 MCM, ACSR Tern, AAC Orchid and ACAR 750 MCM conductors.

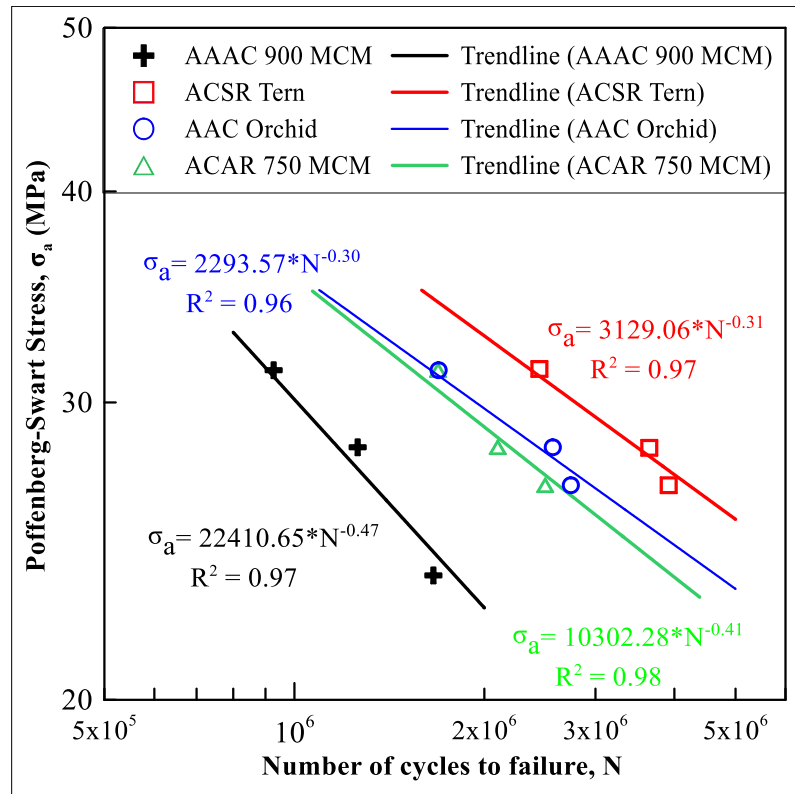


Figure 4.35: Comparison of the mean S-N curves of different conductors tested at $H/w = 1820$ m

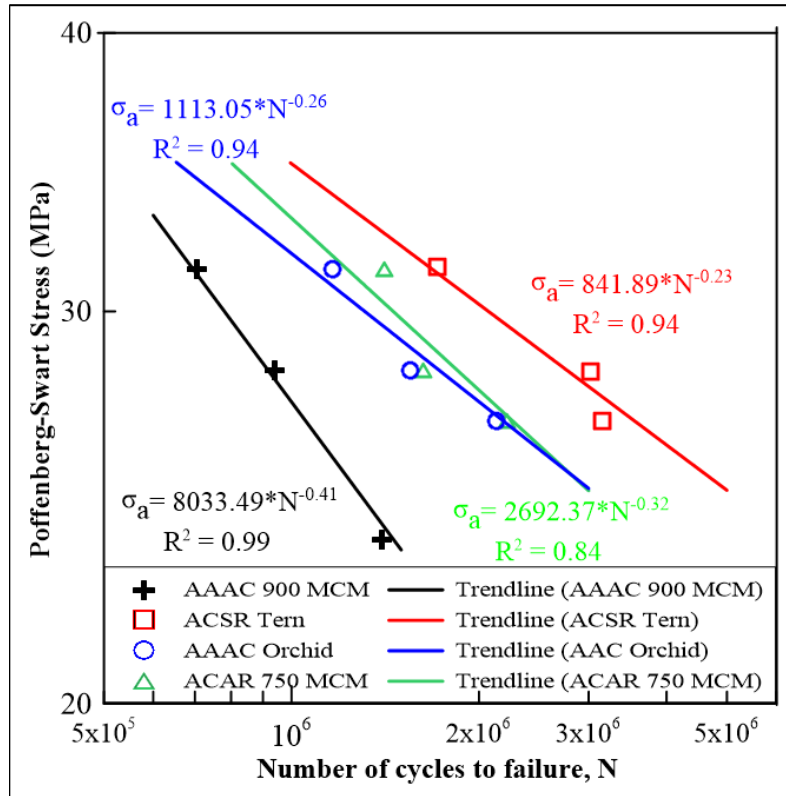


Figure 4.36: Comparison of the mean S-N curves of different conductors tested at $H/w = 2144$ m

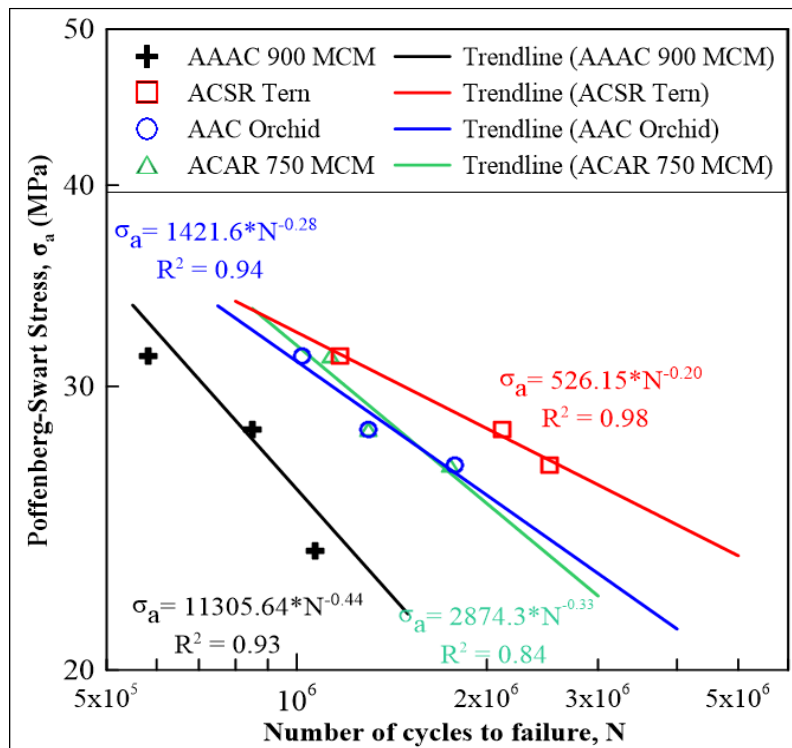


Figure 4.37: Comparison of the mean S-N curves of different conductors tested at $H/w = 2725$ m

The analysis of the graphs presented from Figure 4.35 to Figure 4.37 verify qualitatively that the fatigue behaviour of the AAC Orchid conductor, represented by the blue line, is approximately equal to the one observed for the conductor ACAR 750 MCM, represented by the green line. To verify if the behaviour of the fatigue curves (S-N) of AAC Orchid and ACAR 750 MCM conductors have similar fatigue behaviour, the stability test of the regression coefficients, known as the Chow test (Chow, 1960; Nielsen & Whitby, 2015) was performed. This test aims to verify whether or not the coefficients of a linear regression model (intercept and slope) are different between two sub-samples. The null hypothesis of this test is that the regression coefficients for the two distinct sub-samples are equal in statistical terms, while the alternative hypothesis considers that at least one of the coefficients is different from the other. The results of this analysis are presented in Appendix I, showing the values of the Chow test for the data set analysed (F_{obs}), and the limit value that the statistical test can assume in order to not reject the null hypothesis (F_{crit}), with the standard value of 5% of level of significance adopted for the statistic calculations. Thus, in comparing the values of F_{obs} and F_{crit} , it was observed that there is no statistical evidence to reject the test hypothesis that the fatigue curves (S-N curves) of conductors AAC Orchid and ACAR 750 MCM are similar ($F_{obs} < F_{crit}$). However, when the comparison is performed considering the behaviour of these two conductors with the ACSR Tern conductor, there is statistical evidence to reject the null hypothesis ($F_{obs} > F_{crit}$). In addition to the standardized variable, F_{obs} , and the limit value, F_{crit} , the descriptive level of the test, p-value, is also presented in Appendix I. This parameter represents the probability that the statistic of a hypothesis test (F_{crit} , for example) has an extreme value in relation to the observed value, F_{obs} , when the null hypothesis is true. The values calculated for p-value, besides corroborating the above observations, underline that the application of this test of hypothesis in the specific conditions demonstrate a high probability to affirm that the conductors AAC Orchid and ACAR 750 MCM have similar fatigue behaviour.

Based on the generated S-N curves (Figure 4.35 to Figure 4.37), one could observe that the ACSR Tern conductor could sustain a significantly higher number of cycles before fatigue failure than the AAAC 900 MCM for the value of $H/w = 2144$ m. Meanwhile, the AAC Orchid presents a fatigue life situated between the AAAC 900 MCM and the ACSR Tern conductor. Comparisons between fatigue life ratios of the three conductors showed that, on average, the cables ACSR Tern and AAC Orchid (or ACAR 750 MCM) presented a durability four and two times greater than the AAAC 900 MCM conductor respectively.

Nevertheless, these ratios tend to increase at the low bending displacement and decrease at high bending amplitude, measured at 89 mm from the LPC. This could be explained by the lower relative movement between conductor's layer and also by the no linearity of the dynamic behaviour of conductor (EPRI, 2006). The increase of H/w , from 2144 to 2725 m, or its decrease, from 2144 to 2725 m, caused little change in the durability ratios between these conductors.

A comparison of the mechanical properties of the AA 6201-T81 and the AA 1350-H19 (Table 3.3) revealed that the AA 6201-T81 has a higher yield and ultimate strength than the AA 1350-H19. Consequently, its fatigue resistance also proved higher than the AA 1350-H19, as is usually the case (Hatch, 1984). Therefore, one could in principle expect that the AAAC conductor (made of AA 6201-T81) would also have a higher fatigue strength than the ACSR conductor or the AAC Orchid conductor (ACAR 750 MCM) which are made of AA 1350-H19. However, care must be exercised as, due to the contact loads and the fretting between wires and between the wires of the external layer and the suspension clamp, a complex stress state (with stress concentration) and micro notches may arise. Indeed, as just shown in the previous paragraphs, the fatigue strength of the AAAC conductor was significantly lower than that observed for the others conductors tested. In this setting, notch sensitivity may well explain this behaviour (Kalombo *et al.*, 2015). One can observe that the fatigue resistance of a conductor is a function not only of the fatigue resistance of the wire material, but also of the notch sensitivity and the stress concentration factor associated with discontinuities surface of the conductor (wire), grooves (notches) and fretting marks. On the other hand, a mechanical treatment of the aluminium AA 6201-T81 could influence a fatigue life of an AAAC conductor (Reinke, 2017)

4.3. Constant fatigue life diagram as a function of H/w

The investigation of the H/w parameter was undertaken at constant fatigue life for the four cables tested: the AAAC 900 MCM, ACSR Tern, AAC Orchid and ACAR 750 MCM. With data from the fatigue and static tests presented respectively in sections 4.1 and 4.2, the *constant fatigue life diagrams* were plotted (Figure 4.38 and Figure 4.39) in terms of the parameter H/w versus the bending stress (bending amplitude) for the fatigue life equal to 10^6 cycles. It was observed that to have the same fatigue life at the same H/w parameter, the ACSR Tern conductor must be subjected to bending stress (bending amplitude) greater

than the AAC Orchid (ACAR 750 MCM) conductor which also must be subjected to the bending stress (bending amplitude) greater than for the AAAC 900 MCM (Figure 4.38 and Figure 4.39). For a same life, 10^6 cycles as a reference, the constant life diagram shows that the fatigue strength of the ACSR Tern was 30-40% higher than for the AAAC 900 MCM for different values of H/w . This value is somewhat small (25-30%) when comparing the AAAC 900 MCM to the AAC Orchid (ACAR 750 MCM) conductor.

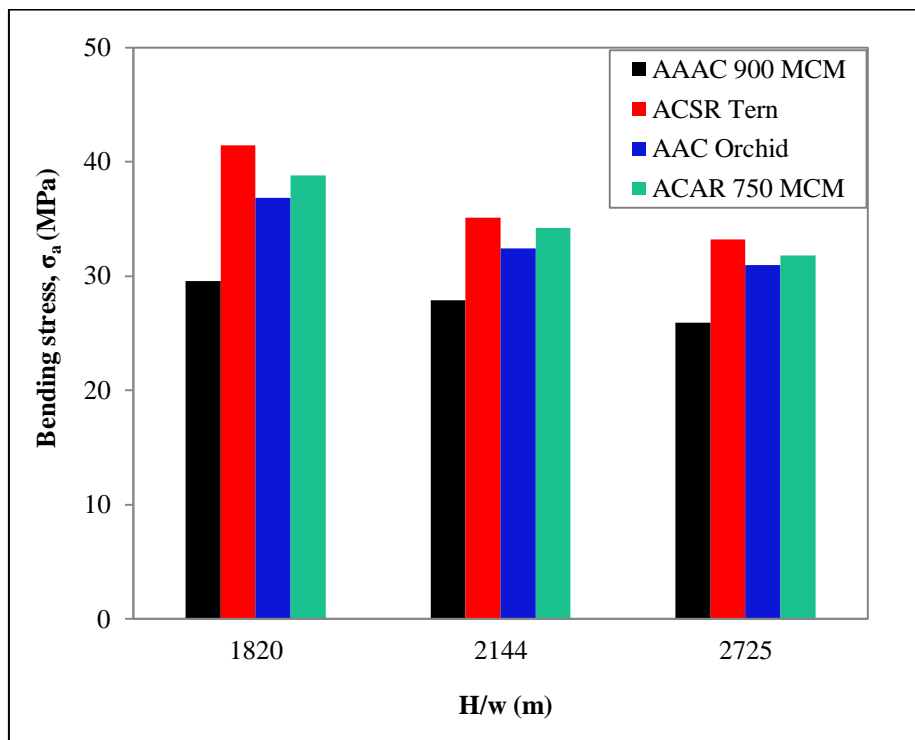


Figure 4.38: Conductor's fatigue strength, term of the H/w parameter versus bending stress, considering 10^6 cycles as a reference

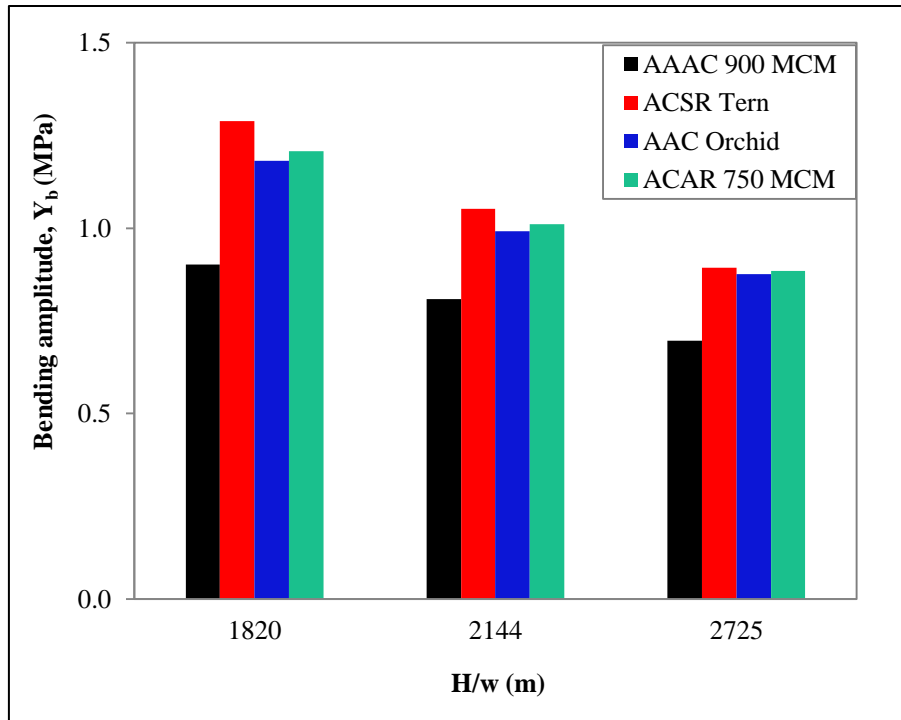


Figure 4.39: Conductor's fatigue strength, term of the H/w parameter versus bending amplitude, considering 10^6 cycles as a reference

4.4. Failure analysis

4.4.1. Macroscopic analysis

The results below are derived from failure analysis of samples tested for fatigue failure to generate the S-N graphs. This information is important for the maintenance of power lines and also in the orientation of equipment to identify the strand fatigue failure. The failure analysis is additionally important as it provides valuable data to compare with a numerical model for the fatigue of the conductor/suspension clamp system in order to more precisely understand this fatigue phenomenon.

The failure analysis was divided into three groups:

- the *position* (failure distance, FD) where the failure occurred on the conductor wire from the suspension clamp mouth;
- the *occurrence* of the wire breaks, referring to the layer of the conductor. With regard to macroscopic failure analysis, the wire break was characterised as internal or external; and
- the *profile* of fracture surface of the wire breaks.

4.4.1.1. Failure analysis related to the failure distance (FD)

The failure analysis relating to the distance at which the wire breaks occur is shown below. The failure distance (FD) was measured from the suspension clamp mouth, a measurement reference towards inside the clamp for all tested cables (AAAC 900MCM, ACSR Tern, AAC Orchid and ACAR 750 MCM conductor) for different values of the parameter H/w as well as for various bending stress (Figure 4.40(a)). The breakdown of the position on the cable layer was observed. When a wire breakage occurred in the upper part of the conductor with respect to the suspension clamp, this was indicated with T (Top), whereas breakage occurring at the bottom of the conductor was indicated with B (Base) as it is shown on the Figure 4.40(b). Details of The failure distance (FD) from the mouth of the suspension clamp for each broken wire of the four tested conductors is presented in Appendix E, as well as the mean failure distance related to the internal (MDF Internal) or external (MDF External) wire break.

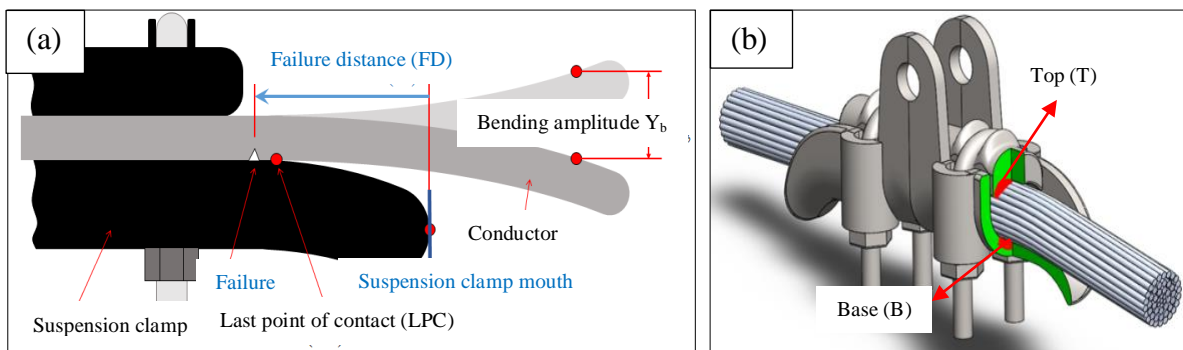


Figure 4.40: Scheme of the system conductor/suspension clamp showing: (a) The failure distance (FD) and (b) the position of the broken wire related to the suspension clamp (Represented with a partial cross section).

For further investigation and discussion, Figure 4.41 to Figure 4.52 were plotted using data from Appendix E. In these graphs, the mean distances have been used for the internal and external wire breaks for the AAAC 900 MCM , ACSR Tern, AAC Orchid and ACAR 750 MCM conductors at different values of H/w parameter.

The MFD of the AAAC 900 MCM conductor ranged between 35 and 45.53 mm for the $H/w = 1820$ m (Figure 4.41). Meanwhile, for the same conductor (AAAC 900MCM), this range was between 40.32 and 49.62 mm, and 28.08 and 46.39 mm for the H/w value of 2144 m and 2725 m respectively (Figure 4.42 and 4.43). For the ACSR Tern conductor, the MFD ranged between 35.16 and 39.42 mm for the H/w value of 1820 m, and 32.65 mm

and 36.37 mm for $H/w = 2144$ m (Figure 4.43 and Figure 4.44). For the highest value of H/w , the MFD ranged between 31.24 and 37.50 mm for the ACSR Tern conductor (Figure 4.45). The MFD of AAC Orchid laid between 29.42 and 35.58 mm, and 32.37 and 38.51 mm for $H/w = 1820$ m and 2144 m respectively (Figure 4.46 and Figure 4.47). Meanwhile, this range was between 35.78 and 40.28 mm for the H/w value of 2725 m (Figure 4.48). The final conductor tested, ACAR 750 MCM, presented the MFD range between 34.46 and 39.23 mm, and 29.91 and 38.97 mm respectively for $H/w = 1820$ and 2144 m respectively (Figure 4.49 and Figure 4.50). The MFD for the ACAR 750 MCM tested with the $H/w = 2725$ m presented the MFD range between 23.60 and 36.86 mm (Figure 4.51).

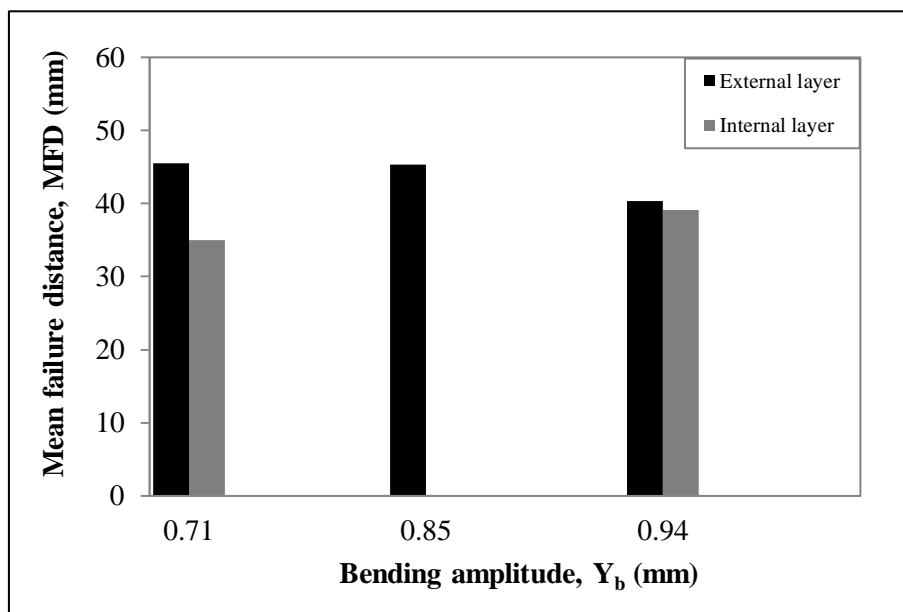


Figure 4.41: Mean failure distance of wire breaks from the suspension clamp mouth function of bending displacement for the AAAC 900 MCM conductor tested at $H/w = 1820$ m

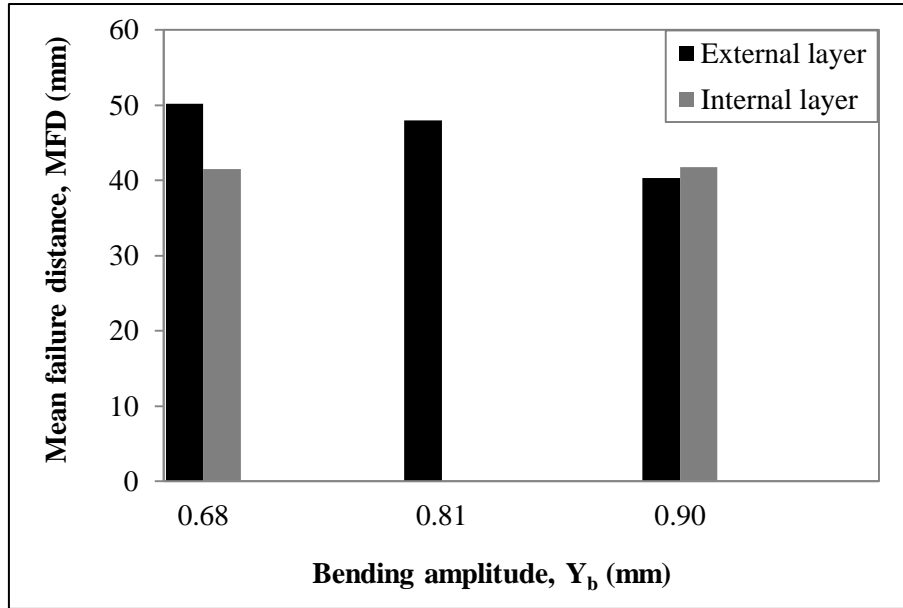


Figure 4.42: Mean failure distance of wire breaks from the suspension clamp mouth function of bending displacement for the conductor AAAC 900 MCM tested at $H/w = 2144$ m

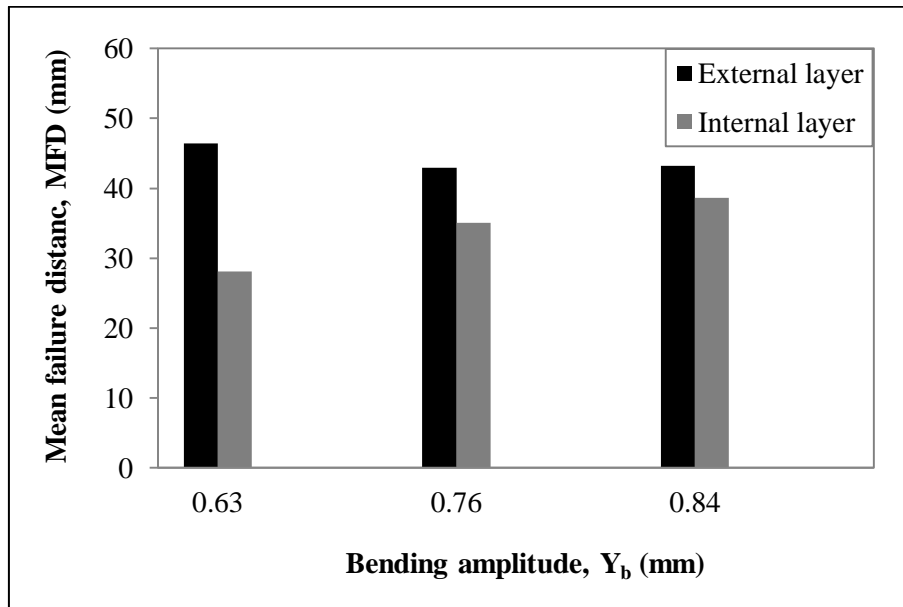


Figure 4.43: Mean failure distance of wire breaks from the suspension clamp mouth function of bending displacement for the AAAC 900 MCM conductor tested at $H/w = 2725$ m

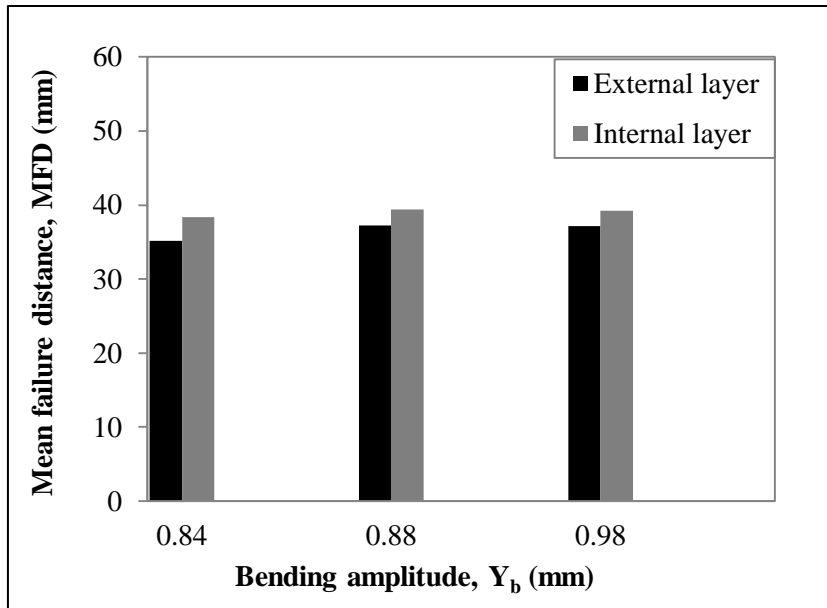


Figure 4.44: Mean failure distance of wire breaks from the suspension clamp mouth function of bending displacement for the ACSR Tern conductor tested at $H/w = 1820$ m

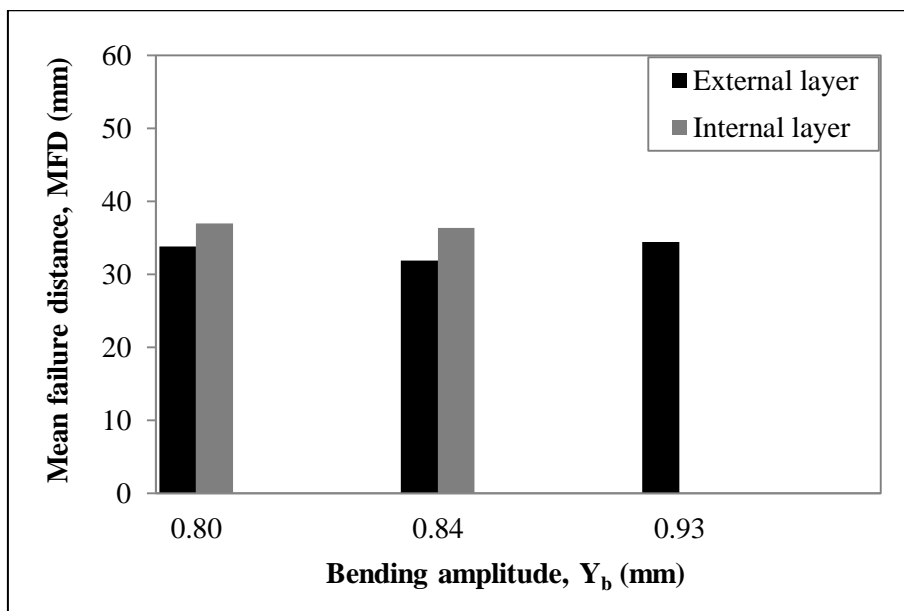


Figure 4.45: Mean failure distance of wire breaks from the suspension clamp mouth function of bending displacement for the ACSR Tern conductor tested at $H/w = 2144$ m

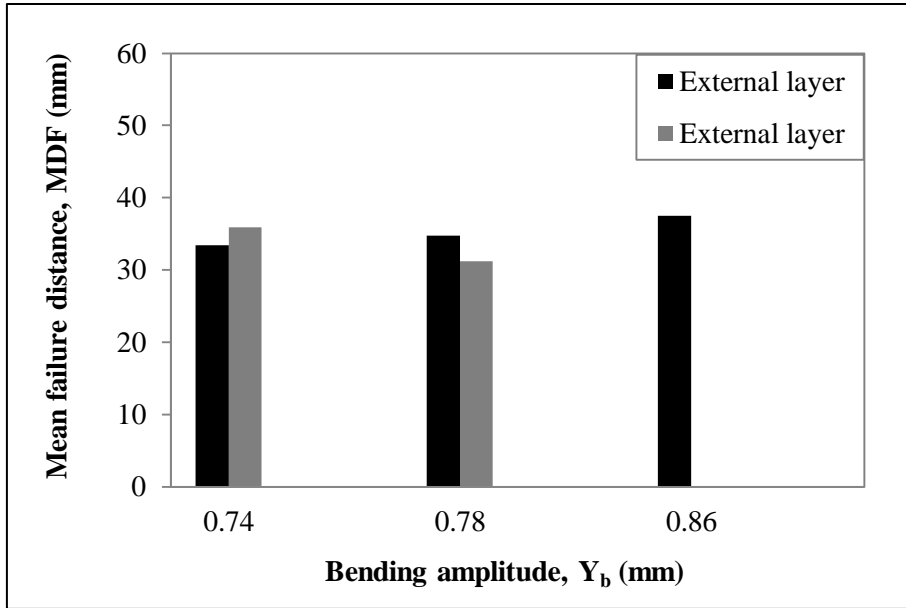


Figure 4.46: Mean failure distance of wire breaks from the suspension clamp mouth function of bending displacement for the ACSR Tern conductor tested at $H/w = 2725$ m

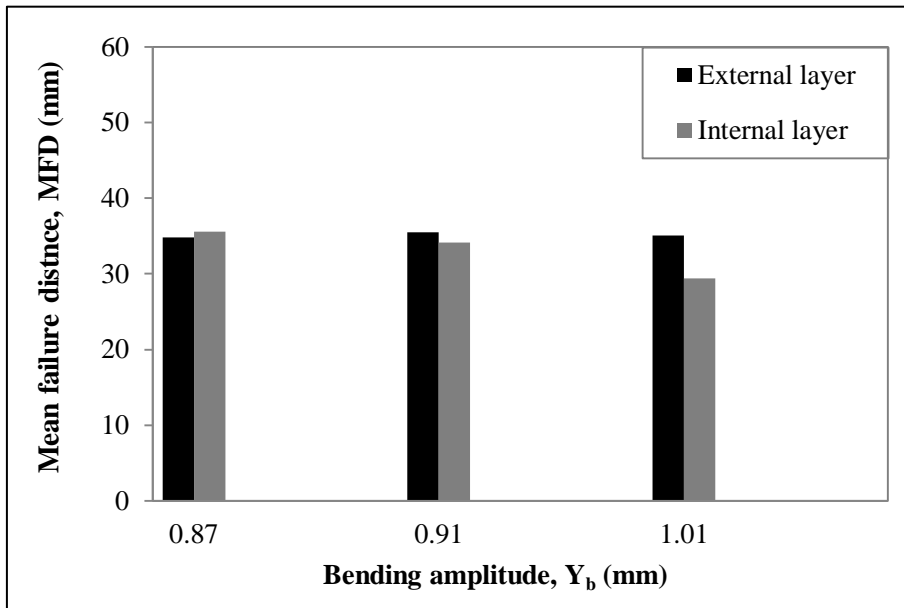


Figure 4.47: Mean failure distance of wire breaks from the suspension clamp mouth function of bending displacement for the AAC Orchid conductor tested at $H/w = 1820$ m

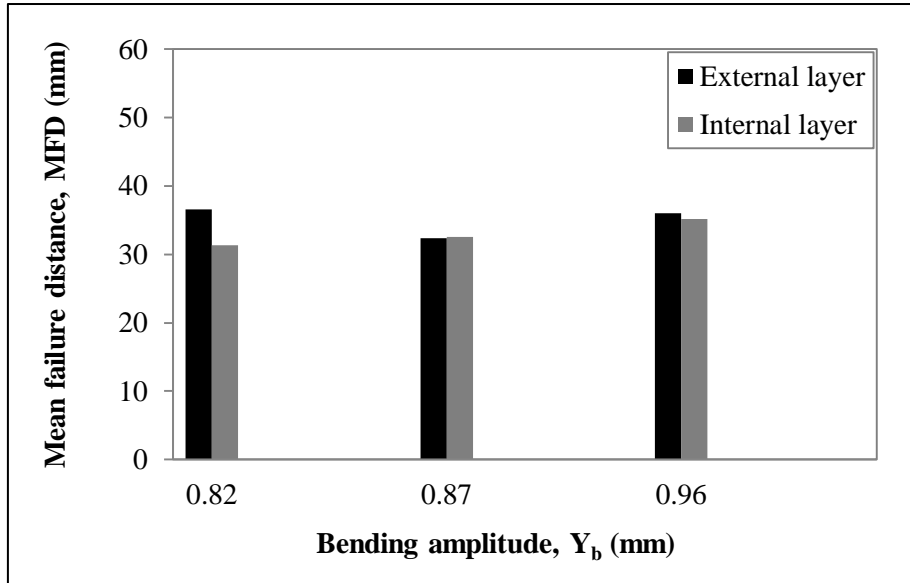


Figure 4.48: Mean failure distance of wire breaks from the suspension clamp mouth function of bending displacement for the AAC Orchid conductor tested at $H/w = 2144$ m

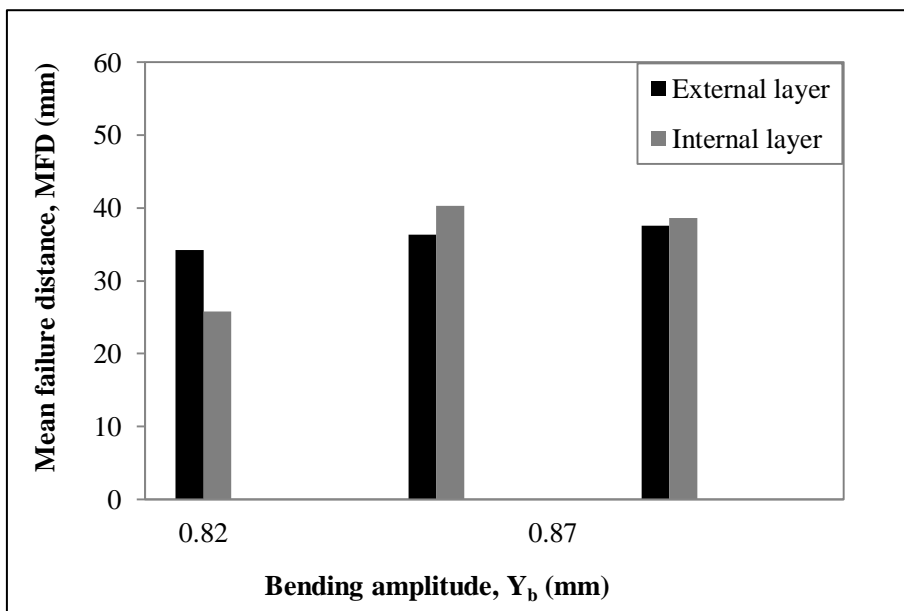


Figure 4.49: Mean failure distance of wire breaks from the suspension clamp mouth function of bending displacement for the AAC Orchid conductor tested at $H/w = 2725$ m

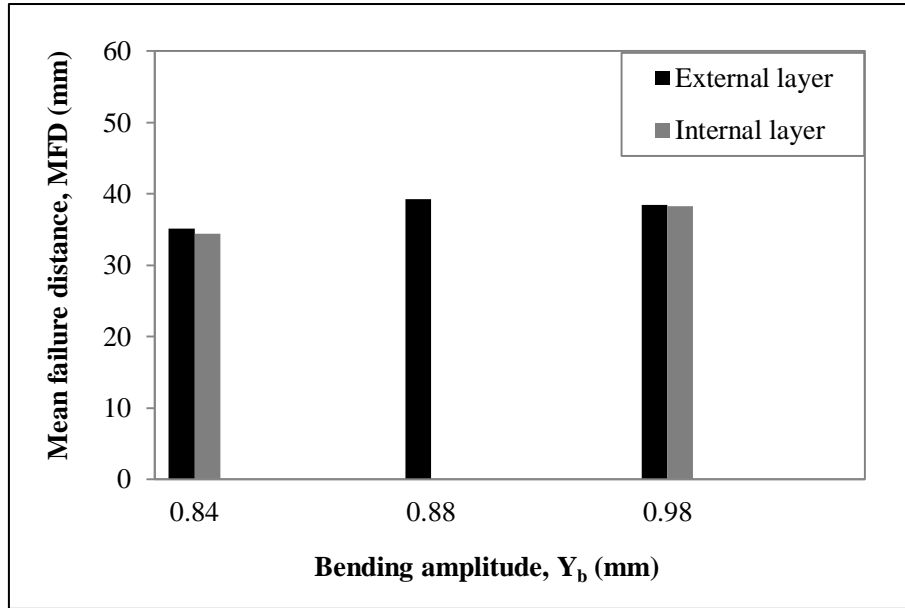


Figure 4.50: Mean failure distance of wire breaks from the suspension clamp mouth function of bending displacement for the ACAR 750 MCM conductor tested at $H/w = 1820$ m

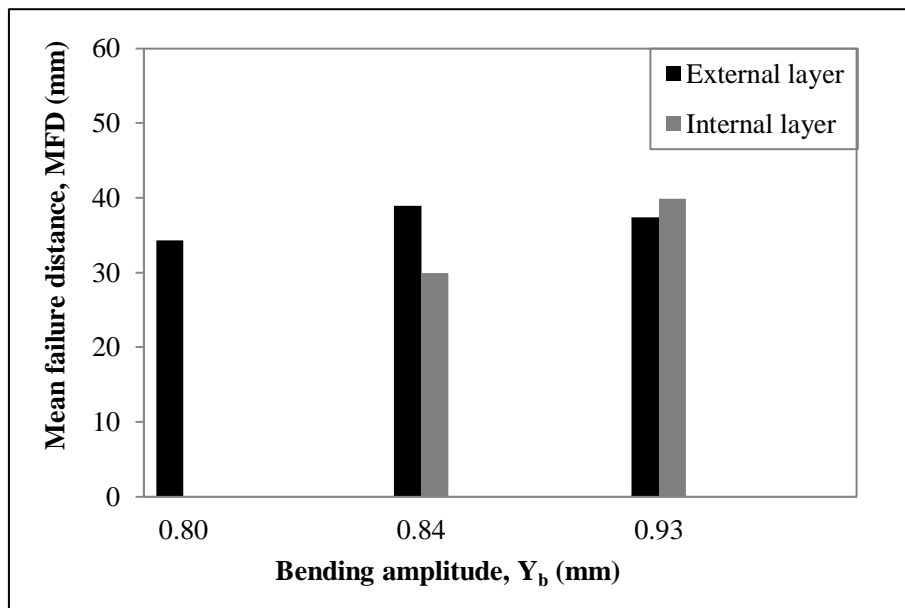


Figure 4.51: Mean failure distance of wire breaks from the suspension clamp mouth function of bending displacement for the ACAR 750 MCM conductor tested at $H/w = 2144$ m

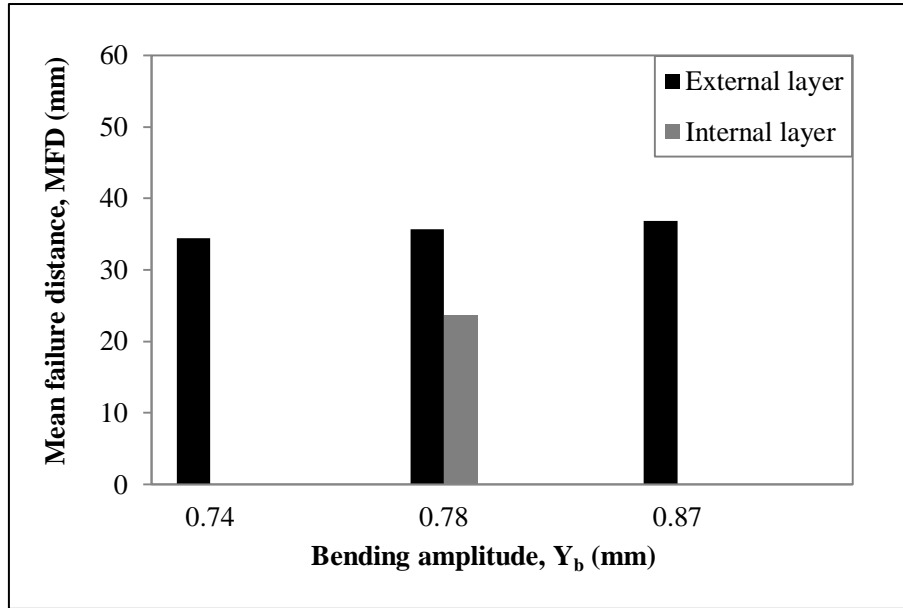


Figure 4.52: Mean failure distance of wire breaks from the suspension clamp mouth function of bending displacement for the ACAR 750 MCM conductor tested at $H/w = 2725$ m

As mentioned above, the importance of the MFD is to predict the wire break location of the conductor to canalize the equipment for maintenance of power line conductors. Thus, the influence of the H/w parameter in function of the distance where the wires break occurred is presented in Figure 4.53. The variation of the mean failure distance is higher for the AAAC 900 MCM conductor and lower for the other three conductors at different values of H/w . Furthermore, there was only little variation of the MFD when the H/w changed from 1820 m to 2144 m and from 2144 m to 2725 m. For the same H/w value, the conductors tested behaviour differently, while the AAC Orchid and ACAR 750 MCM conductor presented almost the same MFD value for the H/w value of 1820 m and 2144 m. It is important to remember that most of the broken wires of the AAAC 900 MCM occurred on the top of the conductor, whereas for the other conductors (ACSR Tern, AAC Orchid and ACAR 750 MCM), they occurred on the base (Appendix E). This behaviour is linked to the material of the broken wires (AA 6201-T81 for AAAC 900 MCM and AA 1350-H19 for the other three conductors) as well as to the diameter of the wires (3.962, 3.38, 3.33 and 3.617 mm respectively for AAAC 900 MCM, ACSR Tern, AAC Orchid and ACAR 750 MCM conductors).

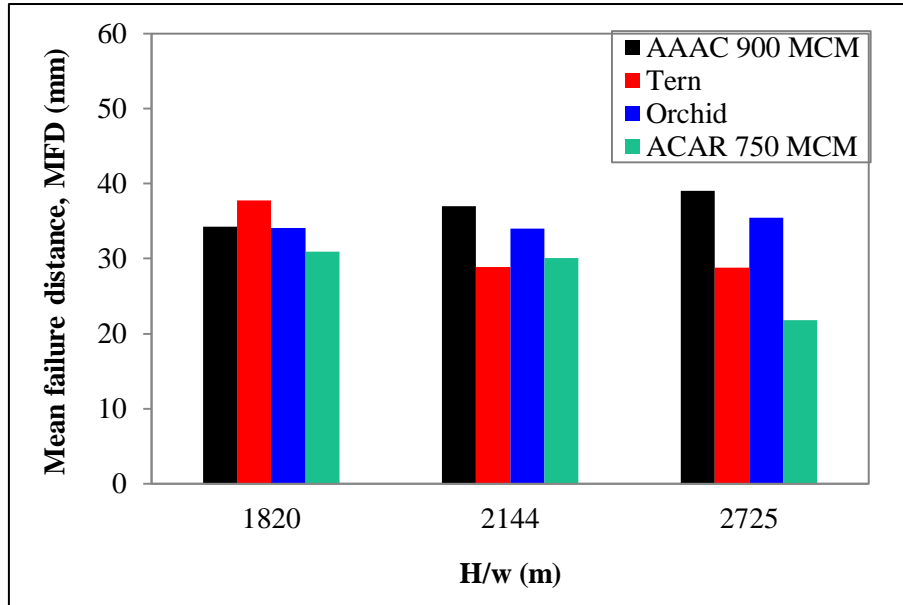


Figure 4.53: Mean failure distance of broken wire measured from the suspension clamp month versus the H/w value for different cables tested

4.4.1.2. Failure analysis related to the layer position

The distribution of failures related to the layer position of the conductors tested (AAAC 900 MCM, ACSR Tern, AAC Orchid and ACAR 750 MCM) for different values of parameter H/w are presented in Appendix F. When the breakage of conductor wires occurred on the outer layer, the wire is indicated by E (external) and by I (internal) when the breakage occurred inside the conductor (Figure 4.54).

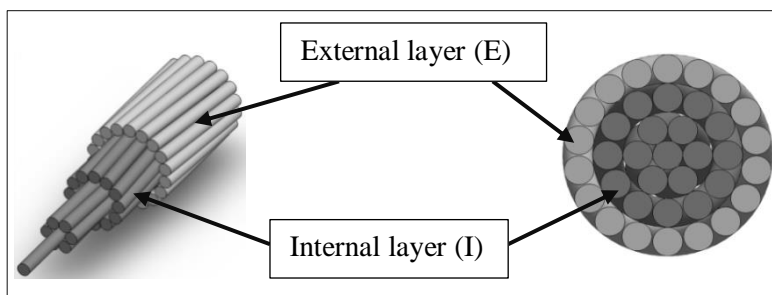


Figure 4.54: Scheme of a conductor with its cross section showing wire from the external (E) and the internal (I) layer

As seen in Appendix F, the percentage distribution of wire breaks were calculated for the tested conductors (AAAC 900 MCM, ACSR Tern, AAC Orchid and ACAR 750 MCM), were shown in Figure 4.55 to Figure 4.58 for the different values of H/w parameter used during the test.

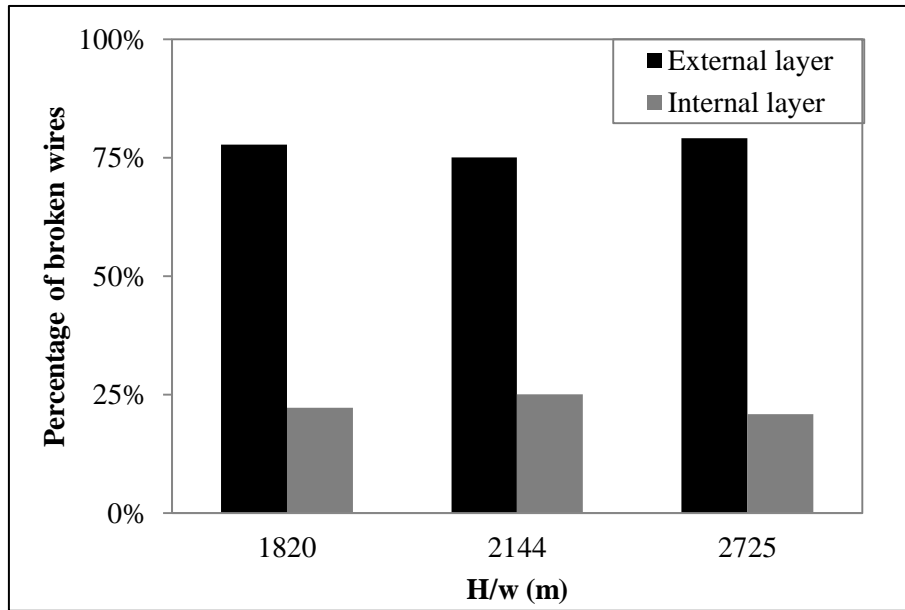


Figure 4.55: Percentage distribution of wire breaks per layer function of the H/w parameter for the AAAC 900 MCM conductor

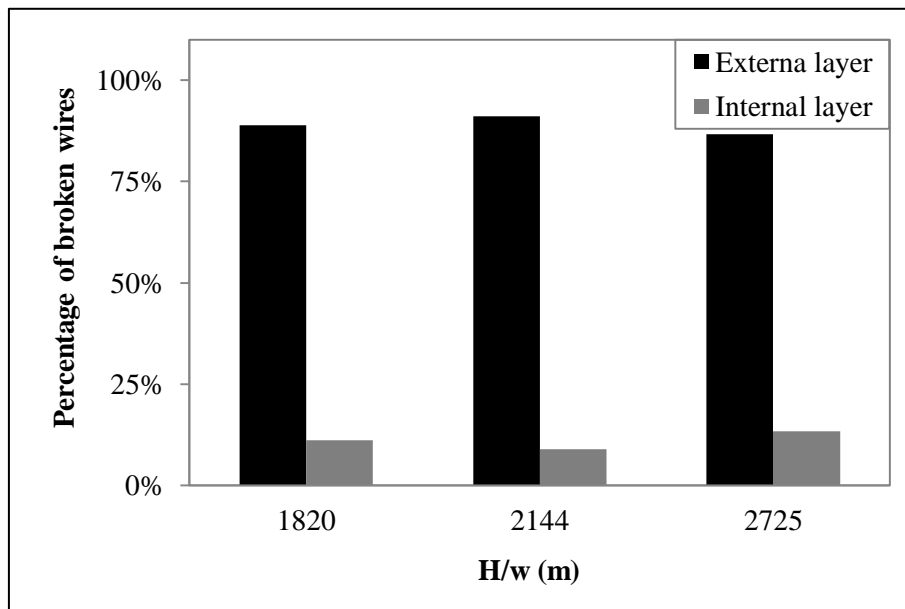


Figure 4.56: Percentage distribution of wire breaks per layer function of the H/w parameter for the ACSR Tern conductor

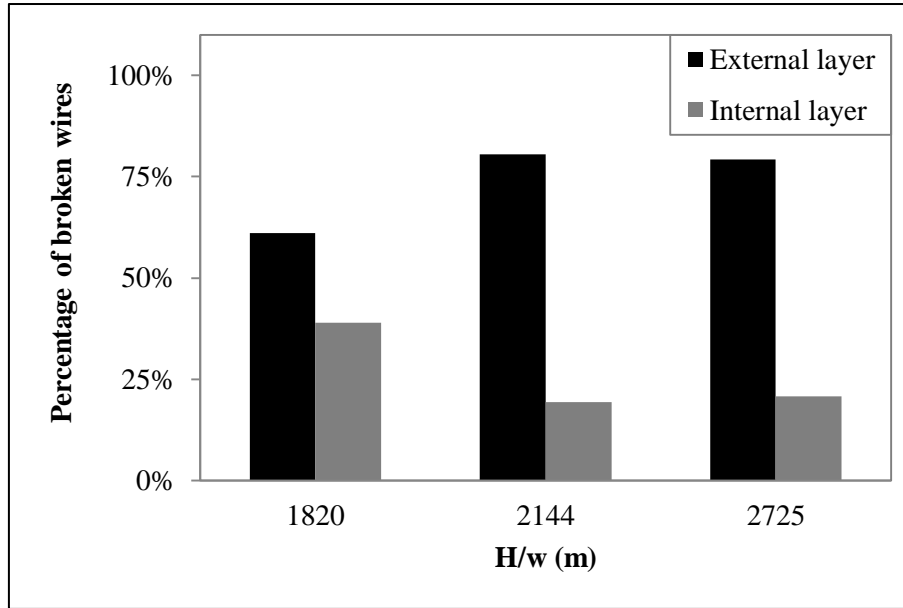


Figure 4.57: Percentage distribution of wire breaks per layer function of the H/w parameter for the AAC Orchid conductor

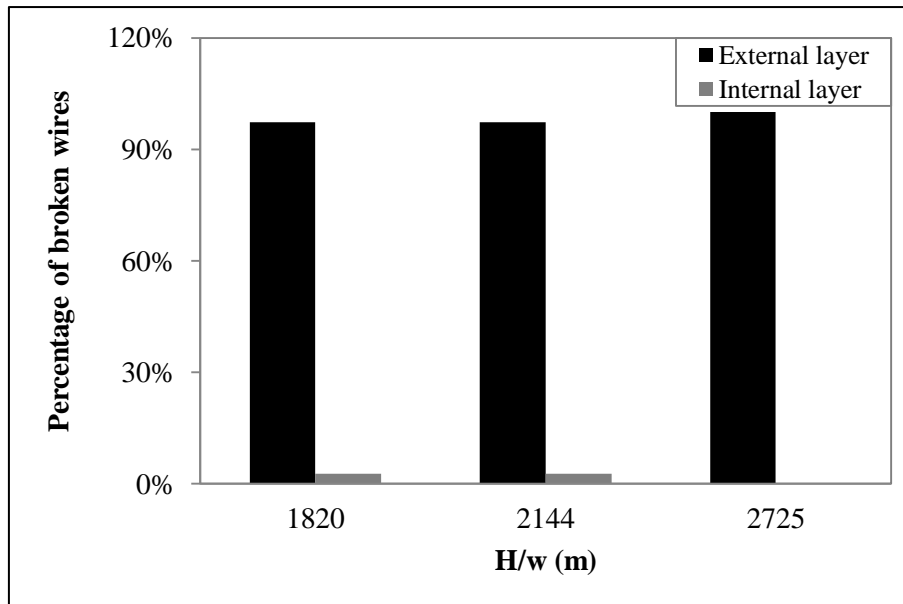


Figure 4.58: Percentage distribution of wire breaks per layer function of the H/w parameter for the ACAR 750 MCM conductor

The analysis of data shows that for all cases, the failure initiates (first wire break) for the external layer for the AAAC 900 MCM, ACSR Tern, AAC Orchid and ACAR 750 MCM conductors. The probability of having a broken wire at an external layer is higher than the internal layer for each value of the H/w parameter. For the same value of H/w , data in Figure 4.59 to Figure 4.61 show that the behaviour of the broken wire relating to the layer position seems to be the same in such a way that the probability for having an external wire break is higher than for internal wire break. However, the probability values are different for each conductor tested (AAAC 900 MCM, ACSR Tern, AAC Orchid and ACAR 750 MCM) for fatigue at different values of H/w parameter. The ACAR 750 MCM conductor presents a higher probability, for each case of H/w value, of having a broken wire from the external layer because of its configuration. The external layer of the ACAR 750 MCM is made of the aluminium AA 1350-H19 and the rest of the layers are in AA 6201-T81. This aluminium has a higher mechanical resistance than the Aluminium AA 1350-H19.

We could notice that most of the broken wires are from outer layers. This situation, identified by other researchers as well, may be associated with the presence of an aggressive superficial damage condition between the suspension clamp and the conductor during vibration. The aggressive condition is presented by the formation of the debris, SiO_2 and Al_2O_3 (Appendix H), between the conductor and the suspension during the fatigue test. This debris has a higher hardness, respectively 1050 and 2000 HV, than the aluminium of a conductor strand (Aggarwal *et al.*, 2000; Azevedo & Cescon, 2002; Fadel *et al.*, 2012)

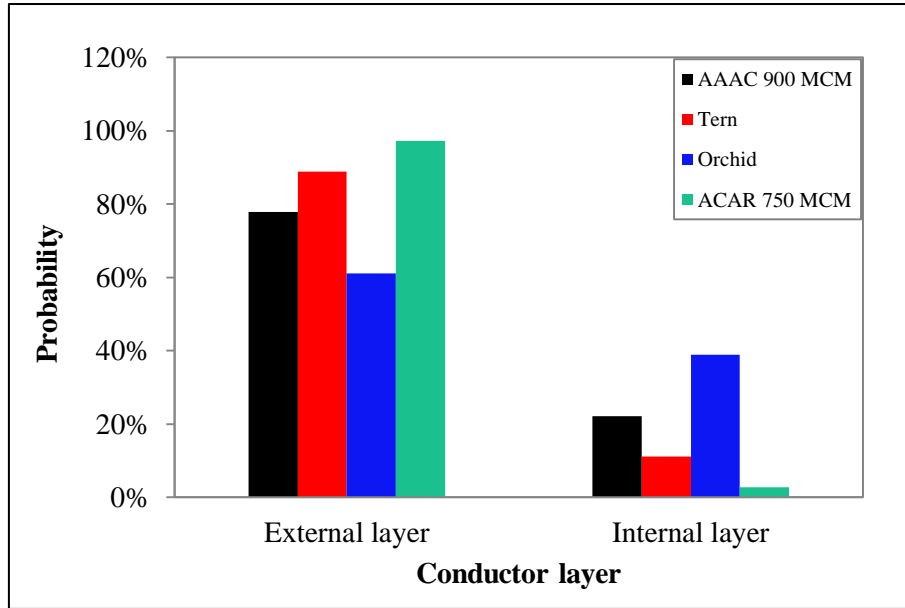


Figure 4.59: Percentage comparison distribution of wire breaks per layer function of the parameter $H/w = 1820$ m for conductors tested

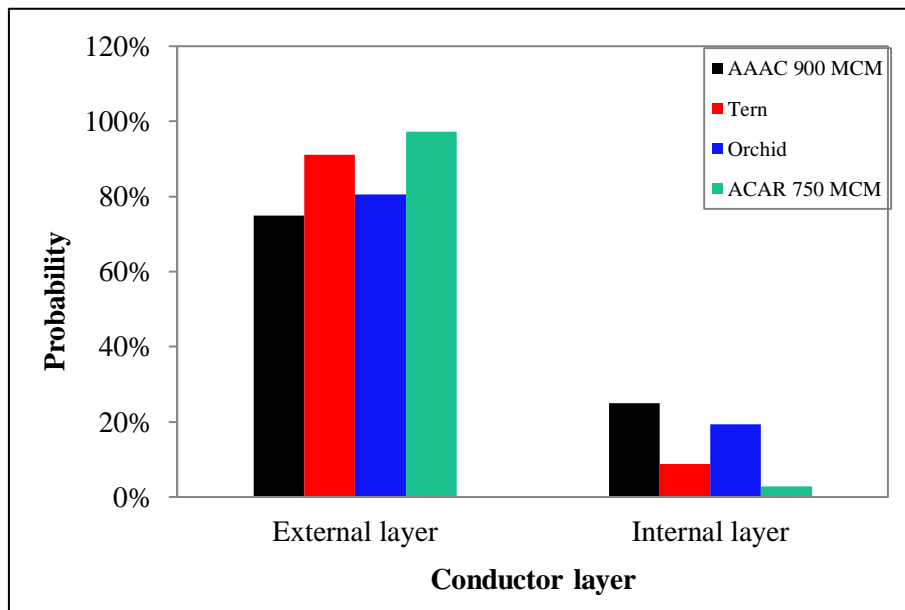


Figure 4.60: Percentage comparison distribution of wire breaks per layer function of the parameter $H/w = 2144$ m for conductors tested

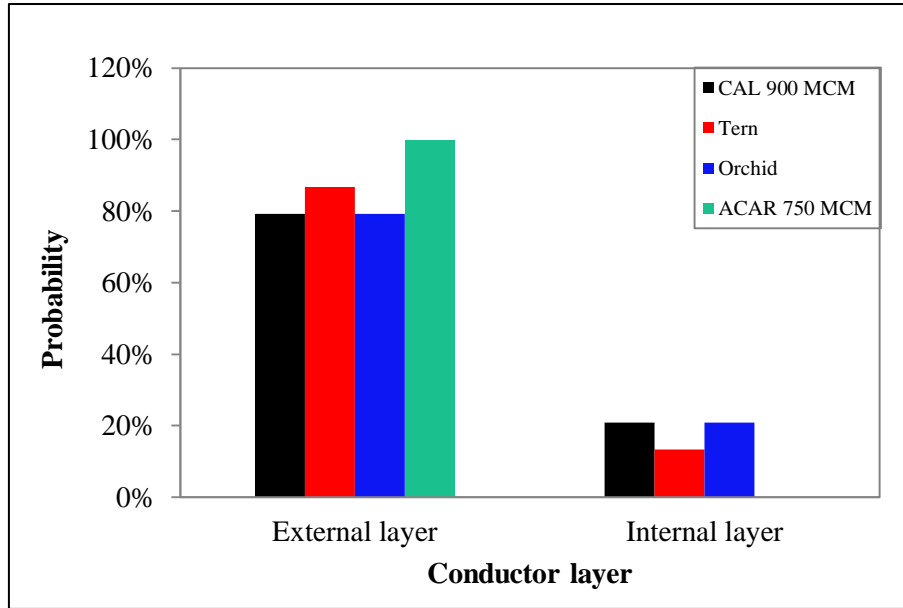


Figure 4.61: Percentage comparison distribution of wire breaks per layer function of the parameter $H/w = 2725$ m for conductors tested

Based on the results presented above, a following discussion can be made on the H/w parameter. At the design stage of a transmission line, perhaps the easiest way to prevent fatigue failure of the conductor is to limit its tension (EPRI, 2006; Kiessling *et al.*, 2003). The control of the tension level in the power line will directly affect the conductor's self-damping, and thereafter its fatigue life (Fadel *et al.*, 2012). As the stranding load increases, the normal contact forces between the wires will also raise, hence the dissipation of frictional energy due to the slip between the wires' contact interface will be reduced for a same wind profile. This means that limiting the level of tension in the cable will prevent excessive bending stresses in the aluminium wires due to severe vibration levels. In this setting, the H/w parameter also takes into account the effect of terrain roughness to determine the most appropriate level of H/w that could be assumed to safely design the line. Limited field data were collected to determine these safe limits for H/w considering different line configurations (single unprotected conductors, single damped conductors, bundled conductors with and without protection, for example) (CIGRÉ, 2005).

It has been pointed out that the H/w parameter represents a clear advance in the design of transmission lines against fatigue due to aeolian vibrations when compared with the former EDS parameter. In contrast with EDS, the H/w parameter is clearly capable of taking into account the diameter of the cable (influencing drag coefficient) and the proportion between steel and aluminium for ACSR conductors (influencing the specific weight and strength) to

define a safe limit value for the tension. Furthermore, the results of the static tests conducted in this research have verified the assumption that H/w controls the measure of the mean stresses in the external layer wires, for cables tested under the different levels of H/w , seems an appropriate one. At a controlled laboratory temperature of 18°C the maximum deviation between the estimated strains (Equation 2.14) in the wires of the external layer and the measured ones was 9% (for the ACSR Tern conductor). Some level of error during strain measurement due to some misalignment during the gauges fixation is quite likely. Although extreme care was taken to position the gauge length aligned as close as possible with respect to the wire's longitudinal direction, there will always be some error involved in this procedure. Then, these results allow us to conclude that the H/w correctly captures the mean (static) stress in the aluminium wires, which has an important effect on the fatigue strength of the material. Moreover, and quite significantly, the results of the fatigue tests for these four conductors allowed us to introduce a new and interesting discussion on the use of the H/w as a solo parameter to design the overhead power line transmission against fatigue. As presented in section 4.2.2, the durability of the ACSR Tern conductor was in average four times higher than the AAAC 900 MCM for the different range of stress amplitudes tested and for the three different H/w values considered (1820 m, 2144 m and 2725 m). This essentially means that the use of a same H/w limit value to design cables made of different configurations can be quite disadvantageous from an economic point of view. To generalise the application of this fatigue design concept to this wide range of cable configurations (ACSR, AAAC, AAC, ACAR), it was necessary to use a lower safe limit value. The tests clearly suggest that it can be excessively conservative to design an ACSR conductor transmission line using an H/w that is appropriate to keep safe a much "weaker" and less durable AAAC. For instance, hypothetically assume that there are two transmission lines constructed, one of them with an ACSR and the other with an AAAC conductor, but so that the wind loads provoke a similar vibration history in these cables. In this specific hypothetic situation, the design of these lines using a same limit value of H/w could provide a safe design for both cables. However, the ACSR would still be safe for a much higher tension in the power line. The fact that the safe tension load in the cable is underestimated will require higher towers and more cable length, and therefore more unnecessary investment to build the line. The determination of a specific H/w limit for each family of overhead conductors could perhaps provide a more optimised design procedure.

4.4.1.3. Failure analysis related to the type fracture of the surface

Four types of fracture surfaces have been identified after the fatigue test on all conductor wire breaks: 1) Quasi-planar (QP) type; 2) 45° type; 3) L type; and 4) V type (Figure 4.62). All four types of fracture surfaces were observed on conductors AAAC 900 MCM, ACSR Tern, AA Orchid and ACAR 750 MCM. The different types were classified according to the value of H/w parameter, as well as by the bending displacement (Y_b) applied at 89 mm from the LPC (last point of the contact) between the conductor and the suspension clamp during the experiment (Appendix G).

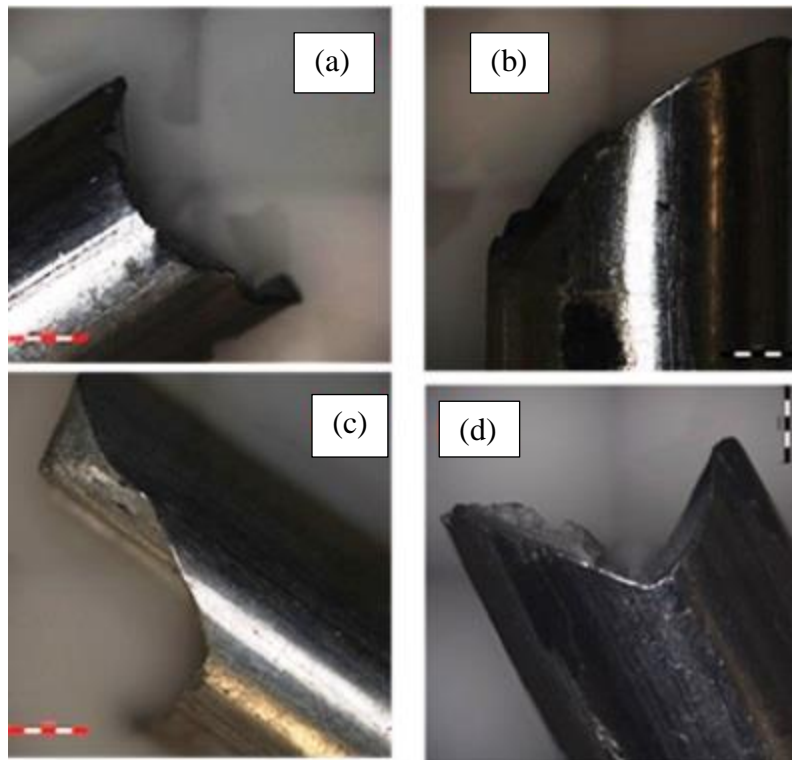


Figure 4.62: Types of strands fracture surface identified on all conductors (AAAC 900MCM, ACSR Tern, AAC Orchid and ACAR 750MCM) tested: (a) Quasi-planar type, (b) 45° type, (c) L type and (d) V type

Data in Appendix F were presented as graphs to facilitate the comparison of fracture type surfaces of wire breaks for different conductors tested in terms of the H/w parameter (Figure 4.63 to Figure 4.66).

The AAAC 900 MCM presented a fractography which included all types presented above. It seems that the type of fracture of the surface does not depend on the H/w parameter for the AAAC 900MCM conductor as the probability of having a type of surface break varied from one H/w value to another (Figure 4.63). Figure 4.64 to Figure 4.66 show the cartography observed, respectively, on the ACSR Tern, AAC Orchid and ACAR 750 MCM conductors. Moreover, these conductors present the behaviour similar to that of AAAC 900 MCM as the probability of the occurrence of the surface fracture type does not depend on the H/w value. We can observe that the QP and 45° type of fracture surface are the most commonly occurring type on the broken wire.

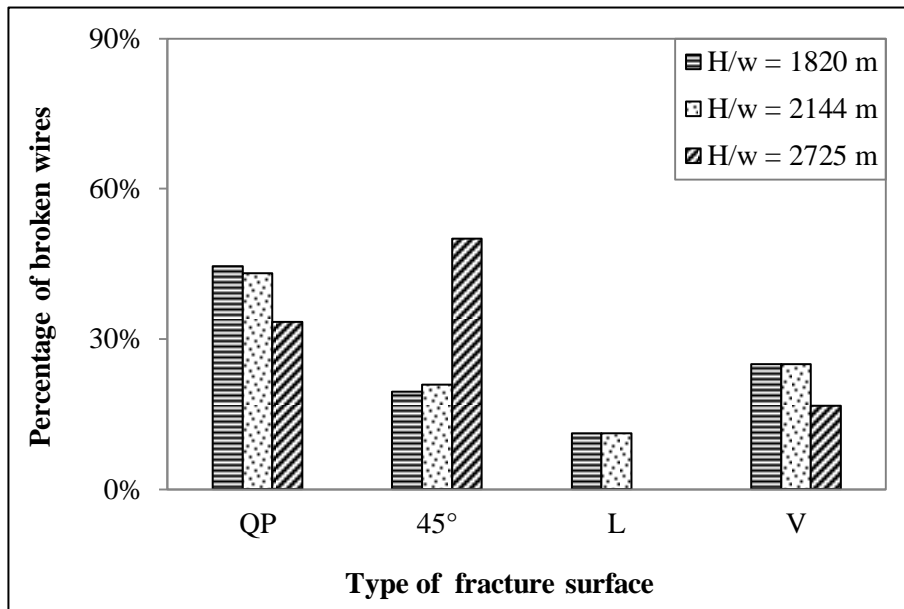


Figure 4.63: Types of fracture surface in function of the different values of the H/w parameter for the AAAC 900 MCM conductor

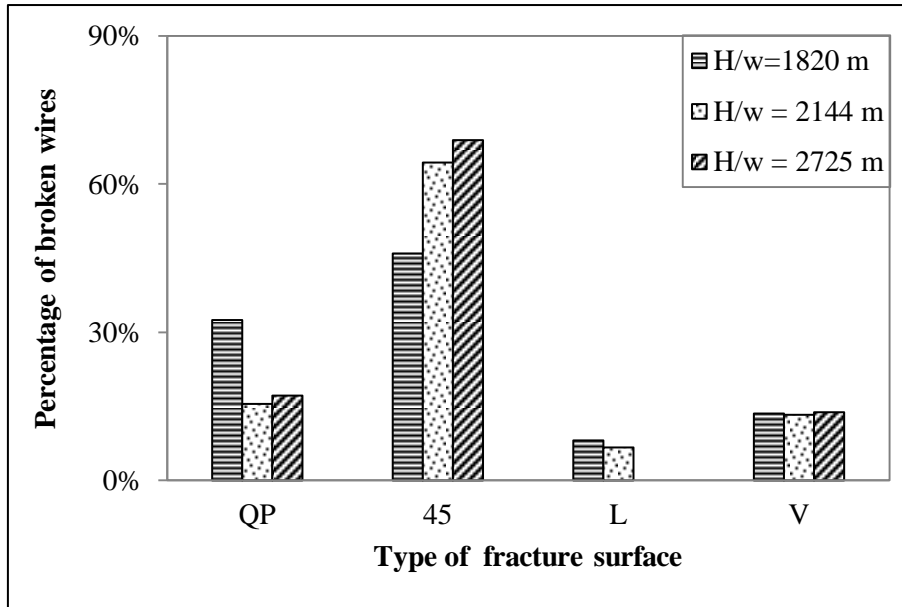


Figure 4.64: Types of fracture surface in function of the different values of the parameter H/w for the ACSR Tern conductor

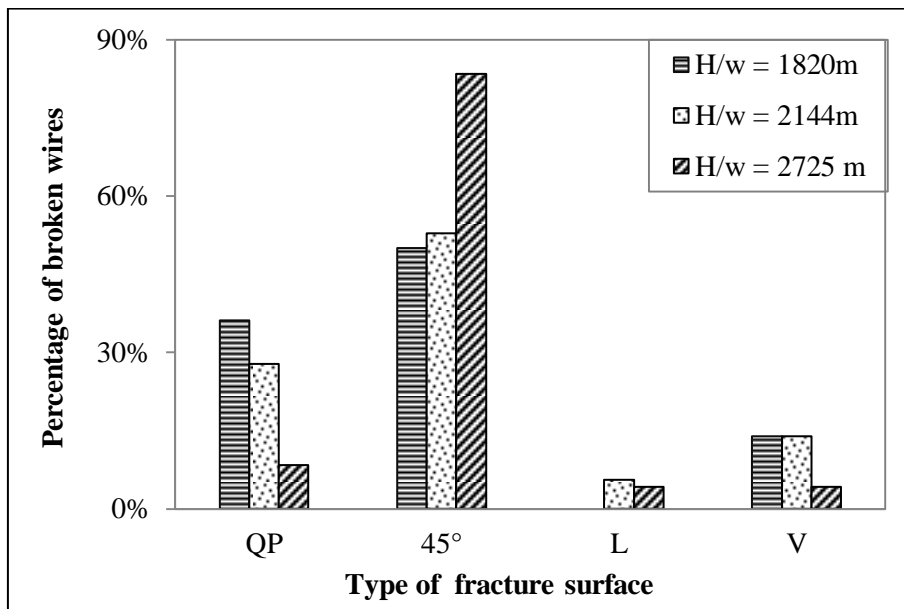


Figure 4.65: Types of fracture surface in function of the different values of the parameter H/w for Orchid conductor

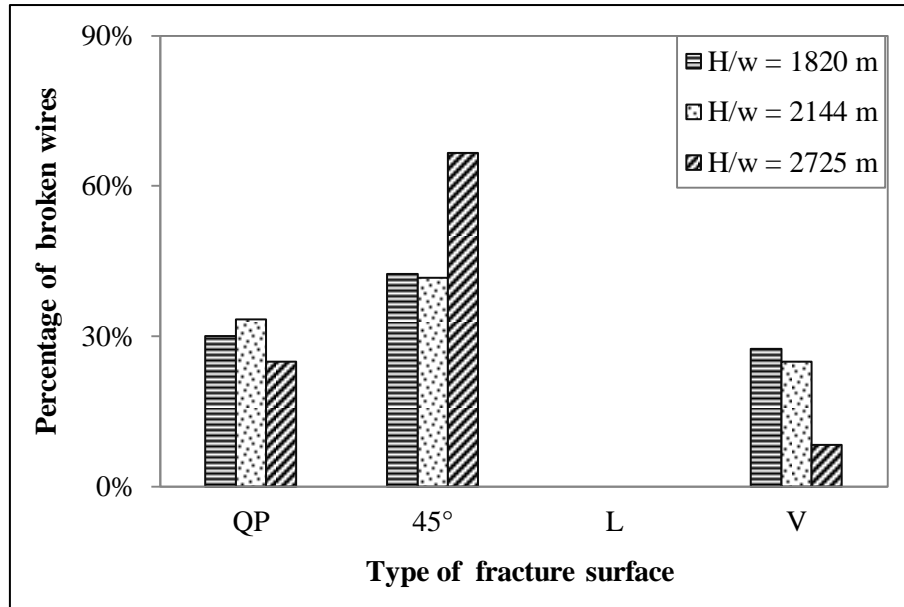


Figure 4.66: Types of fracture surface in function of the different values of the parameter H/w for the ACAR 750 MCM conductor

The comparison of the types of fracture surfaces for AAAC 900 MCM, ACSR Tern, AAC Orchid and ACAR 750 MCM conductors in term of the parameter H/w is presented in Figure 4.67 to Figure 4.69 for different value of H/w parameter (1820, 2144 and 2725 m). Observations determined that the behaviour of occurrence of type of fracture surface is different, even though all conductors tested presented the lowest probability of the L type of fracture surface. From these comparisons, related to H/w , the 45° type has the highest probabilities for the three conductors tested (ACSR Tern, AAC Orchid and ACAR 750 conductors) at all values of the H/w parameter. The AAAC 900 MCM presents, an exception on the preview observation, as the highest probability observed was the QP type however the 45° had the highest probabilities for the $H/w = 2725$ m.

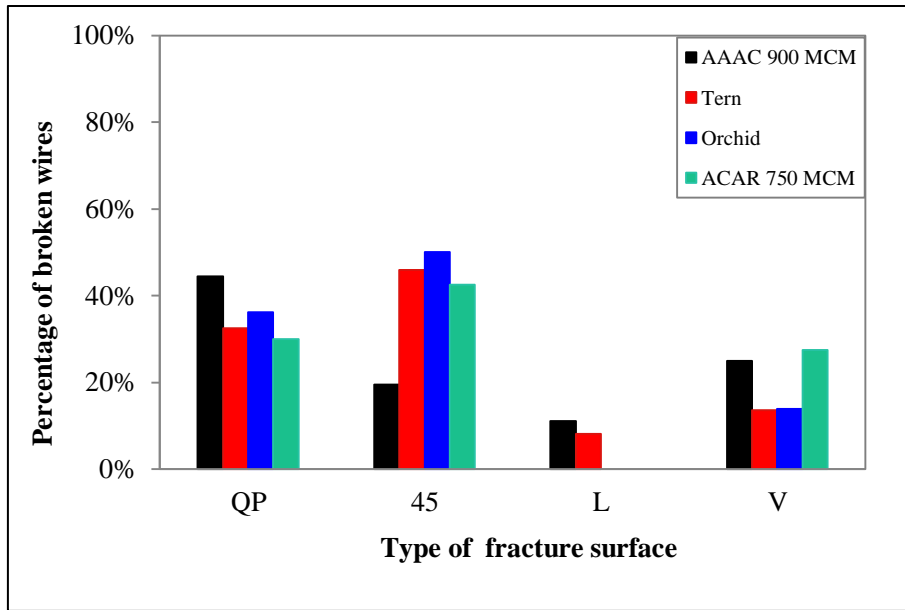


Figure 4.67: Comparison of the types of fracture surfaces for different conductors tested with $H/w = 1820$ m (AAAC 900 MCM, ACSR Tern, AAC Orchid and ACAR 750 MCM)

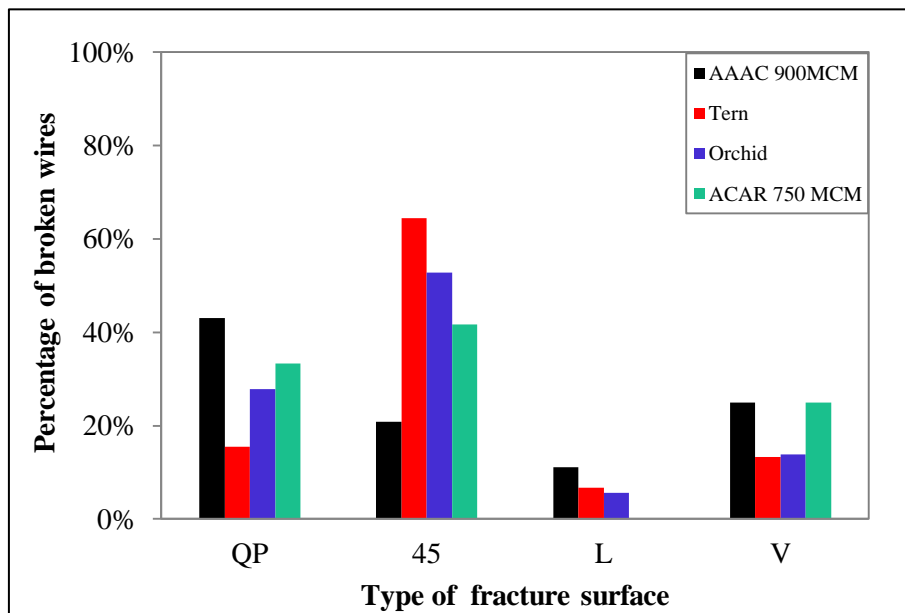


Figure 4.68: Comparison of the types of fracture surfaces for different conductors tested with $H/w = 2144$ m (AAAC 900 MCM, ACSR Tern, AAC Orchid and ACAR 750 MCM)

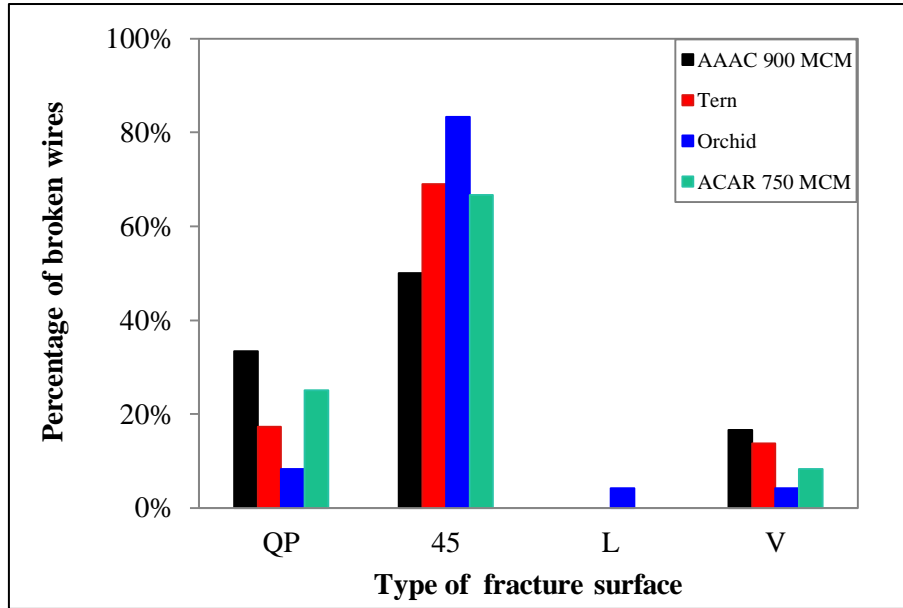


Figure 4.69: Comparison of the types of fracture surfaces for different conductors tested with $H/w = 2725$ m (AAAC 900 MCM, ACSR Tern, AAC Orchid and ACAR 750 MCM)

4.4.2. Microscopic analysis

Microscopic examination of 45° type fractured surfaces of AAAC 900 MCM, ACSR Tern, AAC Orchid and ACAR 750 MCM conductors was conducted with a scanning electron microscope (SEM). These types of fractures were the most commonly encountered following the conductor fatigue test and the failure analyses presented in the subsection 4.4.1.3. The microscopic analysis of the ACAR 750 MCM wires was not presented in this work as they have a similar feature as compared to the AAC Orchid wires. Therefore, through the test, the ACAR 750 MCM is cited at the side of the AAC Orchid and between brackets. Each sample was initially examined using secondary electron imaging to reveal the surface morphology. Additionally, SEM semi-quantitative chemical analysis was performed by energy dispersive x-ray spectroscopy by means of backscattered electron imaging. The fractures were examined in an orientation normal to the wire length and in tilted orientations to obtain more surface details.

For wires of AAAC 900 MCM conductor, most of the fractured surfaces (in both the external and internal layers) were generally transverse to the longitudinal load axis. The fractures had a large relatively quasi-planar zone on one side of the surface (see arrow in Figure 4.70) with a very fine microscopic texture consistent to fatigue fracture. One should

notice that the multiaxial stress conditions in points of the contact interface may generate crack growth in different planes.

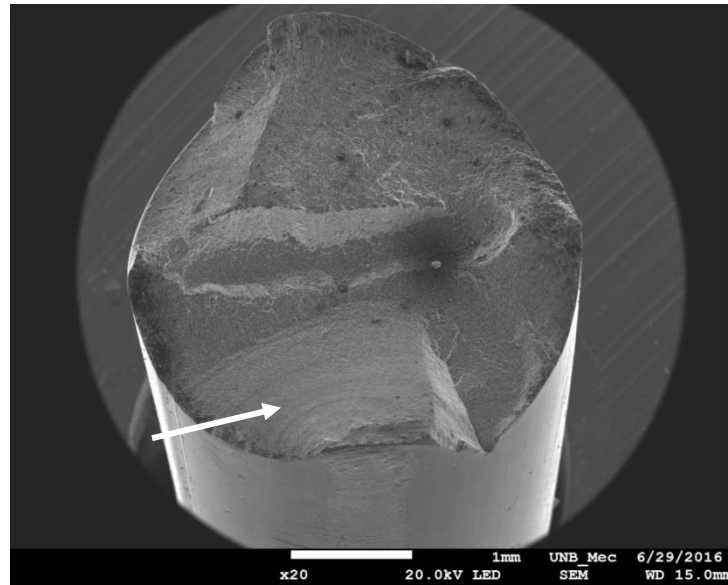


Figure 4.70: Fracture surface of AAAC 900 MCM wire (arrow indicating the quasi-planar area)

Figure 4.71 shows the fracture surface of another AAAC 900 MCM sample. Beach marks from fatigue crack propagation were observed in the quasi-planar portion of the fracture area. The radial markings indicated a single crack initiation site at the surface of the wire (Figure 4.71(a) and (b)). The crack origin is coincident with a fretting wear mark (Figure 4.71(b)) caused by small relative motion at the wire-to-wire contact from different layers or external layer to the suspension clamp during the oscillation of the cable. An high-magnification view in the beach marks zone showed the presence of striations mark which are feature of fatigue failure (Figure 4.71 (d)). The failure progressed through the wire until the applied load caused the remaining section to fail by ductile fracture where dimples were observed (Figure 4.71(c)). As observed in Figure 4.72, the contact surface is typical of a mixed fretting regime, where there is a clear subdivision of the contact area in a central stick zone and a surrounding, annular slip zone.

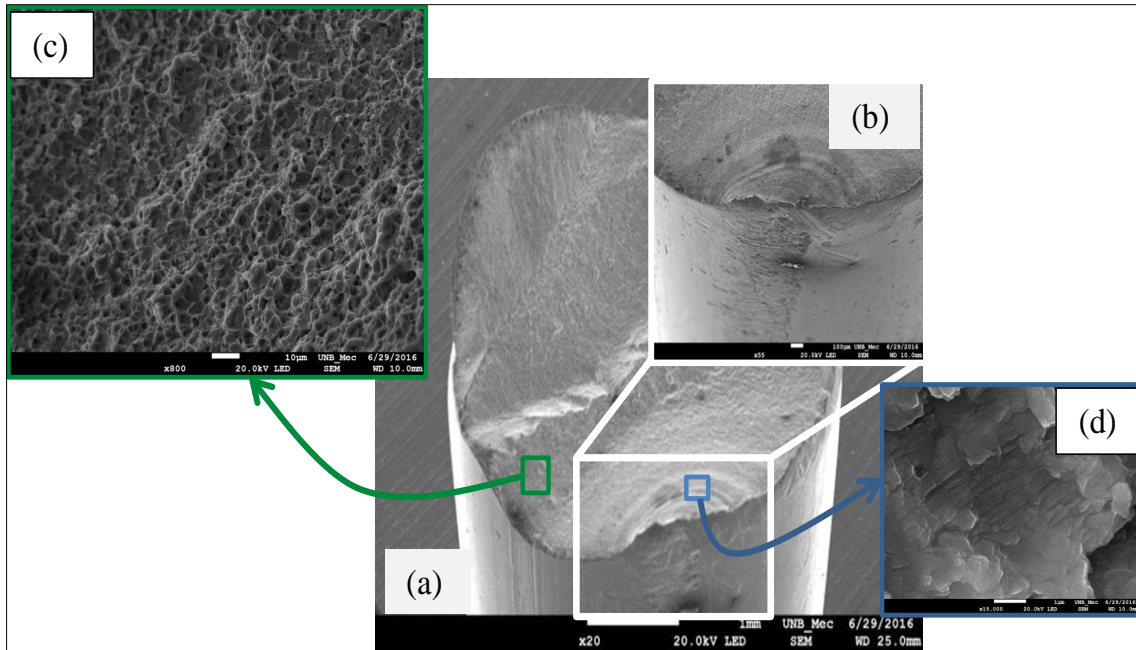


Figure 4.71: SEM of the fracture surface of an AAAC 900 MCM strand: (a) crack initiated in the fretted region and beach marks; (b) zoom of the crack initiation point; (c) dimples and (d) the striations mark.

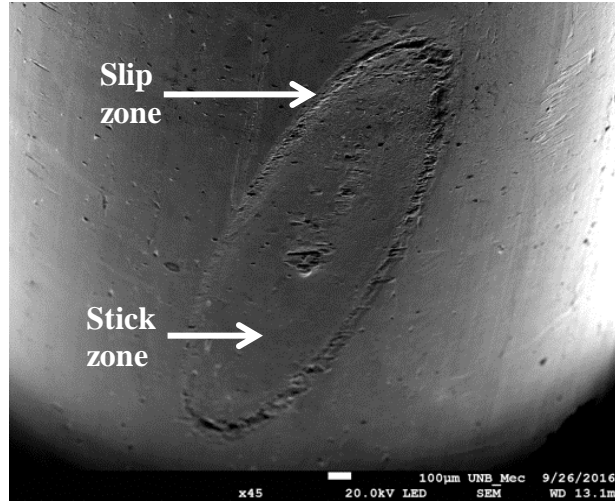


Figure 4.72: Elliptical contact zone in an Aluminum wire (AAAC 900 MCM) from the external layer showing mixed stick/slip fretting regime

For the samples originated from ACSR Tern and AAC Orchid (ACAR 750 MCM) conductor, most of the fractured surfaces were oblique, inclined at an angle around 45° with the longitudinal direction of the wire (Figure 4.73). Usually there was a very small quasi-planar zone on one side of the wire (green arrow). Massive indentation, caused by

the suspension clamp used to sustain the conductor during the fatigue test, can also be identified in Figure 4.73, while the fretting scar and the very small quasi-planar zone can be observed in Figure 4.74.

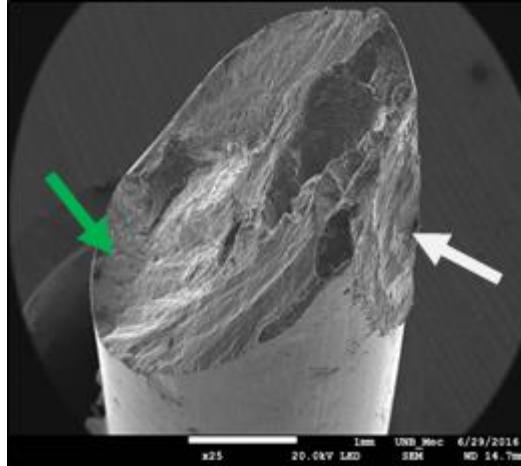


Figure 4.73: Fractured surface of Aluminum 1350-H19 wire, obtained from ACSR Tern conductor after fatigue test, with crack propagation at an oblique angle. Massive clamp indentation is shown at the right edge (arrow)

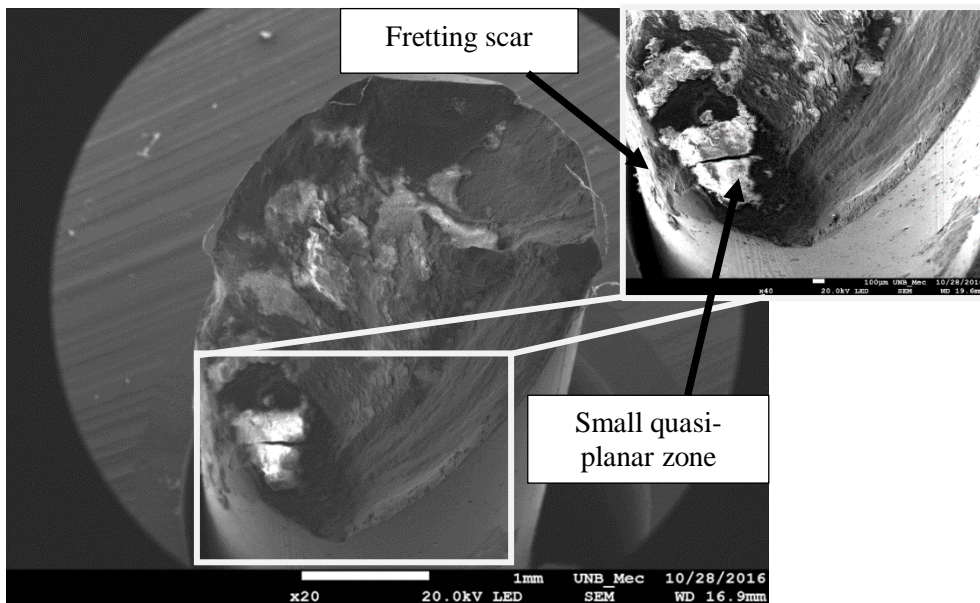


Figure 4.74: SEM of the fracture surface of an ACSR Tern conductor showing the fretting scar and a small quasi-planar zone

Most of the remaining areas of the cross section for the fractured ACSR Tern and AAC Orchid (ACAR 750 MCM) wire showed dimpled fracture morphology, characteristic of a ductile fracture mechanism, as presented in Figure 4.75.

In the crack initiation zone, striation and micro cracks were observed for samples aluminium AA 1350-H19 , AAC Orchid (ACAR 750 MCM) conductor and ACSR Tern (Figure 4.76). Previous researchers reported the same fatigue marks on the broken wires (Fadel *et al.*, 2012; Hou *et al.*, 2016).

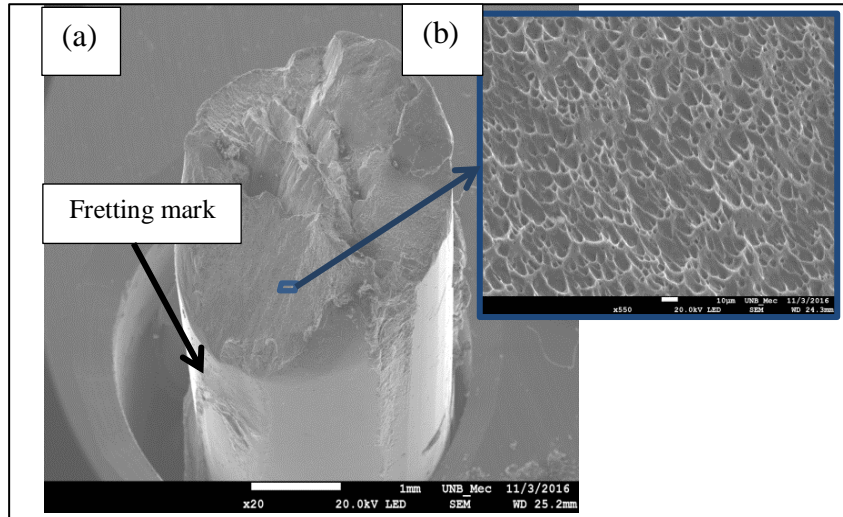


Figure 4.75: Fracture surface of an AAC Orchid conductor showing the fretting mark (a) and (b) the dimples.

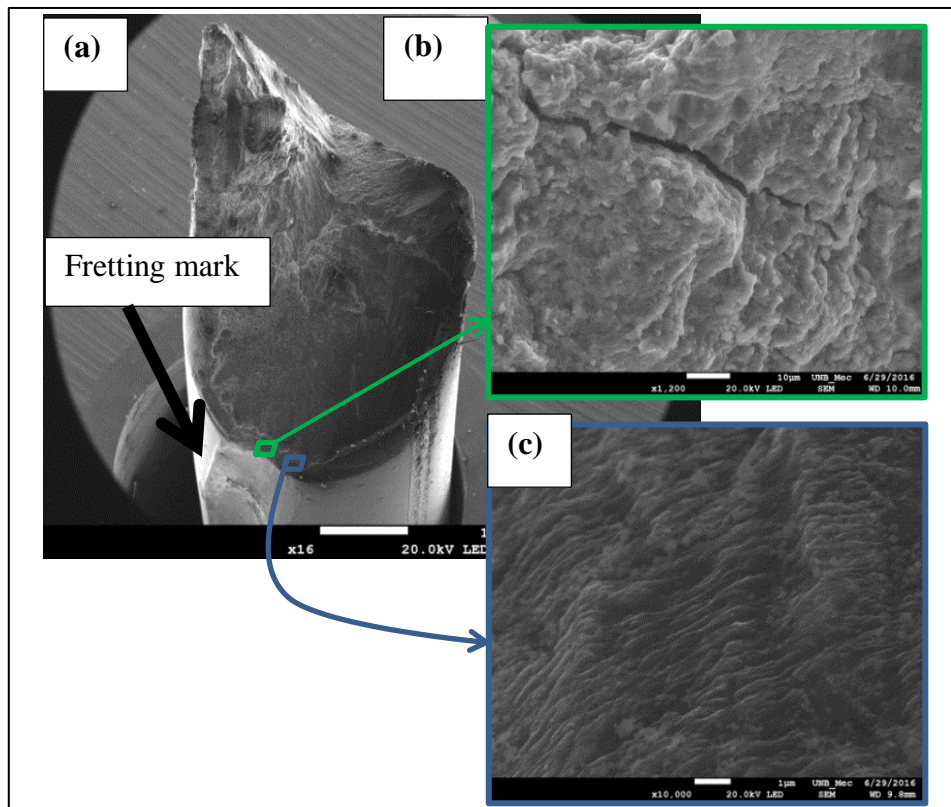


Figure 4.76: Fracture surface of an ACSR Tern conductor showing (a) the fretting mark, (b) the micro crack and (c) the striations mark.

For the samples originating from ACSR Tern, AAC Orchid and ACAR 750 MCM conductor, most of the fractured surfaces were oblique, inclined at an angle around 45° with respect to the longitudinal direction of the wire (Figure 4.73). Other researchers identified a similar failure pattern for broken wires of ACSR conductors (Grosbeak & Ibis) (Fadel *et al.*, 2012; Azevedo *et al.*, 2009; Hou *et al.*, 2016), meanwhile the V type and the quasi-planar types were also reported. A very small quasi-planar zone on one side of the wire was generally observed on the broken wire made of aluminium AA1350-H19. In the case of the ACSR Tern, AAC Orchid and ACAR 750 MCM conductors, the researcher argued that, due to the reduced yield strength and high ductility of Aluminium AA 1350-H19, the final fracture tends to occur in planes of maximum shear stress. Although the state of stress in the crack initiation point is quite complex for this case, the stress gradient generated by the contact is severe and therefore will decay at a short distance from the contact interface. From this point onwards, it seems reasonable to assume that the longitudinal normal stress to the wire (caused by the pre-static load and by the cyclic bending) will be the dominant stress component. Hence, the plane of maximum shear stress should be inclined, close to 45° , with respect to the longitudinal direction of the wire.

Failures in the strands of the AAAC 900 MCM were generally transverse to the longitudinal load axis. The fracture surface had a relatively large quasi-planar zone on one side of the wire. The failure progressed through the wire until the applied load caused the remaining section to fail by ductile fracture. Here the crack propagation area was clearly much larger than for the AA 1350-H19 (ACSR Tern, AAC Orchid and ACAR conductor). The fatigue process progressed in planes of high normal stress (mode I dominated) and only a small part of the final ductile fracture seemed to be shear dominated. This difference in the aspect of the fracture surface compared with the ones in the pure Aluminium (AA 1350-H19) wires may be associated with its much higher strength.

The fractography applied to the strands of the conductors tested by fatigue showed signs of fatigue features such as beach marks, micro cracks and striations. The cracks always initiated from the fretting mark which is due to the contact between the outer layer of conductor and the suspension clamp or inner layer conductor contact. But, the beach marks were difficult to observe on some fracture surfaces of strands, especially for the strands from the pure Aluminium (AA 1350-H19). However, this did not exclude the fact that the strands failed by fatigue, as mentioned earlier. The energy dispersive x-ray spectroscopy microanalyses were completed on the surface fracture of the wire breaks, revealing the

presence of Oxygen (O) and Silicon (Si) which combined with Aluminium (Al) to form the Al_2O_3 and SiO_2 . One of the energy dispersive x-ray spectroscopy microanalyses of different strands of conductors tested are presented in Appendix H.

The analysis of the fracture surfaces revealed that the cracks in the wires always initiate within the fretted zones. Therefore, it seems clear that the fatigue phenomenon in the cable should be governed by local contact stresses in addition to the static stresses due to the tension load and to the bending stresses in the wires. These contact stresses strongly depend on the geometry and clamping loads in the cable/clamp assembly beside the static tension load in the cable. In this setting, to capture in the fatigue analysis the influence of local parameters, such as normal and shear stress between wires, coefficient of friction and surface roughness, a more refined stress analysis would be necessary. It is important to note that a given cable, under the same H/w , could experience quite different fatigue lives, if using a different clamp geometry (and/or with a different surface finishing) or clamping the cable with different pressure levels (different torques in the screw system of the suspension clamp will provide different pressure distribution on the cable surface).

CHAPTER 5

CONCLUSIONS AND RECOMMENDATIONS

5.1. Conclusions

The goal of this research was to investigate the suitability of the H/w parameter as a means to evaluate the fatigue life of conductors via a comparative study involving four types of conductors. For this purpose, a methodology and an experimental procedure for determining fatigue life were developed and applied to AAAC, ACSR, AAC and ACAR conductors to establish their fatigue life function of the H/w parameter. This was followed by failure analysis on each conductor tested. Based on both theoretical studies available in the literature and experimental results obtained in the present study, the following observations were made:

- The fatigue lives for the various conductors tested at the same H/w level and amplitude of stress (AAAC 900 MCM, ACSR Tern, AAC Orchid and ACAR 750 MCM) are different. For instance, the fatigue performance of the AAAC 900 MCM conductor is qualitatively lower than that observed for the other conductors. While comparing mean fatigue lives, it was found that the ACSR Tern and AAC Orchid conductors presented, respectively, a fatigue life almost four and two times higher than that of AAAC 900 MCM when subjected to the same bending stress. This ratio tends to increase at lower bending amplitudes (bending stress) and decrease at higher bending amplitudes. Meanwhile, the AAC Orchid and ACAR 750 MCM conductors presented the similar fatigue lives.
- Measurements at controlled laboratory conditions (18° C) proved that the mean stress in the aluminium wires of cables tested (AAAC 900 MCM, ACSR Tern, AAC Orchid and ACAR 750 MCM) for consideration in this work can in fact be approximated by a linear function of the H/w parameter.
- The fatigue life of the conductors tested increased when the H/w decreased, and vice-versa. The behaviour described above underscores the need to maintain the

levels of dynamic stresses at very low values when increasing the H/w value. Thus, it should be emphasised that the use of dampers is necessary when the conductor is subjected to higher bending amplitude due to Aeolian vibrations and also to higher H/w value.

- For a same life, 10^6 cycles as a reference, the constant life diagram has shown that the fatigue bending displacement of the ACSR Tern is 30 to 40% higher than for the AAAC 900 MCM. This ratio value is little small (25-30%) when comparing the AAAC 900 MCM to the AAC Orchid (ACAR 750 MCM) conductor.
- Cracks always initiated in the fretted regions and in the AAAC 900 MCM were dominated by quasi-planar and 45° type of failures in the wires, while in the ACSR Tern, AAC Orchid and ACAR 750 MCM conductors, they were predominantly inclined at approximately 45° .
- Based on the failure criterion, the ACSR Tern conductor has an almost 91.67% probability of having an external layer; meanwhile, the AAAC 900 MCM presents a probability of 75% for the same H/w value of 2144 m. Concerning the external wire break, the probabilities are 8.33% and 25% respectively for the ACSR Tern and AAAC 900 MCM conductors, showing that the failure of the ACSR Tern conductor can be determined by observing the external layer, but for the AAAC 900 MCM, it is necessary to observe the internal layer as well. For the same H/w value, the behaviour of wire breakage is different for the ACSR Tern conductor to the AAAC 900 MCM conductor. For the value of $H/w = 2144$ m, the ACSR Tern conductor presented almost the same behaviour as the AAC Orchid
- Concerning the types of wire breaks, the ACSR Tern, AAC Orchid and ACAR 750 MCM conductors presented a higher probability of wire break type at 45° while the AAAC 900MCM presented the higher probability of wire break type in quasi-planar. This demonstrates that the breakages are different for the AAAC 900 MCM and the others conductors tested (ACSR Tern, AAC Orchid and ACAR 750 MCM conductors).

- The analysis of the break position from the mouth of the suspension clamp confirmed the occurrence of the break within the suspension clamp, usually in the top of the suspension clamp for AAAC 900 MCM and in the base for the other conductors tested (ACSR Tern, AAC Orchid and ACAR 750 MCM conductors), where visual inspection was not possible.

Based on the above observations, and supported by analysis of the experimental results obtained in this study, it is evident that the H/w parameter represents a clear advance in the design of transmission lines against fatigue due to Aeolian vibrations when compared to the EDS parameter. The H/w parameter controls the mean stress in the external layer wires, which is one of the fatigue parameters influencing the fatigue of overhead conductors. For the same values of H/w , the four conductors presented different fatigue lives as well as different behaviours. This statement refuses collaboration with H/w proponents who believe that all conductors stretched with the same H/w value will have the same fatigue life. Rather than using only the H/w parameter or the EDS criteria for power line design or maintenance, it is reasonable to use the H/w parameter associated to the static tensile stress in the aluminium wire function of the field temperature. Furthermore, as clearly pointed out in this study, the mechanical fatigue of a component often takes two parameters into account: the mean stress and the bending stress.

5.2. Recommendations and suggestions

Recommendations for future research from the experimental perspective are postulated below:

- Comparing of curves obtained to model the influence of mean stress on conductor fatigue life function of the H/w parameter, such as those used by Goodman, Gerber, Smith-Watson-Topper, Walker... model.
- Establishing a link between the observed details (for example, type of surface wire break, fatigue marks) with the mode of conductor dynamic loading, studies which will be useful in the investigation of power line conductors when they fall.
- Referring to the previous recommendation, a similar study could be conducted on the suspension clamp mark after the fatigue test.
- Developing more refined fatigue design procedures for overhead conductors, taking into account not only a simulation of the wind loading on the cable (fluid/structure

interaction) to obtain the fatigue loading on the component, but also a numerical computation (by Finite Element Analysis) of the stress field in the wires within the cable/clamp assembly. This would allow us to include the local characteristics of the contact problem (multiaxial stresses, non-proportional loading and stress gradient effects, for example) in consideration of the life estimation.

References

- Aggarwal, R.K., Johns, A.T., Jayasinghe, J.A.S.B., Su, W., 2000, An overview of the condition monitoring of overhead lines, *Electric Power Systems Research*, Vol. 53, pp. 15–22.
- Araújo, J.A., 2014, *Curso de fadiga em cabos condutores*, Departement de Engenharia Mecânica, Universidade de Brasília.
- Azevedo, C. R. F., Henriques, A. M. D., Pulino Filho, A. R., Ferreira, J. L. A., Araújo, J. A., 2009, Fretting fatigue in overhead conductors: Rig design and failure analysis of Grosbeak aluminium cable steel reinforced conductor, *Engineering Failure Analysis*, 16, 1, 136-151.
- Azevedo, C.R.F. and Cescon, T., 2002, Failure analysis of aluminium cable steel reinforced (ACSR) conductor of the transmission line crossing the Paraná river, *Engineering Failure Analysis*, 9, pp 645–664.
- Barrett, J.S. and Motlis, Y., 2001, Allowable tension levels for overhead line conductors, *IEEE Transmission Distribution*, Vol. 148, No , pp 54-59.
- Braga, G.E., Nakamura, R., Furtado T.A., 2004, *Aeolian vibration of overhead transmission line cables: Endurance limits*, New York: IEEE Press.
- Brunair, R.M., Ramey, G.Ed., Duncan, R.R., 1988, An experimental evaluation of S-N curves and validity of Miner's cumulative damage hypothesis for an ACSR conductor, *IEEE Transactions On Power Delivery*. New York, p. 1131-1140.
- Campbell, W.E., 1969, *Fretting in boundary lubrication: A review of wold literature*, ASM.
- Cardou, A., 2002, *Fretting Fatigue under spectrum load in application to overhead electrical conductors*, Report, Literature Review, University of Laval.
- CEPEL, *Centro de Estudos de Produção de Energia Elétrica*, 2015, *Atlas de Potencial Eólico Brasileiro*, Available:
http://www.cresesb.cepel.br/publicacoes/download/atlas_eolico/mapas_1a.pdf.

- Chow, G.C., 1960, Tests of equality between sets of coefficients in two linear regressions, *Econometrica*, Vol. 23, No 3, pp. 591-605.
- CIGRÉ B2.11.04-273, 2005, Overhead conductor safe design tension with respect to aeolian vibration
- CIGRÉ SC22 WG04, 1988, Endurance capability of conductors, Final Report Paris, 19p.
- CIGRÉ Study Committee 22 (working group 04), 1979, Recommendation for the evaluation of the lifetime of transmission line conductors, *Electra*, 63, 103-145.
- CIGRÉ, SC22, WG04, 1985, Guide for endurance tests of conductors inside clamps, *Electra*, No100, pp. 77-86.
- Cloutier, L., Dalpé, C., Cardou, A., Hardy, C., Goudreau, S., 1999, Fatigue test: Flexural stiffness and fretting Behavior, Third Intl. Symp., On Cable Dynamics, Trondheim, Norway, pp. 197-202
- Dastous, J.B., 2005, Nonlinear finite element analysis of stranded conductors with variable bending stiffness using the tangent stiffness method, *IEEE Transactions On Power Delivery*, New York, pp. 328-338.
- Dulhunty, P.W., 1971, Some recent field experiences with vibration dampers, CIGRÉ ISC22 71WG04.
- Eden, E.M., Rose W.N., Cunningham F.L., 1911, The endurance of metals, *Proc. I. Mech.*, 4,139.
- Edwards, A.T. and J.M. Boyd, 1963, Ontario hydro live-line vibration recorder for transmission line conductors, : *IEEE Transactions on Power Apparatus and Systems*, vol 82, issue 66, pp 269-273.
- EPRI, 2006, Transmission line reference book: Wind induced Conductor motion. EPRI, Palo Alto, CA.
- Fadel, A.A., 2010, *Avaliação do efeito de tracionamento em elevados Níveis de EDS sobre a resistência em fadiga do condutor IBIS (CAA 397,5 MCM)*. Tese de doctorado em

Ciências Mecânicas, Publicação ENM.TD-005/2010, Departamento de engenharia mecânica, Universidade de Brasília, Brasília, DF.

Fadel, A.A., Rosa, D., Murça, L.B., Ferreira, J.L.A., Araújo, J.A., 2012, Effect of high mean tensile stress on the fretting fatigue life of an Ibis steel reinforced aluminium conductor, *International Journal of Fatigue* 42, pp 24-34.

Fricke, Jr.W.G. and Rawlins, C.B., 1968, Importance of fretting in vibration fatigue of stranded conductors, *IEEE Transactions on Power Apparatus and Systems*, vol. PAS-87, no. 6, pp. 1381-1384.

Fuchs, R.D., Almeida, M.T., Labegalini, P., 1992, *Projetos Mecânicos de Linhas Aéreas de Transmissão*, 1ª. Ed. Itajubá:Edgard Blücher, 252p.

Giosan, I., Vortex shedding induced loads on free standing structures, 2013 [Online]. Available: http://www.wceng-fea.com/vortex_shedding.pdf

Gopalan, T.V., 1993, New excitation system for indoor testing of overhead conductors, *Journal of Energy Engineering*, ASCE, p. 159-167.

Goudreau, S., Lévesque, F., Cardou, A., Cloutier, L., 2010, Strain measurements on ACSR conductors during fatigue: Tests I-Experimental method and data, *IEEE Transactions On Power Delivery*, Vol. 25, No. 4.

Goudreau, S., Lévesque, F., Cardou, A., Cloutier, L., 2010, Strain measurements on ACSR conductors during fatigue: Tests II-Stress Fatigue Indicators, *IEEE Transactions On Power Delivery*, Vol. 25, No. 4.

Goudreau, S., Lévesque, F., Cardou, A., Cloutier, L., 2010, Strain measurements on ACSR conductors during fatigue: Tests III-Strains Related to Support Geometry, *IEEE Transactions On Power Delivery*, Vol. 25, No. 4.

Hatch, J.E., 1984, *Aluminum : properties and physical metallurgy*, American Society for Metals.

Heics, R.C. and Havard, D.G., 1994, Influence of vibration recorders on conductor vibration, *IEEE Transactions On Power Delivery*, New York, pp. 919-938.

- Henriques, A.M.D., 2006, *Bancada de ensaios mecânicos à fadiga de cabos condutores de energia*, Tese (Doutorado) – Universidade de Brasília, Brasília.
- Hills, D.A. and Nowell, D., 1994, *Mechanics of fretting fatigue*, Kluwer Academic, The Netherlands.
- Hoepfner, D.W., Adibnazari, S., Moesser, M.W., 1994, Literature review and preliminary studies of fretting and fretting fatigue including special applications to aircraft joints, Final report, Report Number: DOT-FAA-CT-93-2, Utah University.
- Hoepfner, D.W., Elliot, C.B., Moesser, M.W., 1996, The role of fretting fatigue on aircraft rivet hole cracking, Final report, Report number. DOR-FAA-AR-96-10, Utah University.
- Hong, K.J., Kiureghian, A.D., SACKMAN, J.L., 2005, Bending behavior of helically wrapped cables, *Journal of Mechanics of Materials and Structures*, ASCE, pp. 500-511.
- Hou, J.P., Wang Q., Yang H.J., Wu X.M., Li C.H., Zhang Z.F., Li X.W., 2016, Fatigue and fracture behavior of a cold-drawn commercially pure aluminum wire, *Materials*, pp 2-11.
- IEEE Committee Report, 1966, Standardization of conductor vibration measurements, *IEEE Transactions on Power Apparatus and Systems*, Vol. Ps-85. No.1. Pp. 10-20.
- Josiki, Z.A., Kierski, K.L., Lieszkowski, W., 1976, New overhead transmission lines in the Polish Network-service Experience, *CIGRÉ Report 22-05*.
- Kalombo, R.B., Martínez, J.M.G., Ferreira, J.L.A., Da Silva, C.R.M., Araújo, J.A., 2015, Comparative fatigue tests and analysis between an All Aluminium Alloy Conductor (AAAC) and an Aluminium Conductor Steel Reinforced (ACSR), *Procedia Engineering*, 133, pp 223-232.
- Kiessling, F., Nefzger, P., Kaintzyk, U., Nolasco, J.F., 2003, *Ovehead power lines: Planning, Design, Construction*, Spring.

- Langlois, S., Legeron, F., Lévesque, F., 2014, Time history modelling of vibrations on overhead conductors with variable bending stiffness, *IEEE Transactions On Power Delivery*, New York, pp. 607-614. abr.111.
- Lévesque, F., Goudreau, S., Cloutier, L., Cardou, A., 2011, Finite element model of the contact between a vibrating conductor and a suspension clamp, *Tribology International*, 44(9): 1014-1023.
- Lienhard, J.H., 1966, Synopsis of lift, drag, and vortex frequency data for rigid circular cylinders. Washington State University, College of Engineering - Research Division, Pullman, Washington.
- Loredo-Souza, A.M. and Davenport, A.G., 1998, The effects of high winds on transmission lines, *Journal of Wind Engineering and industrial Aerodynamics*, vol. 74-76, pp. 987-994.
- Miner, M.A., 1945, Cumulative damage in fatigue, *Journal of Applied Mechanics*, 67, A159-A164.
- Nefzger. J., 1933, Dérangements occasionnés par les oscillations mécaniques des conducteurs aériens et leur remède, New York, Rapport CIGRÉ.
- Nielsen, B., Whitby, A.A., 2015, Joint Chow test for structural instability, *Econometrics*, Vol. 3, pp. 156-186
- Papailiou, K.O., 1995, Improved calculations of dynamic conductor bending stresses using a variable bending stiffness, In CIGRÉ, SC 22 WG11.
- Papailiou, K.O., 1997, On the bending stiffness of transmission line conductors, *IEEE Transactions on Power Delivery* 12, pp. 1576-1588.
- Poffenberger, J.C. and Swart R.L., 1965, Differential displacement and dynamic conductor strain, *Power Apparatus and Systems*, *IEEE Transactions on*, vol. 84, pp 281-289.
- Raj, M.T. and Parthasarathy, N.S., 2007, A complete review on friction models of composite cables, *International Journal of Mechanics of Composite Materials and constructions*, Russian Academy of Applied Mechanics and Sciences, Vol. 13, No.3, pp.356-384.

- Ramey, G.E. and Silva, J.M., 1981, An experimental evaluation of conductor Aeolian fatigue damage mitigation by amplitude reduction, *IEEE Transactions On Power Apparatus And Systems*, New York, pp. 4935-4940.
- Rawlins, C.B., 1983, Wind tunnel measurement of the imparted to model of vibrating conductor, *IEEE Transactions on power apparatus and Systems*, Vol. PAS-102, No.4.
- Reinke, G., 2017, Influência do tratamento térmico nas propriedades mecânicas de fios de alumínio liga usados em cabos condutores submetidos a ensaios de fadiga, *Dissertação de mestrado em engenharia mecânica*, Departamento de engenharia mecânica, Universidade de Brasília, Brasília, DF.
- Rolim, A.L., Moreira, J.L.R., Veloso, L.A.C.M., De Souza, R.M., Araújo, J.A, 2013, Differential displacement and strain analysis of transmission line cables, *Journal of the Brazilian Society of Mechanical Sciences and Engineering*.
- Smith, E.H. (ed.), 1998, *Mechanical engineer's reference book*, Elsevier.
- Stockbridge, G.H., 1925, Overcoming vibration in transmission cables, *Electrical World*, pp. 1334-1335.
- Tebo, G.B., 1941, Measurement and control of conductor vibration, *Transactions AIEE Power Apparatus and Systems*, vol. 60 (12), pp. 1188-1193
- Tomlinson, G.A., 1927, The rusting of steel surfaces in contact, *Proc. Roy. Society (London)*, A 115; pp. 472-483.
- Varney, T., 1926, Notes on the Vibration of transmission-line conductors, *Associate, A. I. E. E.*, pp. 791-795.
- Vecchiarelli, J., 1997, Aeolian vibration of a conductor with A Stockbridge-Type damper, *PhD thesis*, University of Toronto, Canada.
- Waterhouse, R.B., 1969, Fretting in treatise on materials science and technology, Vol 13, *Wear*, Scott, D. (ed), Academic Press, London.
- Waterhouse, R.B., 1981, *Fretting fatigue*, Elsevier Applied Science, London.

Waterhouse, R.B., 1984, Fretting wear, Vol. 100, pp. 107-118.

Waterhouse, R.B., 1992, Fretting fatigue, International Material Review, Vol. 37, pp. 77-97.

Zetterholm, O.D., 1960, Bare conductors and mechanical calculation of overhead conductors, CIGRÉ Session. Report. No. 223.

Zhao, M., Zhou, Q., Zhao, X., 2011, The fretting fatigue analysis between strands of ACSR, International Conference on Electrical and Control Engineering (ICECE).

Zhou, Z.R., Goudreau, S., Cardou, A., 1995, Single wire fretting fatigue test for electrical conductor bending fatigue evaluation, Wear, Boston, pp. 181-183.

Appendix

Appendix A

A1. Benches for conductor fatigue test at UnB (University of Brasília)

The GFFM, *Grupo de Fadiga, Fracture e Materiais*, has a laboratory called *Laboratório de Fadiga e Integridade Estrutural de Cabos Condutores de Energia* where various types of test on conductors are undertaken. The laboratory has three similar benches for conductor fatigue test. Each bench has a span of 46.8 m which is divided in two parts, the active and the passive span. The scheme of the three benches is showed in Figure A.1(a) as well as the bench description while Figure A.1(b) represents the benches projection in projected two dimensions view.

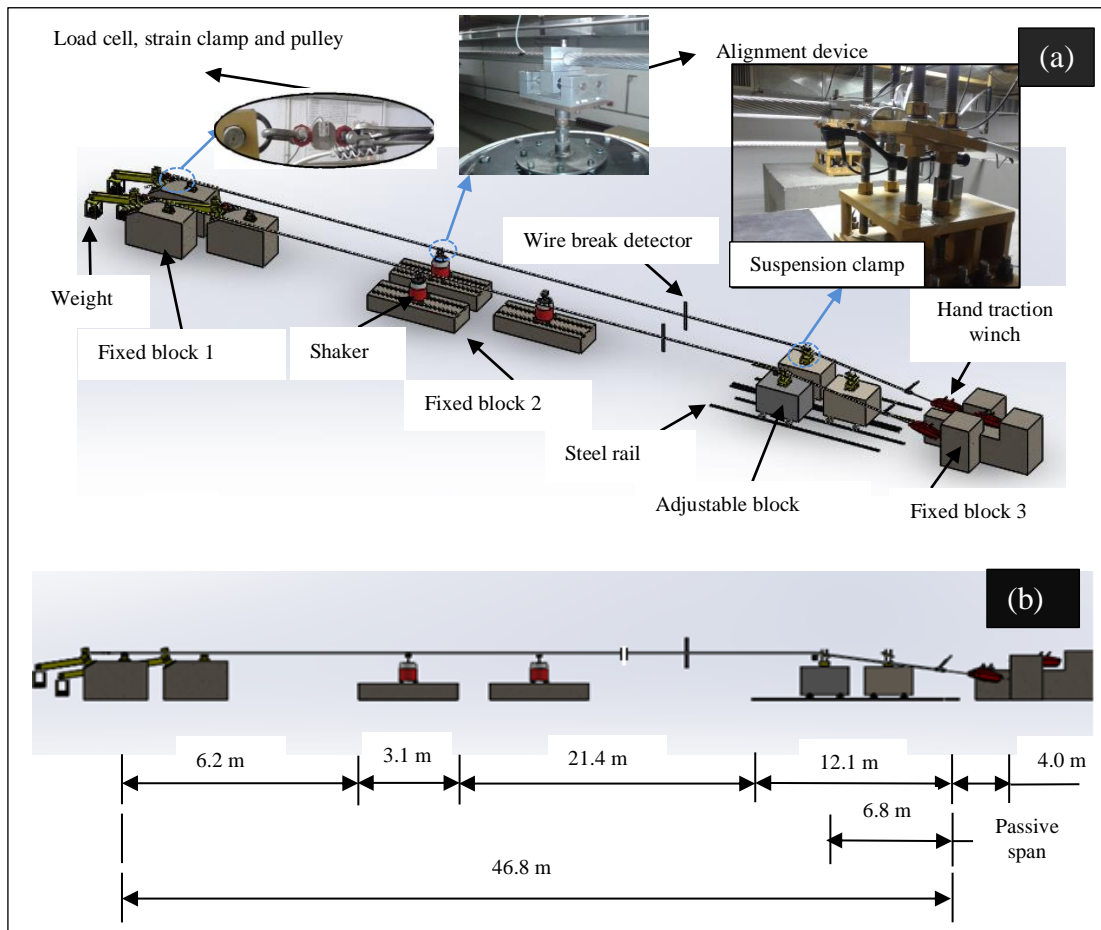


Figure A.1: Scheme of the three fatigue test rigs for overhead conductors at the University of Brasília: (a) overall three dimensional view and (b) projected two dimensional view.

The active span defines the conductor length which is limited by the centre of the pulley on fixed block 1 and the suspension clamp on the adjustable block. The active span can be reduced or augmented by moving the adjustable block when this is necessary.

To ensure the rigidity of the assembly, all blocks are made of solid concrete. The conductor sample is placed on two supports points which act as pivot points, i.e. the suspension clamp (on the adjustable block) and the pulley (on the fixed block 1). It is then fitted at the ends by the strain clamp (pistoled clamp).

During the removing process of the conductor from the drum to the bench, care must be taken to avoid the contact between the conductor and the floor. Furthermore, the conductor must not to be in contact with any metallic material. The same applies to sharp objects such as nails, screws or other material that can crack or damage the conductor (creating a micro crack). For this reason, the use of the auxiliaries pulley mounted on the ceiling the conductor is compulsory (Figure A.2).

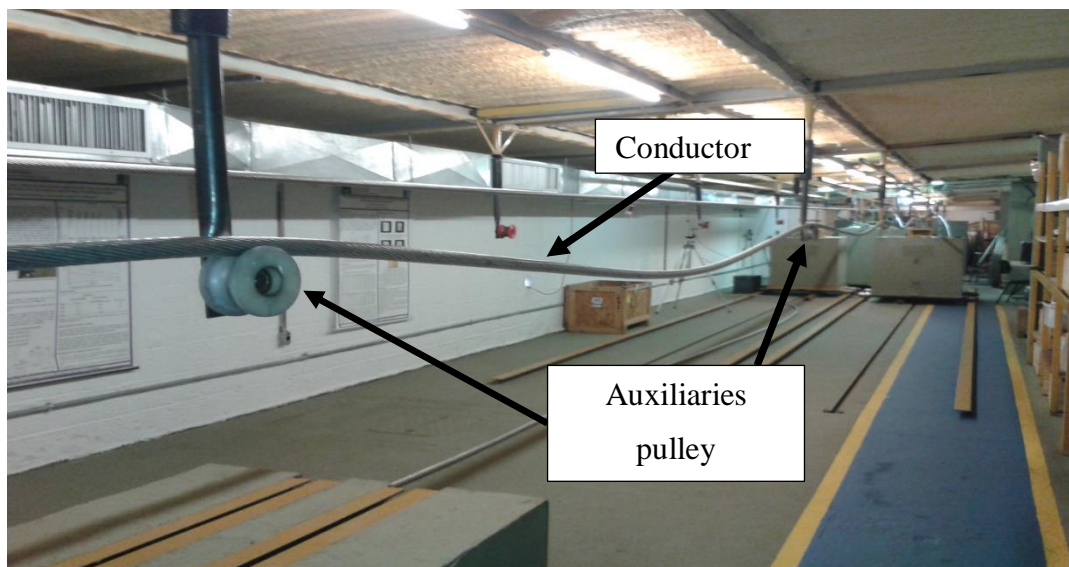


Figure A.2: Conductor on the auxiliary pulley during the montage process on the fatigue bench.

The fixed block 1 is located at the left end where the load is applied through a lever arm. The load cell located between the arm and the strain clamp (Pistoled clamp) represents the stretching load applied on the conductor (Figure A.3)

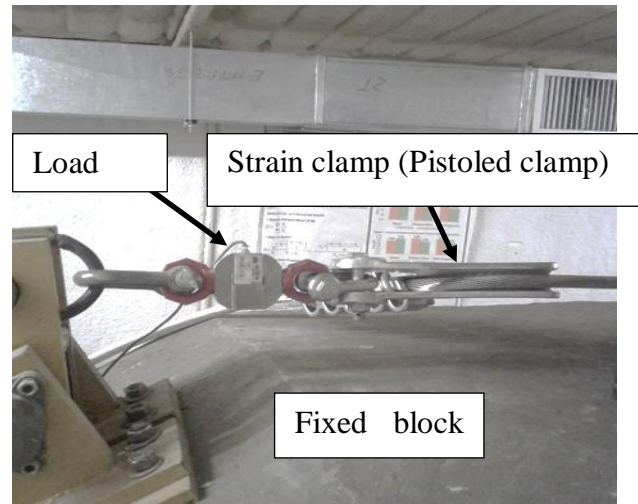


Figure A.3: Cable attached to the fixed block 1 and passing through the strain clamp (pistoled clamp) which is attached to the load cell.

The adjustable block is placed on a thick steel plate fixed to two shafts provided with rollers at the ends. This enables to reduce or augmented the span by moving the adjustable block on the steel rails set out on the laboratory floor (Figure A.4).

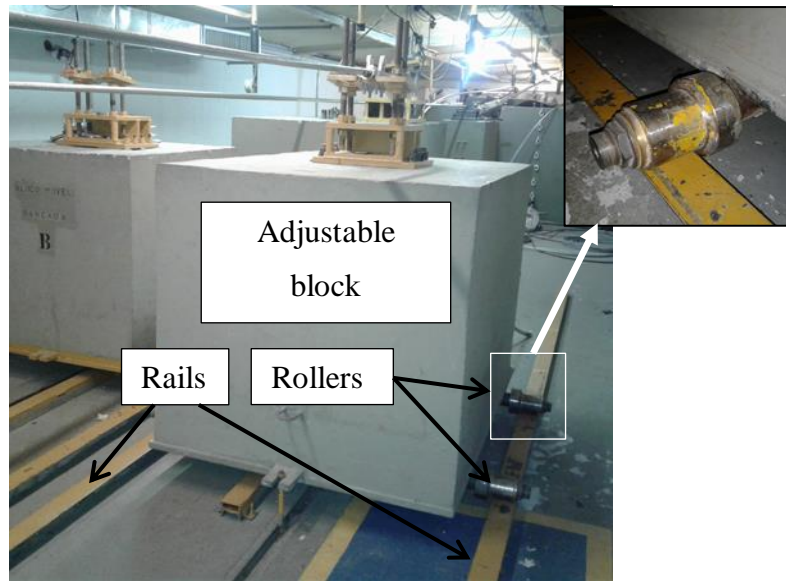


Figure A.4: Adjustable block

The electromechanical shaker is placed on the fixed block 2 which serves as a support and get two steel rails for adjusting the shaker position by moving it on the block 2 (Figure A.5). The move of the shaker allows the improvement of its position in relation to the node or antinode according to the excitation frequency during the fatigue test. This position could sometime improve the control of the fatigue test (Figure A.5).

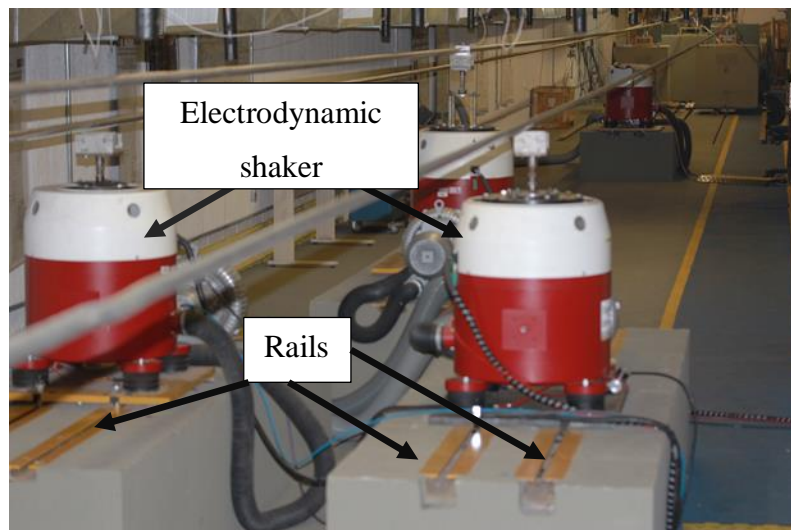


Figure A.5: Fixed block with rail to shaker displacement.

A2. Wire break detection device

The device for wire break detection is installed at the first node of the conductor from the suspension clamp. This device consists of two aluminium rulers attached to the conductor by a screw clamp and two laser displacement sensors with measuring ranges of 16 to 120 mm (Figure A.6). The design of the break detection device is based on the manufacturing process of the power line conductor, from the observation that the conductor is formed by stranding metallic wires.

The conductor manufacturing process causes a conductor to produce tangential and longitudinal components of force when it is stretched. Thus, when there is a wire break of the conductor during the fatigue test, the load supported by the conductor is distributed between the remaining wires so that the balance is maintained. As a result of this accommodation, the conductor turns or is distorted, relatively to its longitudinal axis as it made by strands layers formed into helices. The resulting rotation is caused by the tangential force component of the conductor when the wire breaks, and the rulers of the wire break detection move by the same distance from the longitudinal axis of the conductor. Consequently, the break of a wire located in a conductor's outer layer generates more rotation of the failure of an internal layer. The conductor is made in such way that each layer is in the opposite sense relatively to one another; the direction of the driver rotation depends on the layer in which the broken wire is located. The laser sensors are positioned to measure the displacements L1 and L2 of the reference rules in relation to the horizontal plane, where the distance between the laser sensors and the rules. This distance is converted in angle read through the TFC (*Teste de fadiga em Cabos de Linhas de Transmissão*) software.

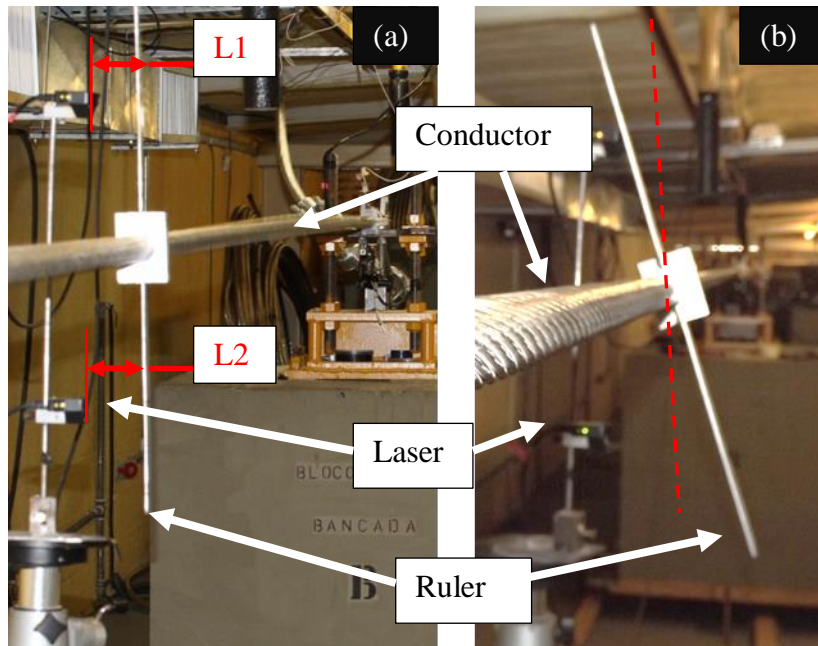


Figure A.6: Wire break detection device mounted on the conductor, (a) during the fatigue test of conductor and (b) after fatigue test

A.3. Data acquisition system

A data acquisition unit manufactured by Lynx Technology (Model ADS2000) has been used for this work. The ADS-2000 consists of two 16-channels acquisition modules. Each bench has its data acquisition system and operates when it is connected to the control computer via internet interface to receive digital and analog signals for control and monitoring (Figure A.7). It allows simultaneous collection of data through the network and signal conditioners. The channels may be configured to thermocouple input, transducer, strain gauge bridge, voltage, current, etc. Appropriate settings of the data acquisition system are made by means of its software.

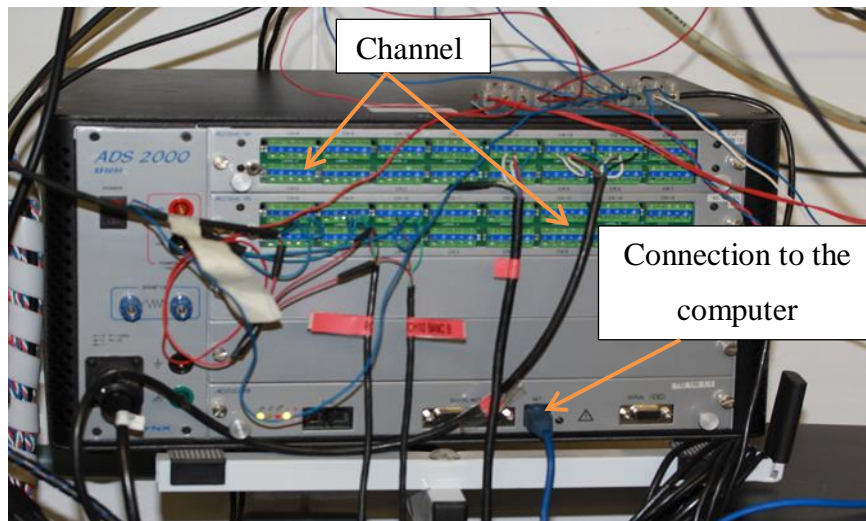


Figure A.7: Data aquisition ADS 2000

The ADS 2000 is able to collect the following data: i) temperature; ii) gauges; iii) flat load cells or instrumented washers, washers load; iv) optical displacement sensor (laser) for both cable rotation measurement (failure detection mechanism) as to the vibration amplitude of the measuring point 89 (Figure A.8); v) accelerometer (vibration amplitude of the measuring point 89).

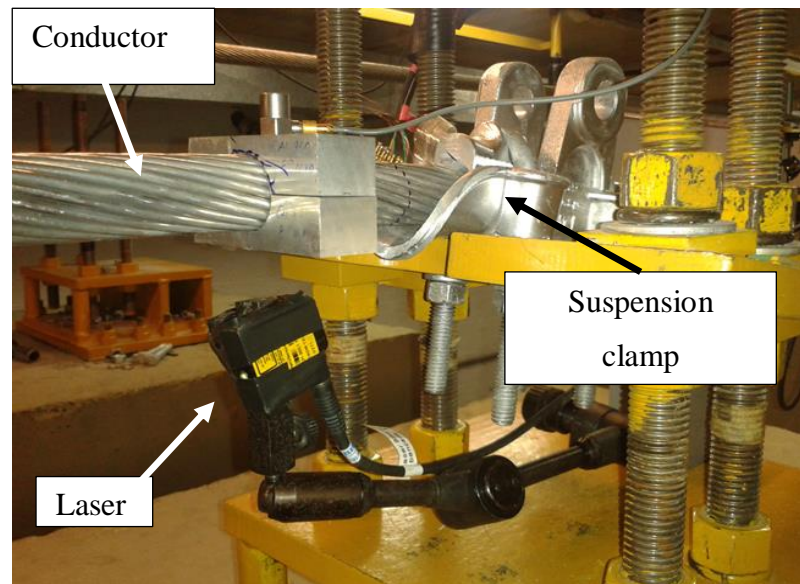


Figure A.8: Laser at 89 mm from the LPC (last point of contact) between the conductor and the suspension clamp

Appendix B

Result of Static Test

Table B.1: Static stress measurements for AAAC 900 MCM conductor

<i>H/w</i> (m)	Tensile stress (MPa)		
	Predicted	Measurement	
		Loading	Unloading
671	17.71	14.72	14.46
1072	28.45	29.84	31.89
1820	48.30	51.74	53.54
2144	56.58	60.98	60.95
2725	71.91	76.94	76.94

Table B.2: Static stress measurements for ACSR Tern conductor

<i>H/w</i> (m)	Tensile stress (MPa)		
	Predicted	Measurement	
		Loading	Unloading
374	9.92	10.17	10.84
1122	29.77	27.86	28.54
1820	48.3	45.22	45.56
2144	56.89	53.24	52.89
2725	72.31	68.17	68.17

Table B.3: Static stress measurements for AAC Orchid conductor

<i>H/w</i> (m)	Tensile stress (MPa)		
	Predicted	Measurement	
		Loading	Unloading
671	15.35	15.53	16.46
1157	30.68	30.39	30.85
1820	48.30	48.02	49.00
2144	56.89	57.02	57.66
2725	72.31	72.90	72.90

Table B.4: Static stress measurements for ACAR 750 MCM conductor

<i>H/w</i> (m)	Tensile stress (MPa)		
	Predicted	Measurement	
		Loading	Unloading
413	10.95	11.44	11.48
1239	32.85	32.34	32.15
1820	48.3	47.13	49.71
2144	56.89	55.63	58.16
2725	72.31	74.18	74.18

Appendix C

Result of dynamic test

Table C.1: Bending stress at 89 mm from the LPC (Last point of contact) between the conductor and the suspension clamp for AAAC 900 MCM conductor ($H/w = 1820$ m)

H/w (m)	Test	Amplitude Y_b (Pk - Pk) (mm)	Calculated stress (MPa)	Experimental Stress (MPa)	Erro (%)
1820	1	0.71	23.70	24.88	4.98
	2	0.71	23.70	27.35	15.40
	3	0.71	23.70	25.63	8.14
	1	0.85	28.22	28.78	1.98
	2	0.85	28.22	31.11	10.24
	3	0.85	28.22	29.97	6.20
	1	0.94	31.35	30.76	1.88
	2	0.94	31.35	31.22	0.41
	3	0.94	31.35	32.57	3.89

Table C.2: Bending stress at 89 mm from the LPC (Last point of contact) between the conductor and the suspension clamp for AAAC 900 MCM conductor ($H/w = 2144$ m)

H/w (m)	Test	Amplitude Y_b (Pk - Pk) (mm)	Calculated stress (MPa)	Experimental Stress (MPa)	Erro (%)
2144	1	0.68	23.70	24.12	1.77
	2	0.68	23.70	23.14	2.36
	3	0.68	23.70	24.11	1.73
	1	0.81	28.22	27.7	1.84
	2	0.81	28.22	26.95	4.50
	3	0.81	28.22	28.1	0.43
	1	0.90	31.35	28.55	8.93
	2	0.90	31.35	28.01	10.65
	3	0.90	31.35	28.49	9.12

Table C.3: Bending stress at 89 mm from the LPC (Last point of contact) between the conductor and the suspension clamp for AAAC 900 MCM conductor ($H/w = 2725$ m)

H/w (m)	Test	Amplitude Y_b (Pk - Pk) (mm)	Calculated stress (MPa)	Experimental Stress (MPa)	Erro (%)
2725	1	0.63	23.70	21.21	10.51
	2	0.63	23.70	24.92	5.15
	1	0.76	28.22	27.01	4.29
	2	0.76	28.22	29.74	5.39
	1	0.84	31.35	30.15	3.83
	2	0.84	31.35	32.09	2.36

Table C.4: Bending stress at 89 mm from the LPC between the conductor and the suspension clamp for ACSR Tern conductor ($H/w = 1820$ m)

H/w (m)	Test	Amplitude Y_b (Pk - Pk) (mm)	Calculated stress (MPa)	Experimental Stress (MPa)	Erro (%)
1820	1	0.84	26.80	26.97	0.65
	2	0.84	26.80	24.95	6.89
	3	0.84	26.80	25.04	6.58
	1	0.88	28.22	30.46	7.93
	2	0.88	28.22	30.91	9.52
	3	0.88	28.22	28.50	1.00
	1	0.98	31.35	33.83	7.91
	2	0.98	31.35	31.47	0.40
	3	0.98	31.35	32.18	2.64

Table C.5: Bending stress at 89 mm from the LPC between the conductor and the suspension clamp for ACSR Tern conductor ($H/w = 2144$ m)

H/w (m)	Test	Amplitude Y_b (Pk - Pk) (mm)	Calculated stress (MPa)	Experimental Stress (MPa)	Erro (%)
2144	1	0.8	26.80	26.95	0.56
	2	0.8	26.80	24.36	9.10
	3	0.8	26.80	23.92	10.75
	1	0.84	28.22	28.18	0.14
	2	0.84	28.22	25.62	9.21
	3	0.84	28.22	28.93	2.52
	1	0.93	31.35	33.12	5.65
	2	0.93	31.35	31.72	1.18
	3	0.93	31.35	31.50	0.48

Table C.6: Bending stress at 89 mm from the LPC between the conductor and the suspension clamp for ACSR Tern conductor ($H/w = 2725$ m)

H/w (m)	Test	Amplitude Y_b (Pk - Pk) (mm)	Calculated stress (MPa)	Experimental Stress (MPa)	Erro (%)
2725	1	0.74	26.80	26.11	2.57
	2	0.74	26.80	27.43	2.35
	1	0.78	28.22	26.53	5.99
	2	0.78	28.22	26.29	6.84
	1	0.86	31.35	32.45	3.51
	2	0.86	31.35	32.13	2.49

Table C.7: Bending stress at 89 mm from the LPC between the conductor and the suspension clamp for AAC Orchid conductor ($H/w = 1820$ m)

H/w (m)	Test	Amplitude Y_b (Pk - Pk) (mm)	Calculated stress (MPa)	Experimental Stress (MPa)	Erro (%)
1820	1	0.87	26.80	26.95	0.56
	2	0.87	26.80	25.43	5.11
	3	0.87	26.80	28.69	7.05
	1	0.91	28.22	27.50	2.55
	2	0.91	28.22	25.95	8.04
	3	0.91	28.22	27.88	1.20
	1	1.01	31.35	31.41	0.19
	2	1.01	31.35	30.67	2.17
	3	1.01	31.35	28.94	7.69

Table C.8: Bending stress at 89 mm from the LPC between the conductor and the suspension clamp for AAC Orchid conductor ($H/w = 2144$ m)

H/w (m)	Test	Amplitude Y_b (Pk - Pk) (mm)	Calculated stress (MPa)	Experimental Stress (MPa)	Erro (%)
2144	1	0.82	26.80	26.93	0.48
	2	0.82	26.80	27.79	3.71
	3	0.82	26.80	27.49	2.56
	1	0.87	28.22	28.70	1.69
	2	0.87	28.22	26.13	7.41
	3	0.87	28.22	29.40	4.20
	1	0.96	31.35	33.30	6.22
	2	0.96	31.35	32.46	3.55
	3	0.96	31.35	33.52	6.92

Table C.9: Bending stress at 89 mm from the LPC (Last point of contact) between the conductor and the suspension clamp for AAC Orchid conductor ($H/w = 2725$ m)

H/w (m)	Test	Amplitude Y_b (Pk - Pk) (mm)	Calculated stress (MPa)	Experimental Stress (MPa)	Erro (%)
2725	1	0.76	26.80	24.53	8.47
	2	0.76	26.80	27.94	4.25
	1	0.8	28.22	25.29	10.38
	2	0.8	28.22	26.51	6.06
	1	0.89	31.35	33.84	7.94
	2	0.89	31.35	30.36	3.16

Table C.10: Bending stress at 89 mm from the LPC between the conductor and the suspension clamp for ACAR 750 MCM conductor ($H/w = 1820$ m)

H/w (m)	Test	Amplitude Y_b (Pk - Pk) (mm)	Calculated stress (MPa)	Experimental Stress (MPa)	Erro (%)
1820	1	0.84	26.80	28.35	5.78
	2	0.84	26.80	26.89	0.34
	3	0.84	26.80	26.41	1.46
	1	0.88	28.22	27.98	0.85
	2	0.88	28.22	27.64	2.06
	3	0.88	28.22	25.59	9.32
	1	0.98	31.35	30.39	3.06
	2	0.98	31.35	28.80	8.13
	3	0.98	31.35	31.26	0.29

Table C.11: Bending stress at 89 mm from the LPC between the conductor and the suspension clamp for ACAR 750 MCM conductor ($H/w = 2144$ m)

H/w (m)	Test	Amplitude Y_b (Pk - Pk) (mm)	Calculated stress (MPa)	Experimental Stress (MPa)	Erro (%)
2144	1	0.80	26.80	24.21	9.66
	2	0.80	26.80	24.94	6.94
	3	0.80	26.80	26.82	0.07
	1	0.84	28.22	25.90	8.22
	2	0.84	28.22	29.80	5.60
	3	0.84	28.22	29.59	4.85
	1	0.93	31.35	30.92	1.37
	2	0.93	31.35	30.37	3.13
	3	0.93	31.35	29.72	5.20

Table C.12: Bending stress at 89 mm from the LPC between the conductor and the suspension clamp for ACAR 750 MCM conductor ($H/w = 2725$ m)

H/w (m)	Test	Amplitude Y_b (Pk - Pk) (mm)	Calculated stress (MPa)	Experimental Stress (MPa)	Erro (%)
2725	1	0.74	26.80	25.34	5.45
	2	0.74	26.80	26.47	1.23
	1	0.78	28.22	30.07	6.56
	2	0.78	28.22	30.33	7.48
	1	0.87	31.35	32.61	4.02
	2	0.87	31.35	33.94	8.26

Appendix D

Fatigue life of conductors for different values of H/w parameter at bending displacement used

Table D.1: Fatigue life of conductor AAAC 900 MCM for different values of H/w parameter at bending displacement (Y_b) used

H/w (m)	Test	Bending Stress (0 - Pk) (MPa)	Bending Amplitude (Pk-Pk) (mm)	Cycles to failure (N)				Mean
				1 st break	2 nd break	3 rd break	4 th break	
1820	1	23.7	0.71	7.60E+05	9.98E+05	1.32E+06	1.79E+06	1.66E+06
	2	23.7	0.71	9.68E+05	1.18E+06	1.29E+06	1.68E+06	
	3	23.7	0.71	8.62E+06	9.75E+05	1.28E+05	1.51E+06	
	1	28.22	0.85	6.74E+05	8.97E+05	8.97E+05	1.45E+06	1.26E+06
	2	28.22	0.85	6.35E+05	7.47E+05	7.47E+05	1.01E+06	
	4	28.22	0.85	5.27E+05	6.78E+05	9.04E+05	1.32E+06	
	1	31.35	0.94	4.24E+05	6.90E+05	8.42E+05	9.55E+05	9.27E+05
	2	31.35	0.94	3.41E+05	7.20E+05	7.20E+05	9.33E+05	
	3	31.35	0.94	3.02E+06	4.44E+06	4.85E+05	8.93E+05	
2144	1	23.7	0.68	1.03E+06	1.12E+06	1.18E+06	1.50E+06	1.40E+06
	2	23.7	0.68	8.87E+05	1.06E+06	1.06E+06	1.40E+06	
	3	23.7	0.68	6.88E+05	7.78E+05	1.11E+06	1.29E+06	
	1	28.22	0.81	5.46E+05	6.82E+05	1.06E+06	1.04E+06	9.39E+05
	2	28.22	0.81	4.00E+05	4.40E+05	6.00E+05	9.21E+05	
	3	28.22	0.81	5.40E+05	6.35E+05	7.30E+05	8.57E+05	
	1	31.35	0.9	4.34E+05	4.63E+05	6.93E+02	7.44E+05	7.05E+05
	2	31.35	0.9	2.93E+05	5.68E+04	6.45E+05	7.63E+05	
	3	31.35	0.9	5.47E+05	5.77E+03	6.00E+05	6.08E+05	
2725	1	23.7	0.63	5.47E+05	7.30E+05	8.03E+05	9.85E+05	1.07E+06
	2	23.7	0.63	4.64E+05	7.41E+05	1.11E+06	1.16E+06	
	1	28.22	0.76	5.48E+05	6.21E+05	6.58E+05	7.67E+05	8.49E+05
	2	28.22	0.76	5.87E+05	6.97E+05	9.30E+05	9.30E+05	
	1	31.35	0.84	3.29E+05	3.66E+05	4.39E+05	5.12E+05	5.83E+05
	2	31.35	0.84	5.14E+05	5.60E+05	6.07E+05	6.53E+05	

Table D.2: Fatigue life of conductor ACSR Tern for different values of H/w parameter at bending displacement (Y_b) used

H/w	Bending stress	Amplitude Y_b	Cycles to failure (N)					Mean	
			1 st break	2 nd break	3 rd break	4 th Break	5 th Break		
(m)	(0-Pk) (MPa)	(Pk-Pk) (mm)							
1820	26.8	0.84	1	1.16E+06	1.52E+06	1.91E+06	2.34E+06	3.99E+06	3.92E+06
			2	1.23E+07	1.59E+06	2.55E+06	3.13E+06	4.22E+06	
			3	1.47E+06	1.83E+06	2.12E+06	2.78E+06	3.54E+06	
	28.2	0.88	1	1.27E+06	2.12E+06	2.15E+06	2.26E+06	3.63E+06	3.65E+06
			2	1.08E+06	1.36E+06	1.93E+06	2.59E+06	3.52E+06	
			3	1.47E+06	1.63E+06	2.35E+06	2.99E+06	3.80E+06	
	31.4	0.98	1	9.56E+05	1.13E+06	1.21E+06	1.57E+05	2.52E+06	2.44E+06
			2	1.44E+06	1.81E+06	2.00E+06	2.30E+06	2.71E+06	
			3	1.38E+06	1.58E+06	1.80E+06	1.94E+06	2.10E+06	
2144	26.8	0.8	1	2.54E+06	2.54E+06	2.90E+06	2.90E+06	3.09E+06	3.16E+06
			2	1.38E+06	1.38E+06	1.38E+06	2.07E+06	2.96E+06	
			3	1.12E+06	1.12E+06	2.21E+06	2.77E+06	3.43E+06	
	28.2	0.84	1	1.64E+06	1.64E+06	2.00E+06	2.94E+06	3.04E+06	3.03E+06
			2	9.88E+05	1.35E+06	2.10E+06	2.53E+06	2.89E+06	
			3	1.45E+06	1.67E+06	1.67E+06	3.11E+06	3.14E+06	
	31.4	0.93	1	1.36E+06	1.36E+06	1.36E+06	1.36E+06	1.65E+06	1.71E+06
			2	1.30E+06	1.33E+06	1.33E+06	1.33E+06	1.49E+06	
			3	1.10E+06	1.10E+06	1.99E+06	1.99E+06	1.99E+06	
2725	26.8	0.74	1	1.06E+06	1.14E+06	1.21E+06	1.92E+06	2.47E+06	2.51E+06
			2	1.28E+06	1.41E+06	1.79E+06	2.08E+06	2.55E+06	
	28.2	0.78	1	7.17E+05	1.11E+06	1.63E+05	1.86E+06	2.18E+06	2.11E+06
			2	1.10E+06	1.17E+06	1.33E+06	1.56E+06	2.03E+06	
	31.4	0.86	1	6.04E+05	7.25E+05	8.51E+05	9.02E+05	1.04E+06	1.17E+06
			2	8.15E+05	1.08E+06	1.14E+06	1.21E+06	1.30E+06	

Table D.3: Fatigue life of conductor AAC Orchid for different values of H/w parameter at bending displacement (Y_b) used

H/w (m)	Test	Bending Stress (0 - Pk) (MPa)	Bending Amplitude (Pk-Pk) (mm)	Cycles to failure (N)				Mean
				1 st break	2 nd break	3 rd break	4 th break	
1820	1	26.8	0.87	1.08E+06	1.46E+06	2.59E+06	2.72E+06	2.74E+06
	2	26.8	0.87	1.34E+06	1.66E+06	2.56E+06	2.96E+06	
	3	26.8	0.87	1.10E+06	1.44E+06	2.21E+06	2.54E+06	
	1	28.22	0.91	8.53E+05	1.07E+06	2.23E+06	2.43E+06	2.57E+06
	2	28.22	0.91	8.53E+05	1.07E+06	2.27E+06	2.70E+06	
	3	28.22	0.91	8.17E+05	1.25E+06	2.22E+06	2.57E+06	
	1	31.35	1.01	7.03E+05	1.17E+06	1.41E+06	1.83E+06	1.69E+06
	2	31.35	1.01	8.03E+05	1.24E+06	1.47E+06	1.77E+06	
	3	31.35	1.01	7.37E+05	1.11E+06	1.37E+06	1.47E+06	
2144	1	26.8	0.82	1.29E+06	1.62E+06	1.75E+06	1.98E+06	2.14E+06
	3	26.8	0.82	1.42E+06	1.62E+06	1783620	2.05E+06	
	4	26.8	0.82	1.06E+06	1.83E+06	2.19E+06	2.38E+06	
	1	28.22	0.87	7.24E+05	9.88E+05	1.12E+06	1.32E+06	1.55E+06
	2	28.22	0.87	1.23E+06	1.26E+06	1.33E+06	1.49E+06	
	4	28.22	0.87	6.05E+05	9.10E+05	1.59E+06	1.84E+06	
	1	31.35	0.96	5.25E+05	6.24E+05	6.90E+05	1.08E+06	1.16E+06
	2	31.35	0.96	3.32E+05	4.28E+05	8.26E+05	1.15E+06	
	3	31.35	0.96	9.56E+05	1.12E+06	1.19E+06	1.25E+06	
2725	1	26.8	0.76	6.85E+05	1.08E+06	1.41E+06	1.66E+06	1.78E+06
	2	26.8	0.76	5.58E+05	1.04E+06	1.49E+06	1.90E+06	
	1	28.22	0.8	8.56E+05	1.26E+06	1.41E+06	1.48E+06	1.30E+06
	2	28.22	0.8	6.85E+05	8.56E+05	9.59E+05	1.13E+06	
	1	31.35	0.89	5.89E+05	7.28E+05	1.00E+06	1.10E+06	1.02E+06
	2	31.35	0.89	5.68E+05	8.14E+05	8.65E+05	9.30E+05	

Table D.4: Fatigue life of conductor ACAR 750 MCM for different values of H/w parameter at bending displacement (Y_b) used

H/w (m)	Test	Bending Stress (0 - Pk) (MPa)	Bending Amplitude (Pk-Pk) (mm)	Cycles to failure (N)				Mean
				1 ^a Break	2 nd break	3 rd break	4 th break	
1820	1	26.8	0.84	1.46E+06	1.71E+06	2.15E+06	2.80E+06	2.50E+06
	2	26.8	0.84	1.37E+06	1.98E+06	2.21E+06	2.40E+06	
	3	26.8	0.84	1.11E+06	1.62E+06	1.94E+06	2.29E+06	
	1	28.22	0.88	1.24E+06	1.46E+06	1.71E+06	2.15E+06	2.10E+06
	2	28.22	0.88	8.56E+05	1.12E+06	1.84E+06	2.14E+06	
	3	28.22	0.88	1.04E+06	1.56E+06	1.84E+06	2.01E+06	
	1	31.35	0.98	6.70E+05	8.10E+05	1.19E+06	1.40E+06	1.69E+06
	2	31.35	0.98	8.00E+05	1.22E+06	1.56E+06	1.71E+06	
	3	31.35	0.98	7.93E+05	1.01E+06	1.23E+06	1.96E+06	
2144	1	26.8	0.8	8.53E+05	1.24E+06	1.54E+06	2.26E+06	2.22E+06
	2	26.8	0.8	9.37E+05	1.08E+06	1.66E+06	1.98E+06	
	3	26.8	0.8	1.09E+06	1.60E+06	1.83E+06	2.42E+06	
	1	28.22	0.84	5.90E+05	9.37E+05	1.14E+06	1.39E+06	1.63E+06
	2	28.22	0.84	6.55E+05	1.09E+06	1.31E+06	1.67E+06	
	3	28.22	0.84	8.29E+05	9.53E+05	1.33E+06	1.82E+06	
	1	31.35	0.93	3.76E+05	6.16E+05	6.75E+05	1.47E+06	1.41E+06
	2	31.35	0.93	3.30E+05	6.18E+05	1.03E+06	1.28E+06	
	3	31.35	0.93	4.56E+05	7.87E+05	1.28E+06	1.49E+06	
2725	1	26.8	0.74	8.57E+05	1.50E+06	1.68E+06	1.83E+06	1.75E+06
	2	26.8	0.74	6.78E+05	1.04E+06	1.48E+06	1.67E+06	
	2	28.22	0.78	4.79E+05	7.71E+05	1.14E+06	1.43E+06	1.30E+06
	3	28.22	0.78	3.63E+05	6.90E+05	1.05E+06	1.16E+06	
	1	31.35	0.87	3.64E+05	6.19E+05	7.65E+05	1.02E+06	1.13E+06
	2	31.35	0.87	3.99E+05	5.08E+05	8.71E+05	1.23E+06	

Appendix E

Failure distance (FD) measured from the suspension clamp mouth for different conductor tested

Table E.1: Failure distance (FD) measured from the suspension clamp mouth for the AAAC 900 MCM conductor at different values of parameter H/w and failure position related to the suspension clamp. The distance between the suspension clamp mouth and the LPC is 30.03 mm.

H/w (m)	Y_b (mm)	#	Failure distance from the suspension clamp mouth (mm)				MFD External (mm)		MFD Internal (mm)	
			1 st break	2 nd break	3 rd break	4 th break				
1820	0.71	1	44.60 ^T	48.71 ^T	52.52 ^T	29.63 ^T	48.61		29.63	
		2	42.65 ^T	42.65 ^T	43.50 ^T	42.70 ^T	42.88	45.53	0.00	35.03
		3	41.38 ^T	45.86 ^T	48.10 ^T	32.75 ^T	45.11		40.43	
	0.85	1	48.88 ^T	44.36 ^T	43.35 ^T	44.04 ^T	45.16		0.00	
		2	42.76 ^T	42.95 ^T	46.26 ^T	44.08 ^T	44.01	45.32	0.00	0.00
		3	50.25 ^T	45.50 ^T	46.20 ^T	45.20 ^T	46.79		0.00	
	0.94	1	43.92 ^T	40.81 ^T	43.27 ^T	42.21 ^T	42.55		0.00	
		2	40.18 ^T	37.91 ^T	38.75 ^T	38.38 ^T	38.95	40.37	38.38	39.11
		3	41.17 ^T	38.06 ^T	40.32 ^T	39.37 ^T	39.62		39.85	
2144	0.68	1	50.11 ^T	47.41 ^T	46.26 ^T	45.96 ^T	47.93		45.96	
		2	50.81 ^T	55.28 ^T	52.92 ^T	33.77 ^T	53.00	50.21	33.77	41.50
		4	50.14 ^T	49.23 ^T	38.13 ^T	51.42 ^T	49.69		44.78	
	0.81	1	54.91 ^T	48.59 ^T	47.63 ^T	29.65 ^T	45.20		0.00	
		2	56.58 ^T	54.23 ^T	59.97 ^T	56.10 ^T	56.72	47.98	58.04	0.00
		3	45.30 ^T	41.34 ^T	41.24 ^T	40.24 ^T	42.03		0.00	
	0.90	1	33.92 ^B	46.48 ^T	47.27 ^T	45.10 ^T	45.79		0.00	
		2	29.92 ^B	34.37 ^B	48.07 ^T	43.17 ^T	38.77	40.32	0.00	41.72
		3	32.53 ^B	36.41 ^B	38.23 ^T	41.72 ^T	36.41		41.72	
2725	0.63	1	37.82 ^B	39.47 ^B	46.26 ^T	45.96 ^T	42.38		0.00	
		2	49.52 ^T	56.02 ^T	45.68 ^B	28.08 ^T	50.41	46.39	28.08	28.08
	0.76	1	39.29 ^T	41.51 ^T	33.16 ^B	33.73 ^T	37.99		33.73	
		2	46.88 ^T	46.28 ^T	50.38 ^T	36.35 ^T	47.85	42.92	36.35	35.04
	0.84	1	41.66 ^T	35.73 ^T	35.71 ^T	41.49 ^T	38.70		38.60	
		2	50.40 ^T	51.28 ^T	39.99 ^T	49.42 ^T	47.77	43.23	0.00	38.60

Table E.2: Failure distance (FD) measured from the suspension clamp mouth for the ACSR Tern conductor at different values of parameter H/w and failure position related to the suspension clamp. The distance between the suspension clamp mouth and the LPC is 29.75 mm.

H/w (m)	Y_b (mm)	Test	Failure distance from the suspension clamp mouth (mm)					MFD External (mm)		MFD Internal (mm)	
			1 st break	2 nd break	3 rd Break	4 th Break	5 th Break				
1820	0.84	1	37.70 ^B	36.29 ^B	33.52 ^B	33.95 ^B	40.43 ^B	36.38		0.00	
		2	38.73 ^B	36.67 ^B	37.95 ^B	44.88 ^T	47.01 ^T	37.78	35.16	45.95	38.39
		3	32.34 ^B	30.85 ^B	30.77 ^B	32.82 ^B	30.84 ^B	31.32		30.84	
	0.88	1	33.88 ^B	31.68 ^B	34.85 ^B	34.62 ^B	44.99 ^T	36.00		0.00	
		2	40.30 ^B	38.24 ^B	35.69 ^B	37.49 ^B	39.33 ^B	38.21	37.27	0.00	39.42
		3	39.02 ^B	37.41 ^B	36.33 ^B	38.24 ^T	40.59 ^T	37.59		39.42	
	0.98	1	36.39 ^B	34.47 ^B	31.12 ^B	31.03 ^B	35.18 ^B	33.64		0.00	
		2	39.79 ^B	38.79 ^B	40.39 ^B	38.42 ^B	46.40 ^T	40.76	37.14	0.00	39.23
		3	34.19 ^B	33.46 ^B	33.98 ^B	38.99 ^B	44.47 ^T	37.02		39.23	
2144	0.80	1	36.1 ^B	32.32 ^B	36.15 ^B	38.7 ^B	45.57 ^T	37.77		45.57	
		2	35.89 ^B	32.77 ^B	32.08 ^B	34.48 ^B	34.73 ^T	33.58	33.79	34.61	36.96
		4	32.69 ^B	28.69 ^B	25.62 ^B	33.12 ^B	30.7 ^B	30.03		30.70	
	0.84	1	29.16 ^B	33.04 ^B	34.86 ^B	41.12 ^T	41.41 ^T	35.92		0.00	
		2	28.83 ^B	27.83 ^B	25.34 ^B	27.74 ^B	29.48 ^B	27.84	31.88	0.00	36.37
		3	35.68 ^B	35.9 ^B	35.42 ^B	46.46 ^T	36.37 ^B	38.37		36.37	
	0.93	1	32.83 ^B	30.35 ^B	25.4 ^B	28.55 ^B	32.48 ^B	30.35		0.00	
		2	39 ^B	35.63 ^B	29.79 ^B	38.49 ^B	47.37 ^T	38.49	34.42	0.00	0.00
		3	37.12 ^B	34.89 ^B	27.34 ^B	32.19 ^B	35.07 ^B	34.89		0.00	
2725	0.74	1	35.29 ^B	30.98 ^V	32.63 ^B	27.61 ^B	27.61 ^B	31.63	33.46	27.61	35.94
		2	36.52 ^B	35.44 ^B	34.33 ^B	34.86 ^B	44.26 ^T	35.29		44.26	
	0.78	1	35.80 ^B	34.36 ^B	29.82 ^B	31.34 ^B	31.43 ^B	32.83	34.73	31.43	31.24
		2	35.82 ^B	30.66 ^B	31.98 ^B	48.08 ^T	31.05 ^B	36.64		31.05	
	0.86	1	30.96 ^B	31.09 ^B	31.11 ^B	40.50 ^T	38.88 ^T	34.51	37.50	0.00	0.00
		2	40.03 ^B	46.63 ^B	33.62 ^B	35.02 ^B	47.20 ^T	40.50		0.00	

Table E.3: Failure distance (FD) measured from the suspension clamp mouth for the AAC Orchid conductor at different values of parameter H/w and failure position related to the suspension clamp. The distance between the suspension clamp mouth and the LPC is 31.27 mm.

H/w (m)	Y_b (mm)	Test	Failure distance from the suspension clamp mouth (mm)								MFD External (mm)		MFD Internal (mm)	
			1 st break	2 nd break	3 rd break	4 th break								
1820	0.87	1	35.07 ^B	34.31 ^B	35.57 ^B	36.64 ^B			35.40		0.00			
		2	36.56 ^B	32.52 ^B	33.07 ^B	35.05 ^B	34.05	34.81	35.05	35.58				
		3	34.87 ^B	35.09 ^B	35.00 ^B	36.10 ^B	34.99		36.10					
	0.91	1	33.99 ^B	31.96 ^B	29.92 ^B	33.77 ^B	31.96		33.77					
		2	33.83 ^B	31.62 ^B	31.52 ^B	36.60 ^T	32.73	35.48	34.06	34.15				
		3	41.76 ^B	31.79 ^B	37.41 ^B	34.70 ^T	41.76		34.63					
	1.01	1	35.32 ^B	34.27 ^B	35.48 ^B	28.29 ^B	34.80		31.89					
		2	33.94 ^B	35.08 ^B	27.06 ^B	31.78 ^B	34.51	35.07	29.42	29.42				
		3	36.01 ^B	35.77 ^B	26.10 ^B	27.81 ^B	35.89		26.96					
2144	0.82	1	35.17 ^B	34.89 ^B	37.06 ^B	44.24 ^T	37.84		0.00					
		2	36.19 ^B	32.81 ^B	36.63 ^B	29.32 ^T	35.21	36.58	29.32	31.37				
		3	37.81 ^B	35.90 ^B	36.35 ^B	33.42 ^T	36.69		33.42					
	0.87	1	29.94 ^B	28.22 ^B	30.24 ^B	34.13 ^B	29.47		34.13					
		2	33.41 ^B	31.43 ^B	22.22 ^B	39.89 ^T	32.42	32.37	31.06	32.59				
		3	33.14 ^B	32.18 ^B	34.83 ^B	40.70 ^B	35.21		0.00					
	0.96	1	37.85 ^B	34.50 ^B	37.10 ^B	38.80 ^B	37.48		0.00					
		2	36.89 ^B	34.50 ^B	44.13 ^T	35.21 ^B	38.51	36.01	35.21	35.21				
		3	28.27 ^B	30.28 ^B	29.71 ^B	39.98 ^T	32.06		0.00					
2725	0.76	1	34.71 ^B	35.08 ^B	24.79 ^B	26.83 ^B	34.90	34.19	25.81	25.78				
		2	34.34 ^B	32.30 ^B	33.84 ^B	25.74 ^B	33.49		25.74					
	0.80	1	37.74 ^B	34.27 ^B	32.45 ^B	33.24 ^B	36.01	36.35	32.85	40.28				
		2	36.74 ^B	36.65 ^B	47.36 ^T	48.06 ^T	36.70		47.71					
	0.89	1	36.84 ^T	38.37 ^T	40.55 ^T	36.79 ^T	38.59	37.56	38.59	38.59				
		2	39.07 ^B	36.18 ^B	34.02 ^B	36.88 ^B	36.54		0.00					

Table E.4: Failure distance (FD) measured from the suspension clamp mouth for the ACAR 750 MCM conductor at different values of parameter H/w and failure position related to the suspension clamp. The distance between the suspension clamp mouth and the LPC is 32.29 mm.

H/w (m)	Y_b (mm)	Test	Failure distance from the suspension clamp mouth (mm)								MFD External (mm)		MFD Internal (mm)	
			1 ^a break		2 ^a break		3 ^a break		4 ^a break					
1820	0.84	1	34.22	B	33.28	B	32.95	B	32.95	B	33.48		32.95	
		2	35.97	B	36.84	B	36.35	B	41.61	T	37.69	35.17	0.00	34.46
		3	32.07	B	35.91	B	35.02	B	36.93	B	34.33		35.98	
	0.88	1	39.20	B	39.70	B	37.45	B	30.85	B	36.80		0.00	
		2	41.16	B	44.82	B	44.06	T	47.60	T	44.41	39.23	0.00	0.00
		3	34.91	B	34.38	B	33.04	B	43.58	T	36.48		0.00	
	0.98	1	38.11	B	37.04	B	35.61	B	37.19	B	36.99		0.00	
		2	41.88	B	37.65	B	40.33	B	41.84	B	39.95	38.45	41.84	38.25
		3	36.67	B	40.13	B	33.92	B	35.41	B	38.40		34.67	
2144	0.80	1	35.01	B	37.90	B	34.51	B	35.82	B	35.81		0.00	
		2	31.52	B	31.50	B	31.24	B	29.75	B	31.00	34.27	0.00	0.00
		3	36.02	B	38.47	B	32.01	B	37.46	B	35.99		0.00	
	0.84	1	36.30	B	37.79	B	46.51	B	44.20	B	41.20		0.00	
		2	35.76	B	34.65	B	35.53	B	29.91	T	35.31	38.97	29.91	29.91
		3	36.34	B	36.57	B	44.37	T	44.32	T	40.40		0.00	
	0.93	1	33.95	B	34.71	B	36.18	B	46.40	T	35.45		0.00	
		2	34.64	B	35.84	B	37.73	B	39.86	T	36.07	37.35	39.86	39.86
		3	37.63	B	37.51	B	38.14	B	48.84	T	40.53		0.00	
2725	0.74	2	33.66	B	34.75	B	31.37	B	36.99	B	34.21	34.46	0.00	0.00
		4	33.10	B	34.99	B	34.44	B	41.99	B	34.72		0.00	
	0.78	1	39.74	B	33.96	B	33.11	B	35.94	B	34.95	35.73	0.00	23.60
		3	36.51	B	36.35	B	37.35	B	23.60	T	36.51		23.60	
	0.87	1	39.66	B	34.74	B	36.54	B	37.61	B	37.14	36.86	0.00	0.00
		2	34.47	B	32.60	B	33.40	B	45.84	T	36.58		0.00	

Appendix F

Position of wire break by layer for different conductors tested at different values of H/w parameter

Table F.1: Position of wire break by layer for conductor AAAC 900 MCM for different values of parameter H/w

H/w (mm)	Y_b (mm)	Test	Position of wire break by layer			
			1 st break	2 nd break	3 rd break	4 th break
1820	0.71	1	E	E	E	I
		2	E	E	I	I
		3	E	E	I	I
	0.85	1	E	E	E	E
		2	E	E	E	E
		3	E	E	E	E
	0.94	1	E	E	E	E
		2	E	E	E	I
		3	E	E	I	I
2144	0.68	1	E	E	E	I
		2	E	E	E	I
		3	E	E	I	I
	0.81	1	E	E	E	I
		2	E	E	I	I
		3	E	E	E	I
	0.90	1	E	E	E	E
		2	E	E	E	E
		3	E	E	E	I
2725	0.63	1	E	E	E	E
		2	E	E	E	I
	0.76	1	E	E	E	I
		2	E	E	E	I
	0.84	1	E	E	I	I
		2	E	E	E	E

Table F.2: Position of wire break by layer for conductor ACSR Tern for different values of parameter H/w

H/w (mm)	Y_b (mm)	Test	Position of wire break by layer				
			1 st break	2 nd break	3 rd break	4 th break	5 th break
1820	0.84	1	E	E	E	E	E
		2	E	E	E	I	I
		3	E	E	E	E	I
	0.88	1	E	E	E	E	E
		2	E	E	E	E	E
		3	E	E	E	I	I
	0.98	1	E	E	E	E	E
		2	E	E	E	E	E
		3	E	E	E	E	E
2144	0.8	1	E	E	E	E	E
		2	E	E	E	I	I
		3	E	E	E	E	I
	0.84	1	E	E	E	E	E
		2	E	E	E	E	E
		3	E	E	E	E	I
	0.93	1	E	E	E	E	E
		2	E	E	E	E	E
		3	E	E	E	E	E
2725	0.74	1	E	E	E	E	I
		2	E	E	E	E	I
	0.78	1	E	E	E	E	I
		2	E	E	E	E	I
	0.86	1	E	E	E	E	E
		2	E	E	E	E	E

Table F.3: Position of wire break by layer for conductor AAC Orchid for different values of parameter H/w

H/w (mm)	Y_b (mm)	Test	Position of wire break by layer			
			1 st break	2 nd break	3 rd break	4 th break
1820	0.87	1	E	E	E	E
		2	E	E	E	I
		3	E	E	E	I
	0.91	1	E	E	E	I
		2	E	E	I	I
		3	E	I	I	I
	1.01	1	E	E	I	I
		2	E	E	I	I
		3	E	E	I	I
2144	0.82	1	E	E	E	E
		2	E	E	E	I
		3	E	E	E	I
	0.87	1	E	E	E	I
		2	E	E	I	I
		3	E	E	E	I
	0.96	1	E	E	E	E
		2	E	E	E	I
		3	E	E	E	E
2725	0.76	1	E	E	I	I
		2	E	E	E	I
	0.80	1	E	E	I	I
		2	E	E	E	E
	0.89	1	E	E	E	E
		2	E	E	E	E

Table F.4: Position of wire break by layer for conductor ACAR 750 MCM for different values of parameter H/w

H/w (mm)	Y_b (mm)	Test	Position of wire break by layer			
			1 st break	2 nd break	3 rd break	4 th break
1820	0.84	1	E	E	E	I
		2	E	E	E	E
		3	E	E	E	E
	0.88	1	E	E	E	E
		2	E	E	E	E
		3	E	E	E	I
	0.98	1	E	E	E	E
		2	E	E	E	E
		3	E	E	E	E
2144	0.8	1	E	E	E	E
		2	E	E	E	E
		3	E	E	E	E
	0.84	1	E	E	E	E
		2	E	E	E	I
		3	E	E	E	E
	0.93	1	E	E	E	E
		2	E	E	E	E
		3	E	E	E	E
2725	0.74	1	E	E	E	E
		2	E	E	E	E
	0.78	1	E	E	E	E
		2	E	E	E	E
	0.87	1	E	E	E	E
		2	E	E	E	E

Appendix G

Fracture type surface of wire breaks for conductors at different values of H/w

Table G.1: Fracture type surface of wire breaks for the AAAC 900 MCM conductor at different values of H/w

H/w (m)	Y_b (mm)	Test	Fracture type surface of wire			
			1 st break	2 nd break	3 rd break	4 th Break
1820	0.71	1	QP	QP	QP	V
		2	QP	45°	QP	45°
		3	45°	QP	QP	V
	0.85	1	QP	L	V	QP
		2	45°	V	QP	V
		3	45°	QP	45°	QP
	0.94	1	QP	L	QP	L
		2	45°	V	V	QP
		3	QP	L	V	V
2144	0.68	1	L	QP	V	V
		2	L	QP	45°	45°
		4	QP	QP	45°	V
	0.9	1	45°	45°	L	QP
		2	L	45°	QP	QP
		3	L	QP	V	QP
	0.63	1	45°	QP	V	V
		2	QP	45°	QP	QP
		3	QP	QP	V	V
2725	0.76	1	45°	QP	45°	QP
		2	V	QP	QP	45°
	0.84	1	V	V	45°	45°
		2	45°	45°	QP	QP
	0.84	1	45°	45°	QP	QP
		2	45°	45°	V	45°

Table G.2: Fracture type surface of wire breaks for the ACSR Tern conductor at different values of H/w

H/w (m)	Y_b (mm)	Test	Fracture type surface of wire				
			1 st break	2 nd break	3 rd break	4 th break	5 th break
1820	0.84	1	V	QP	QP	45°	45°
		2	V	45°	QP	L	V
		3	45°	45°	V	QP	45°
	0.88	1	45°	QP	45°	45°	QP
		2	V	45	QP	QP	V
		3	45	QP	QP	QP	QP
	0.98	1	V	45	45	45	45
		2	45°	45°	45°	45°	v
		3	V	45°	45°	V	V
2144	0.8	1	V	45	45	45	QP
		2	45	45	45	QP	45
		4	45	45	45	45	L
	0.84	1	45	45	QP	L	45
		2	QP	45	V	45	V
		3	45	45	QP	QP	L
	0.93	1	45	45	45	45	45
		2	45	V	45	45	QP
		3	V	45	45	V	45
2725	0.74	1	45°	V	45°	45°	45°
		2	QP	45°	45°	45°	45°
	0.78	1	QP	QP	45°	V	QP
		2	QP	V	V	45°	45°
	0.84	1	45°	V	45°	45°	45°
		2	45°	45°	45°	45°	45°

Table G.3: Fracture type surface of wire breaks for the AAC Orchid conductor at different values of H/w

H/w (m)	Y_b (mm)	Test	Fracture type surface of wire			
			1 st break	2 nd break	3 rd break	4 th break
1820	0.87	1	45°	45°	45°	45°
		2	QP	QP	QP	45°
		3	45°	QP	QP	45°
	0.91	1	QP	V	45°	45°
		2	45°	QP	45°	45°
		3	QP	V	QP	45°
1.01	1	QP	45°	V	45°	
	2	QP	QP	V	45°	
	3	V	QP	45°	45°	
2144	0.82	1	QP	45	45	45°
		2	45	L	QP	45°
		3	QP	45	V	45°
	0.87	1	V	45°	45°	45°
		2	QP	45°	L	45°
		3	45°	V	45	QP
0.96	1	V	45°	45°	L	
	2	45°	L	45°	45°	
	3	45°	QP	QP	V	
2725	0.76	1	45°	45°	V	45°
		2	45°	45°	45°	45°
	0.8	1	45°	L	QP	QP
		2	45°	45°	45°	45°
	0.89	1	45°	45°	45°	45°
		2	45°	45°	45°	45°

Table G.4: Fracture type surface of wire breaks for the ACAR 750 MCM conductor at different values of H/w

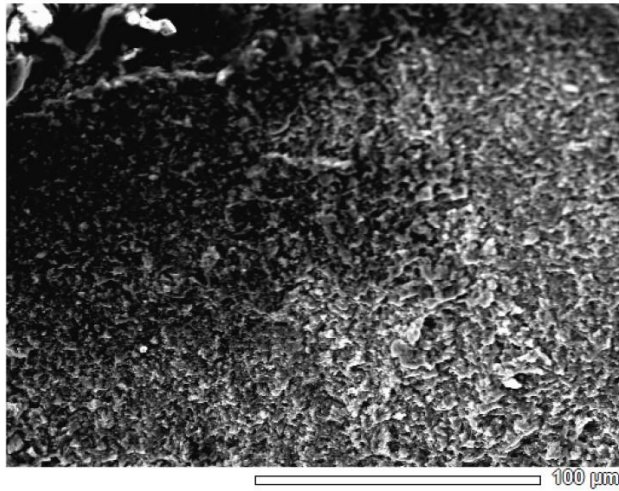
H/w (m)	Y_b (mm)	Test	Fracture type surface of wire			
			1 st break	2 nd break	3 rd break	4 th break
1820	0.84	1	QP	QP	45°	V
		2	45°	45°	QP	45°
		3	QP	45°	QP	45°
	0.88	1	V	45°	45°	V
		2	QP	45°	QP	45°
		3	QP	V	V	QP
	0.98	1	45°	45°	V	45°
		2	QP	QP	45°	QP
		3	45°	45°	45°	V
2144	0.8	1	QP	45°	QP	V
		2	QP	V	45°	QP
		3	QP	V	V	45°
	0.84	1	V	45°	V	45°
		2	QP	45°	V	45°
		3	QP	45°	45°	45°
	0.93	1	45°	45°	QP	45°
		2	45°	QP	QP	V
		3	V	QP	QP	45°
2725	0.74	1	45°	QP	45°	45°
		2	V	45°	45°	45°
	0.78	1	45°	QP	V	45°
		2	QP	QP	QP	45°
	0.87	1	45°	45°	45°	45°
		2	QP	45	45	45

Appendix H

Microscopic Energy dispersive x-ray spectroscopy analysis

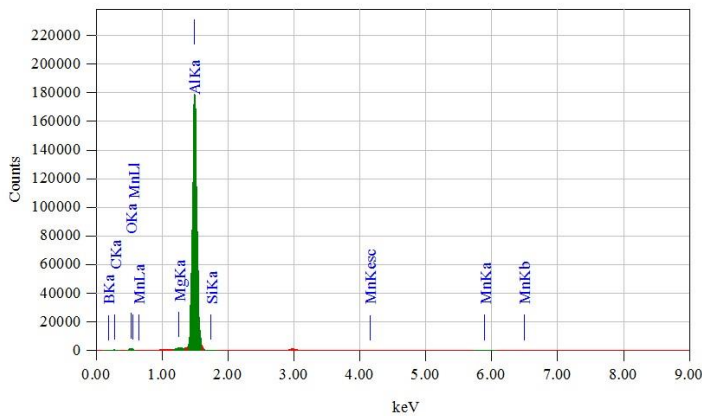
Figure H.1: Energy dispersive x-ray spectroscopy of AAAC 900 MCM. Peaks related to aluminium, magnesium and silicon elements can be identified, representatives of chemical composition. The high amount of oxygen identified can be related to aluminium oxide formation (Al_2O_3) by fretting wear during conductor vibration on fatigue tests.

View003



Lab 1/1

Title : IMG1
 Instrument : 7100F
 Volt : 20.00 kV
 Mag. : x 550
 Date : 2017/11/28
 Pixel : 512 x 384



Acquisition Parameter
 Instrument : 7100F
 Acc. Voltage : 20.0 kV
 Probe Current: 1.00000 nA
 PHA mode : F3
 Real Time : 70.41 sec
 Live Time : 50.00 sec
 Dead Time : 28 %
 Counting Rate: 37141 cps
 Energy Range : 0 - 20 keV

ZAF Method Standardless Quantitative Analysis

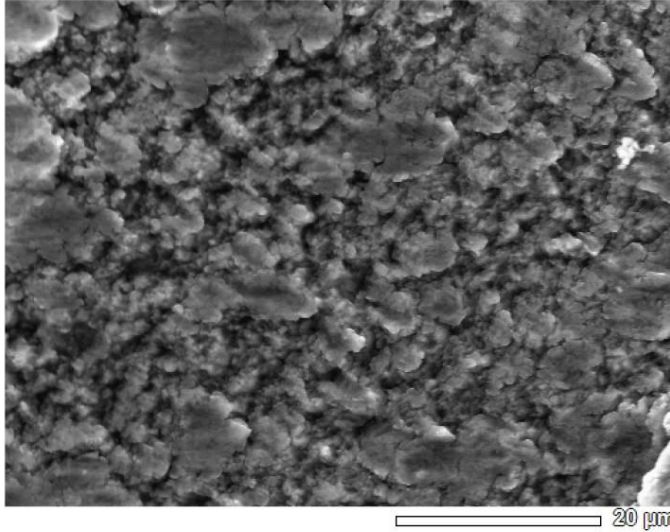
Fitting Coefficient : 0.0121

Element	(keV)	Mass%	Sigma	Atom%	Compound	Mass%	Cation	K
B								
C	0.277	13.81	0.15	25.21				1.0691
O	0.525	8.49	0.11	11.64				6.5826
Mg	1.253	0.51	0.01	0.46				0.5069
Al	1.486	76.81	0.11	62.41				91.6674
Si	1.739	0.38	0.01	0.29				0.1738
Mn	5.894	0.00	0.01	0.00				0.0001
Total		100.00		100.00				

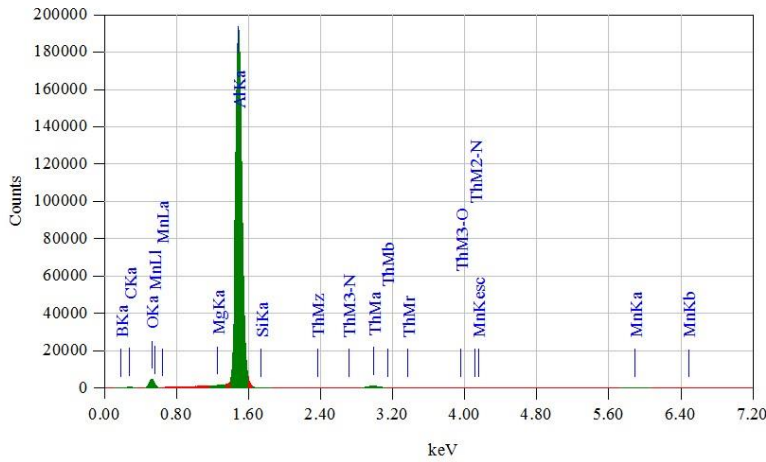
Figure H.2: Energy dispersive x-ray spectroscopy of ACSR Tern wire. Peaks related to aluminium can be identified, representatives of chemical composition. Smaller amount of oxygen was measured, indicative of less aluminium oxide formation (Al_2O_3) than the AAAC 900 MCM wire.

View001

Lab 1/1



Title : IMG1
 Instrument : 7100F
 Volt : 20,00 kV
 Mag. : x 1,800
 Date : 2017/11/28
 Pixel : 512 x 384



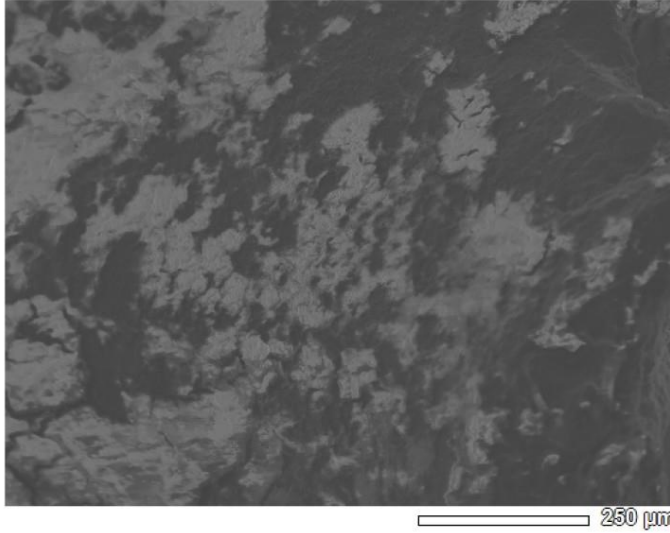
Acquisition Parameter
 Instrument : 7100F
 Acc. Voltage : 20.0 kV
 Probe Current: 1.000000 nA
 PHA mode : T3
 Real Time : 68.96 sec
 Live Time : 50.00 sec
 Dead Time : 27 %
 Counting Rate: 37526 cps
 Energy Range : 0 - 20 keV

ZAF Method Standardless Quantitative Analysis
 Fitting Coefficient : 0.0066

Element	(keV)	Mass%	Sigma	Atom%	Compound	Mass%	Cation	K
B	K*							
C	K	0.277	11.10	0.11	20.08			1.0162
O	K	0.525	17.24	0.13	23.41			15.3530
Mg	K*							
Al	K	1.486	70.01	0.09	56.35			82.2616
Si	K*	1.739	0.02	0.01	0.01			0.0082
Mn	K*							
Th	M	2.991	1.63	0.03	0.15			1.3611
Total			100.00		100.00			

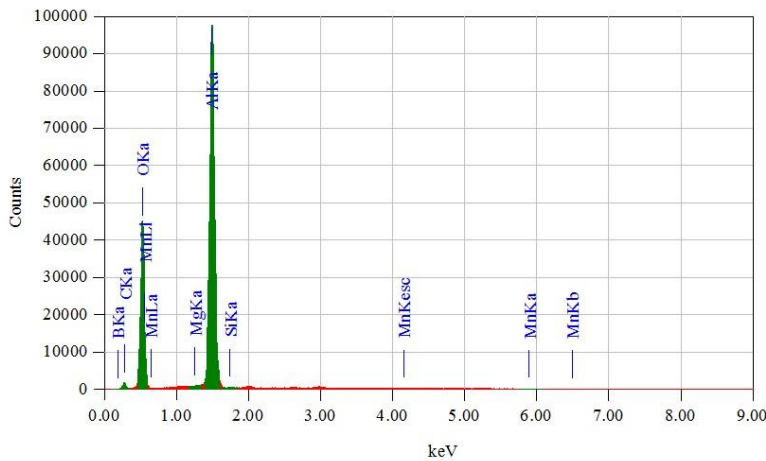
Figure H.2: Energy dispersive x-ray spectroscopy of AAC Orchid wire. Peaks related to aluminium can be identified, representatives of chemical composition. Smaller amount of oxygen and silicon was measured, indicative of less aluminium oxide formation (Al_2O_3) and SiO_2 .

View000



Lab 1/1

Title : IMG1
 Instrument : 7100F
 Volt : 20,00 kV
 Mag. : x 120
 Date : 2017/11/28
 Pixel : 512 x 384



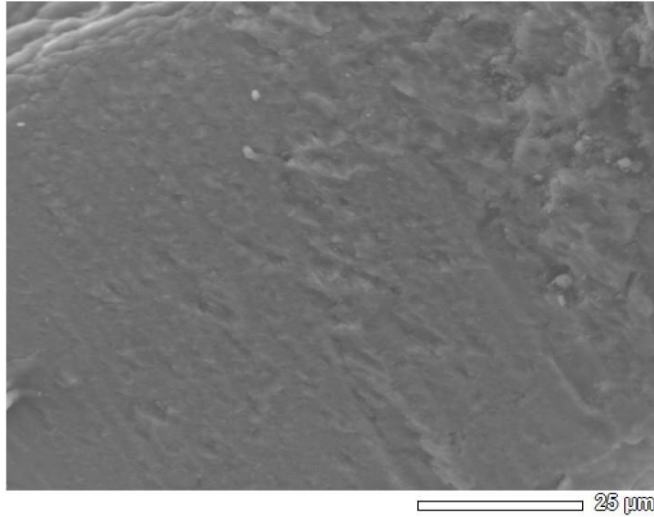
Acquisition Parameter
 Instrument : 7100F
 Acc. Voltage : 20.0 kV
 Probe Current: 1.00000 nA
 PHA mode : T3
 Real Time : 63.72 sec
 Live Time : 50.00 sec
 Dead Time : 21 %
 Counting Rate: 28195 cps
 Energy Range : 0 - 20 keV

ZAF Method Standardless Quantitative Analysis
 Fitting Coefficient : 0.0070

Element	(keV)	Mass%	Sigma	Atom%	Compound	Mass%	Cation	K
B K	0.183	7.10	0.11	10.91				0.4221
C K	0.277	8.20	0.05	11.34				1.1878
O K	0.525	60.50	0.14	62.84				77.4913
Mg K								
Al K	1.486	24.15	0.05	14.87				20.8630
Si K	1.739	0.05	0.00	0.03				0.0320
Mn K	5.894	0.00	0.00	0.00				0.0038
Total		100.00		100.00				

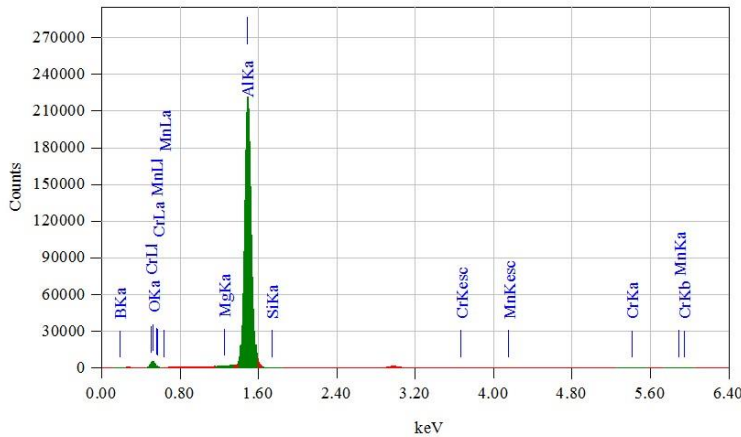
Figure H.2: Energy dispersive x-ray spectroscopy of ACAR 750 wire. Peaks related to aluminium can be identified, representatives of chemical composition. Smaller amount of oxygen and Silicium was measured, indicative of less aluminium oxide formation (Al_2O_3) and SiO_2 .

View005



Lab 1/1

Title : IMG1
 Instrument : 7100F
 Volt : 20,00 kV
 Mag. : x 1,200
 Date : 2017/11/22
 Pixel : 512 x 384



Acquisition Parameter
 Instrument : 7100F
 Acc. Voltage : 20.0 kV
 Probe Current: 1,00000 nA
 PHA mode : T3
 Real Time : 72.52 sec
 Live Time : 50.00 sec
 Dead Time : 31 %
 Counting Rate: 43024 cps
 Energy Range : 0 - 20 keV

ZAF Method Standardless Quantitative Analysis

Fitting Coefficient : 0.0244

Element	(keV)	Mass%	Sigma	Atom%	Compound	Mass%	Cation	K
B K								
O K	0.525	17.47	0.12	26.30				15.3094
Mg K								
Al K	1.486	82.41	0.10	73.59				84.6439
Si K	1.739	0.12	0.01	0.10				0.0467
Cr K								
Mn K								
Total		100.00		100.00				

Appendix I

Results of Chow test on the fatigue behaviour between conductors

Table I.1: Chow test results comparing the S-N curve of ACAR and AAC Orchid conductor.

H/w (m)	F_{obs}	F_{crit}	p-value (%)
1820	1.60	3.74	23.76
2144	0.89	3.74	43.44
2725	0.10	4.46	90.56

Table I.2: Chow test results comparing the S-N curve of AAC Orchid and ACSR Tern conductor.

H/w (m)	F_{obs}	F_{crit}	p-value (%)
1820	16.56	3.74	0.03
2144	15.82	3.74	0.03
2725	6.10	4.46	2.46

Table I.3: Chow test results comparing the S-N curve of ACAR 750 MCM and ACSR Tern conductor.

<i>H/w (m)</i>	F_{obs}	F_{crit}	p-value (%)
1820	14.79	3.74	0.04
2144	9.05	3.74	0.30
2725	4.47	4.46	4.98